PERMISSION TO MICROFILM — AUTORISATION DE MICROFILMER

• Please print or type — Écrire en lettres moulées ou dactylographier

Full Name of Author — Nom complet de l'auteur

Edward David Cooper

Date of Birth — Date de naissance	Country of Birth — Lieu de naissance
4/2/54	Great Britain

Permanent Address — Résidence fixe

THE TERRACE, BRIDGE STREET,
ISLIP, OXFORD
ENGLAND   OX5 2TE

Title of Thesis — Titre de la thèse

Dirac Phenomenology and Its Application
to Proton Induced Pion Production
Reactions

University — Université

Alberta

Degree for which thesis was presented — Grade pour lequel cette thèse fut présentée

PhD

Year this degree conferred — Année d'obtention de ce grade	Name of Supervisor — Nom du directeur de thèse
1981	Dr. Helmy Sherif

Date	Signature
27th April 1981	E. Cooper

NL-91 (4/77)

NOTICE

AVIS

The quality of this microfiche is heavily dependent upon the quality of the original thesis submitted for microfilming. Every effort has been made to ensure the highest quality of reproduction possible.

If pages are missing, contact the university which granted the degree.

Some pages may have indistinct print especially if the original pages were typed with a poor typewriter ribbon or if the university sent us a poor photocopy.

Previously copyrighted materials (journal articles, published tests, etc.) are not filmed.

Reproduction in full or in part of this film is governed by the Canadian Copyright Act, R.S.C. 1970, c. C-30. Please read the authorization forms which accompany this thesis.

La qualité de cette microfiche dépend grandement de la qualité de la thèse soumise au microfilmage. Nous avons tout fait pour assurer une qualité supérieure de reproduction.

S'il manque des pages, veuillez communiquer avec l'université qui a conféré le grade.

La qualité d'impression de certaines pages peut laisser à désirer, surtout si les pages originales ont été dactylographiées à l'aide d'un ruban usé ou si l'université nous a fait parvenir une photocopie de mauvaise qualité.

Les documents qui font déjà l'objet d'un droit d'auteur (articles de revue, examens publiés, etc.) ne sont pas microfilmés.

La reproduction, même partielle, de ce microfilm est soumise à la Loi canadienne sur le droit d'auteur, SRC 1970, c. C-30. Veuillez prendre connaissance des formules d'autorisation qui accompagnent cette thèse.

THIS DISSERTATION
HAS BEEN MICROFILMED
EXACTLY AS RECEIVED

LA THÈSE A ÉTÉ
MICROFILMÉE TELLE QUE
NOUS L'AVONS REÇUE

THE UNIVERSITY OF ALBERTA

DIRAC PHENOMENOLOGY AND ITS APPLICATION TO PROTON INDUCED

PION PRODUCTION REACTIONS

by

(C) Edward David Cooper

ρ

A THESIS

SUBMITTED TO THE FACULTY OF GRADUATE STUDIES AND RESEARCH

IN PARTIAL FULFILMENT OF THE REQUIREMENTS FOR THE DEGREE

OF Doctor of Philosophy .

IN

Nuclear Physics

DEPARTMENT OF PHYSICS

EDMONTON, ALBERTA

SPRING 1981

THE UNIVERSITY OF ALBERTA

RELEASE FORM

NAME OF AUTHOR   Edward David Cooper

TITLE OF THESIS   DIRAC PHENOMENOLOGY AND ITS APPLICATION

TO PROTON INDUCED PION PRODUCTION

REACTIONS

DEGREE FOR WHICH THESIS WAS PRESENTED   Doctor of Philosophy

YEAR THIS DEGREE GRANTED   SPRING 1981

Permission is hereby granted to THE UNIVERSITY OF ALBERTA LIBRARY to reproduce single copies of this thesis and to lend or sell such copies for private, scholarly or scientific research purposes only.

The author reserves other publication rights, and neither the thesis nor extensive extracts from it may be printed or otherwise reproduced without the author's written permission.

(SIGNED) ....

PERMANENT ADDRESS:

.THE. .TERRACE.........

.BRIDGE. sT. ..ISLIP...

.OXFORD,.ENGLAND....

DATED 27./.4/.1981

THE UNIVERSITY OF ALBERTA

FACULTY OF GRADUATE STUDIES AND RESEARCH

The undersigned certify that they have read, and recommend to the Faculty of Graduate Studies and Research, for acceptance, a thesis entitled DIRAC PHENOMENOLOGY AND ITS APPLICATION TO PROTON INDUCED PION PRODUCTION REACTIONS submitted by Edward David Cooper in partial fulfilment of the requirements for the degree of Doctor of Philosophy in Nuclear Physics.

....
Supervisor

....
....
....

....
External Examiner

Date....April 10, 1981......

DEDICATION

To Mum and Dad

ABSTRACT

A relativistic description of the bulk features of the nucleon-nucleus interaction is developed and used in a relativistic DWBA approach to the (p,π^+) reaction.

The nucleon-nucleus interaction is described by vector and scalar potentials. For the bound state these potentials are real and are similar to those obtained from Dirac Hartree Fock calculations. For continuum states, namely the proton distorted wave, the vector and scalar potentials are taken to be complex. The parameters are varied to fit the elastic scattering data by a search program called *RUNT*; which has been specifically developed for this purpose. The fits so obtained are generally of superior quality to those obtained from a non-relativistic optical model.

Two distinct classes of potential emerged from the search, one having large imaginary potentials of opposite sign in accord with the earlier work, the other having two small absorptive potentials.

The pion distorted waves are calculated from a standard optical potential.

Both pseudoscalar and pseudovector descriptions of the πNN vertex are used in the DWBA calculations. The energy and angular dependences of the (p,π^+) cross-section data on the closed shell nuclei ^{40}CA and ^{12}O are reproduced with the pseudovector coupling, but not with the pseudoscalar coupling. The pseudovector coupling also reproduces the

analysing power data on ^{12}C in the forward hemisphere. The rather curious experimental observation of the state independence of the analysing power is born out by this model.

ACKNOWLEDGEMENTS

translating it into the Queen's English, and also to my committe for accepting the thesis whilst it was still a little "ragged".

Last , but by no means least, I'd like to thank my wife Karyn for her patience, love and support during this last year, when the many deadlines I had promised her for completion of the thesis slipped by.

Table of Contents

xi

List of Tables

List of Figures

1. INTRODUCTION

If a nucleus is bombarded with protons which have kinetic energies greater than 140 MeV, then many things can happen. The most common occurrences are the following: the proton can elastically scatter from the nucleus leaving the latter in its ground state; The proton can give up some of its kinetic energy leaving the nucleus in a bound, excited state; or else the proton can break up the nucleus. In this thesis we are primarily interested in a less probable event, namely that of pi meson production with the nucleus left intact in some definite state. The cross-section for pion production is very small around threshold; for example if 160 MeV protons are scattered from ^{40}Ca, the total cross-section for producing a pion and leaving the final nucleus in its ground state is of order 0.5 μb. The total reaction cross-section is around 650 mb, almost a million times larger.

Experimentally the low cross-section makes the reaction hard to study, so it is really only with the recent advent of the meson factories that the reaction has gained much importance. The reaction is, however, very important *theoretically* since it involves large momentum transfer and therefore probes the higher momentum components of nuclear wavefunctions.

1

1.1 The Pion-Nucleon Interaction

Let us consider the possible interactions of pions with nucleons. The simplest Lagrangian we can write down is:

$$\mathcal{L} = \mathcal{L}_N + \mathcal{L}_\pi + \mathcal{L}_{INT} \qquad 1.1$$

$$\mathcal{L}_N = \bar{\psi}(x)(i\gamma^\mu \partial_\mu - m_N)\psi(x) \qquad 1.2$$

$$\mathcal{L}_\pi = \tfrac{1}{2}(\partial_\mu \underline{\phi} \cdot \partial^\mu \underline{\phi} - m_\pi^2 \underline{\phi}^2) \qquad 1.3$$

$$\mathcal{L}_{INT} = -ig\bar{\psi}(x)\Gamma\,\underline{\tau}\cdot\psi(x)\,\underline{\phi}(x) \qquad 1.4$$

$$\Gamma = \gamma_5 \qquad or \qquad \Gamma = (2m_N)^{-1}\gamma_5\gamma^\mu \partial_\mu^{(\pi)} \qquad 1.5$$

where the first interaction is called the pseudoscalar interaction (or coupling) and the second is called the pseudovector coupling (GE60).

In the above, ψ is a Dirac spinor describing the nucleon field and $\underline{\phi}$ is the pion field wavefunction.

There exists another model, due to Schwinger (SC57), called the sigma model which has derivative coupling (as in the pseudovector interaction) and entails the presence of another field, that of sigma mesons. It turns out that the sigma model and the pseudoscalar interaction give renormalisable theories, whereas the pseudovector interaction gives a theory which is unrenormalisable.

From equation 1.1 we use the Euler-Lagrange equations to get the field equations for the pseudoscalar vertex from

$$\frac{\partial \mathcal{L}}{\partial X} = \partial_\mu \left(\frac{\partial \mathcal{L}}{\partial_\mu X} \right)$$

1.6

Putting $X = \bar{\psi}$ in 1.6 gives us the equation

$$(i\gamma^\mu \partial_\mu - m_N)\psi(x) = ig\gamma_5 \underline{\tau} \cdot \psi(x) \underline{\phi}(x)$$

1.7

and putting $X = \phi$ we get

$$(\partial^\mu \partial_\mu - m_\pi^2)\phi(x) = ig\bar{\psi}(x)\gamma_5 \underline{\tau} \psi(x)$$

1.8

The top equation is the one we are interested in; only the bottom equation changes its *form* when we use a different interaction. One should note that the source term on the right of equation 1.8 gives the overlap of nucleons and antinucleons; this is reminiscent of the old Bootstrap model of the pion being made up of a nucleon-antinucleon in a bound state.

From equation 1.4 we see that the only vertex in the model is that shown in figure 1.1

In free space, energy and momentum conservation prohibit a proton emitting a free pion; however, if there is a nucleus nearby to remove the excess momentum a pion can be so produced. We can write this symbolically as in figure 1.2 If we take this diagram literally then we can write down the matrix element (in the zero range approximation) as
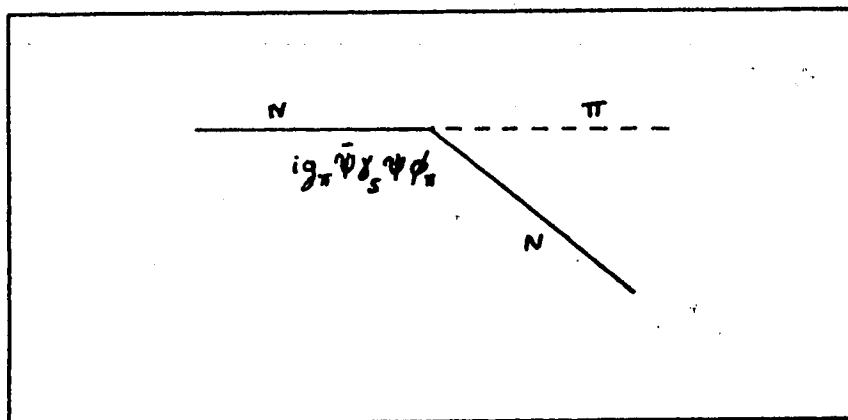
Figure 1.1 The vertex for pseudo scalar coupling.

$$T_{fi} = \int \bar{\psi}_f(x) \, \Gamma \, \underline{\gamma} \cdot \underline{\phi}(x) \, \psi(x) \, d^4x$$

1.9

where Γ is the pion-nucleon vertex.

If we attempt to use the usual nuclear physics technique of doing a non-relativistic reduction (Foldy-Wouthuysen) of the vertex, we get an expression

$$T_{fi} = \int \psi_f^\dagger(\underline{r}) \, H_{\pi NN}(\underline{r}) \, \phi_\pi(\underline{r}) \, \psi_i(\underline{r}) \, d^3r$$

1.10

where ψ_f, ψ_i ,are the nucleon distorted waves from a Schrödinger equation and $H_{\pi NN}(r)$ is the FW reduced vertex. There is an ambiguity with the FW reduction which leads to an ambiguity in $H_{\pi NN}$.

Friar (FR74) has shown that this ambiguity can be expressed as
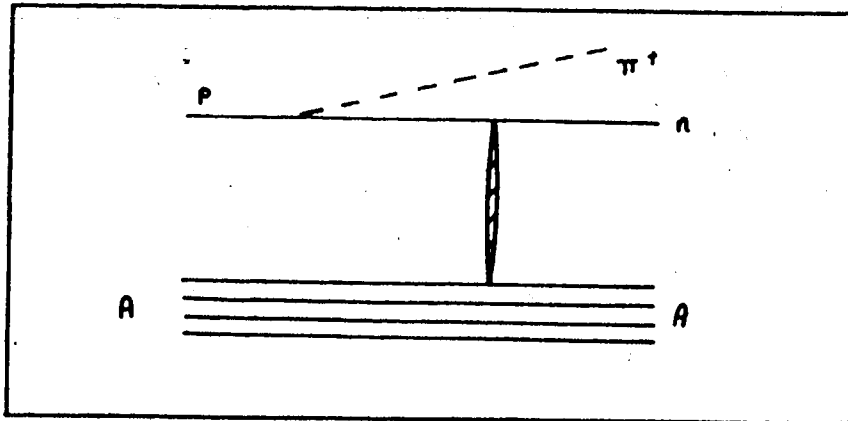
Figure 1.2 Pionic stripping in the viscinity of a nucleus.

$$H_{\pi N\underline{N}}(\underline{r}) = -\frac{g}{2\pi}\,\underline{\sigma}\cdot\underline{\nabla}\,\phi(\underline{r}) - \frac{(\mu+\frac{1}{2})}{4\pi^2}\left\{\underline{\sigma}\cdot\underline{p}\,,\,\dot{\phi}(\underline{r})\right\}$$

$$+\frac{g}{8m^3}\left\{\underline{p}^2,\,\underline{\sigma}\cdot\underline{\nabla}\,\phi(\underline{r})\right\} + \frac{\mu g}{8m^3}\left\{\underline{\sigma}\cdot\underline{\nabla}\,,\,[\nabla^2,\,\phi(\underline{r})]\right\}$$

$$+\frac{g}{2m^2}\,\underline{\sigma}\cdot\underline{\nabla}\,\left(\phi(\underline{r})U_s(r)\right) + \frac{g(\mu-\frac{1}{2})}{2m^2}\,\phi(\underline{r})\,\underline{\sigma}\cdot\underline{\nabla}\,U(\underline{r})$$

1.11

where

$$U(\underline{r}) = U_s(\underline{r}) + U_v(\underline{r})$$

1.12

and where μ is *completely arbitrary*. In equation 1.12 Uv and Us are the vector and scalar potentials experienced by the incident proton. Friar points out, however, that to first order in the coupling constant g the *physics* does not depend on μ. Assuming for the sake of argument that $\mu = 0$ (the static approximation), that the proton and pion

are free and that the final neutron enters a bound state, then we get terms (ignoring spin) like

$$T_{fi} = \int \psi_f^+(r) e^{-i \frac{p_f \cdot r}{\hbar}} \cdot e^{i p_\pi \cdot r} \, d^3r \quad = \phi(q) \tag{1.13}$$

where

$$q = p_\rho - p_\pi \tag{1.14}$$

is the three momentum transfer. Here $\phi(q)$ is the bound state in momentum space. We can, crudely, say that the angular distribution of pions gives us *directly* the single particle wavefunctions in momentum space. Knowledge of these high momentum components of the (single particle) nuclear wavefunctions is highly desirable from a nuclear structure point of view.

Now things are certainly not this rosy. If the target nucleus has A nucleons then the problem, from the point of view of quantum mechanics, is an A+1 body problem. In order to explain the data and extract at least *some* information we must rely on a model. There are two popular ways of modelling the problem: they are called the *one nucleon model* (or *mechanism*) and the *two nucleon model*.

1.2 The One Nucleon Model

This model is schematically depicted in figure 1.3 The assumptions being made here are:

1.   The pion is emitted from the incident proton.

2.   Before emitting the pion, the proton will undergo
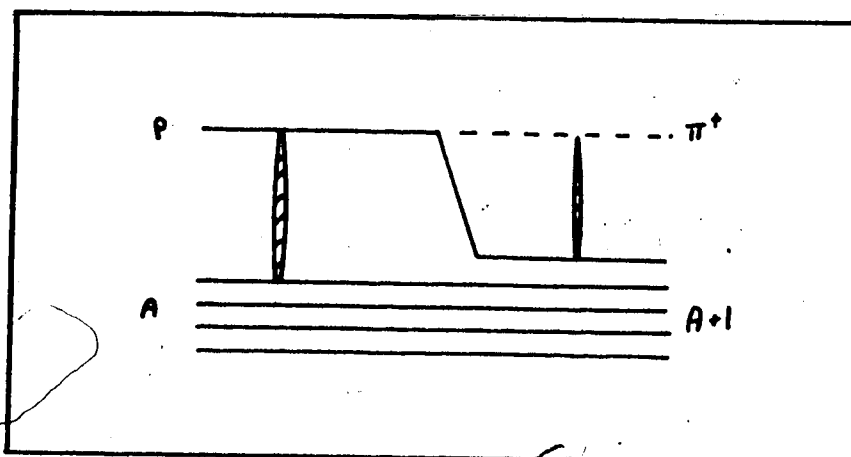
Figure 1.3 The One Nucleon Model.

interactions with all the other A nucleons in the problem and this interaction can be represented by a potential.

3. After it is produced, the pion will interact with the A+1 nucleons in the final nucleus.

4. The neutron formed from the nucleon which emitted the pion goes immediately into its final bound state.

Given that the incident proton interacts by a potential in the incident channel, the question remains how to find this potential, or rather what is the best potential to use. Weber and Eisenberg (WE78) have shown that the pion production cross-section and analysing power are very sensitive to this potential. These authors used a standard Woods-Saxon Optical potential with real, imaginary and spin-orbit parts.

There is one major problem: if we fix our potential by assuming a phenomenological shape and then obtain the parameters in this shape by fitting the elastic scattering data, we can learn a lot about the proton wavefunctions at large distances from the nucleus, whereas we can learn little about them at short range.

Elastic scattering at intermediate energies is mostly sensitive to the following properties of the potential:

1. the volume integral

2. the root mean square radius

3. the gradient at the nuclear surface.

This is clearly demonstrated in the work of Amado et al. (AM80).

Let us consider the real central potential. Most analyses assume a Woods-Saxon form for this potential. This is actually not such a good idea if we want to know the small distance behaviour, for the following reason: the N-N interaction is mediated by meson exchange. At long range the lightest mesons are the most important (pi and sigma); these lead to an attractive component. Thus no matter what energy we are dealing with, we expect the *tail* of the NN interaction, and hence the optical potential, to be attractive. The volume integral of the potential for energies above 400 MeV is known to be positive and so the potential must change sign at some radius. The Woods-Saxon parameterisation does not allow for this to happen, and so while we may use the Woods-Saxon potential to fit

phase-shift data, generally the wavefunction resulting will
not be correct deep inside the nucleus. The pion potential
also has this feature of being known only at the nuclear
surface. We discuss the potential used to generate the pion
wave functions in Chapter 5.

1.3 The Two Nucleon Model

The basic graph for the process is depicted in figure
1.4
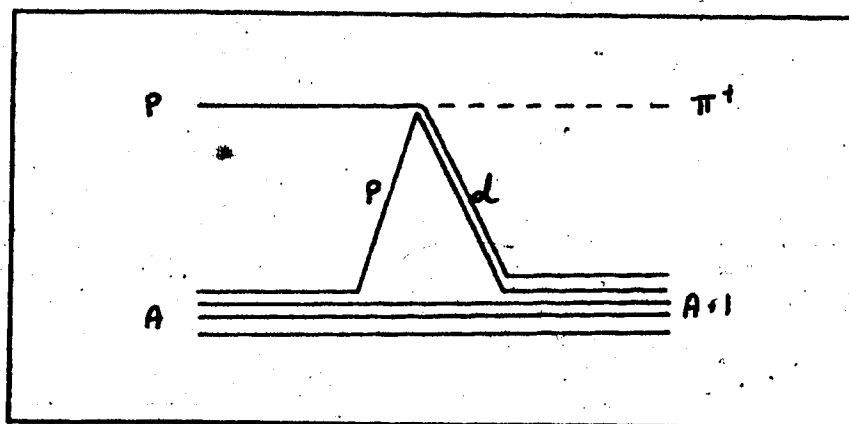
Figure 1.4 The Two Nucleon Model.

The incident nucleon strikes a nucleon in the target
and produces a pion by the reaction

$$p + p \rightarrow p + n + \pi^+$$

The cross-section for the process

$$p + n \rightarrow n + n + \pi^+$$

is much smaller and usually neglected.

There are two ways of proceeding with this model: one microscopic and the other phenomenological.

1.3.1 The Microscopic Two Nucleon Model

In the first case the amplitudes from the sub-process

$$p + p \rightarrow p + n + \pi^+$$

are obtained from some model (e.g. (GR79)) and are folded in with the nuclear wavefunctions. The advantage of this model is that the huge momentum transfer is shared between 2 nucleons, so we expect it to be less sensitive to the distorting potentials.

1.3.2 The Phenomenological Two Nucleon Model

In the more phenomenological approach (the Fearing/Ruderman model) (FE77), the assumption is that in $p + p \rightarrow p + n + \pi^+$ the dominant final state is that in which the proton and neutron form a deuteron. By means of a suitable factorisation of the matrix element it is possible to get the $p + A \rightarrow (A+1) + \pi^+$ cross-section written in terms of the $p + p \rightarrow d + \pi^+$ cross-section (plus a form factor). This model has the pleasing feature that knowedge of the πNN vertex is not necessary, although this also means it is not possible to extract any information about the vertex from the model.

1.4 Discussion of The Models

In the ONM it seems we are very sensitive to the distorting potentials, and also to the ambiguity in the non-relativistic reduction of the vertex.

In the two nucleon model we have a serious problem with the distorting potentials, namely in calculating observables for the reaction p + A → (A + 1) + π⁺, we need the p + (A-1) potential *In the presence* of a spectator nucleon. We can not usually get this from experimental data and must therefore rely on a model for it.

These models, it should be remembered, are just *models* of a complex system; it is meaningless to say the mechanism is a one body mechanism or a two body mechanism. In figure 1.5 is depicted a graph looking like the TNM. Writing down the T-matrix element from the graph, we get

$$T = \int \psi_1^+(r_1)\,\psi_2^+(r_2)\,H(r_1,r_2)\,\psi_1(r_1)\,\psi_2(r_2)\,d^3r_1\,d^3r_2 \qquad 1.15$$

$$= \int \psi_1^+(r_1)\int \psi_2^+(r_2)\,H(r_1,r_2)\,\psi_2(r_2)\,d^3r_2\;\;\psi_1(r_1)\,d^3r_1 \qquad 1.16$$

$$= \int \psi_1^+(r_1)\,H_{\pi NN}(r_1)\,\psi_1(r_1)\,d^3r \qquad 1.17$$

Thus by averaging over the positions of the nucleon in the nucleus we can obtain something which resembles the ONM from the TNM.
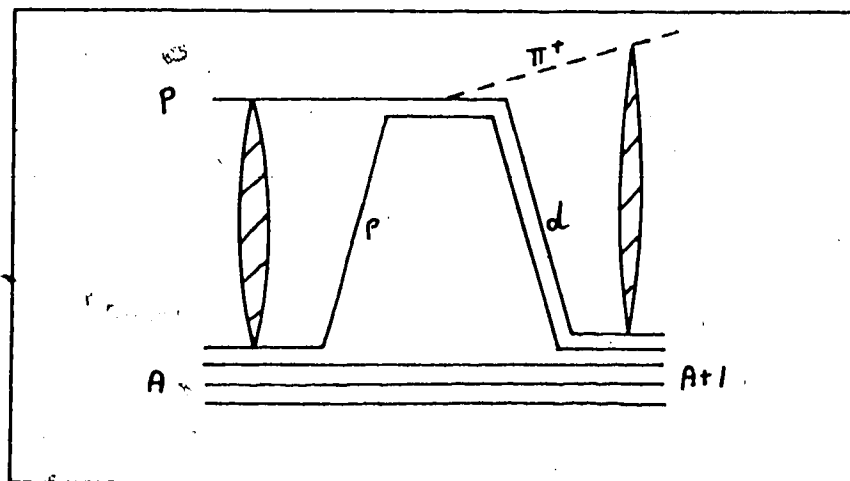
Figure 1.5 The connection between the ONM and the TNM.

1.5 Present Contribution

The model which is the cleanest as far as inputs and extractable information, is clearly the ONM. In this thesis the model is given a new chance by treating the protons as Dirac particles.

The DWBA calculation is done entirely using 'relativistic' potentials and wavefunctions. This not only handles the lower components previously treated in a hand waving manner (BR77), but also eliminates the ambiguity in the non-relativistic reduction in the pion-nucleon vertex. We employ one of the best pion distortion potentials available at present, namely the Stricker potential (ST79) which reproduces not only the pion elastic scattering data up to 50 MeV but also the pionic atom data. From

relativistic potentials, we also generate a bound state wavefunction which exhibits properties not found when using a non-relativistic model.

1.6 Organisation of Thesis

In Chapter 1 we have outlined the (p,π^+) problem and the current ways of dealing with it. In Chapter 2 we briefly review the literature available on the ONM, and discuss what we might expect to be the result of doing the full relativistic DWBA calculation.

For the DWBA calculation we will need both pion and proton distorted waves, as well as a bound state wavefunction for the neutron. We first show how these separate components are calculated: Chapter 3 derives a bound state wavefunction from relativistic Hartree Fock arguments; Chapter 4 extends the resulting formalism to the continuum and also demonstrates how to extract elastic scattering results; Chapter 5 shows how to the get the pion potential and from it the pion distorted wave. Chapter 6 accumulates the results of the three preceeding Chapters and uses them to calculate a T matrix for the (p,π^+) reaction. Chapter 7 shows the quality of fits obtainable to the proton elastic scattering data and presents the potentials used in the fits. In Chapter 8 we present the (p,π^+) predictions and compare them to the experimental data (where available). Chapter 9 concludes the relativistic one nucleon model

discussion, summarising the results of Chapters 7 and 8 and drawing what conclusions are possible as to the physics contained in the (p,π^+) reaction. Technical details of some of the 'ingredients' of the calculation are discussed in the appendices.

2. BRIEF HISTORICAL REVIEW OF THE ONM

In this Chapter we outline the historical development of the one nucleon model (ONM) for the (p,π⁺) reaction. For other models of this reaction, and for more details of the ONM, the reader is referred to the excellent reviews of the (p,π⁺) reaction by

1. Fearing (FE80)

2. Gell-Mann and Watson (GE54)

3. Höistad (HO77)

4. Measday and Miller (ME80)

2.1 Pion Production in N-N Collisions

The first measurement of the pion production cross-section was done in 1943, and Heitler and Pang (HE43) tried to explain the result as a form of bremstrahlung in which the virtual pions forming a cloud around the bare nuclear core were knocked on shell by interacting with a second nucleon. (This is essentially the process we call pionic stripping today.) This idea was taken up by Morette and Pang (MO48) where they included distortion (a delta function potential) in the incident channel. Foldy and Marshak (FO49) did the same thing but instead of a delta function they used a spin and isospin dependent realistic NN potential with spacial extent given by Yukawa terms.

Modern day calculations do not differ much from the spirit of these early calculations. Alberg ét al. (AL78) have recently performed a field theoretic calculation for

the process p + p → d + π⁺ at various intermediate energies.
These authors used the *static* operator for the pion-nucleon
non-relativistic vertex but were unable to get good fits to
the intermediate energy data.

2.2 Vertex Reduction

Non relativistic ONM calculations require a
non-relativistic reduction of the vertex. The first such
reduction was done by Chew (CH51) who obtained the
expression,

$$H_I(r) = t_1 e^{i \underline{\sigma} \cdot \underline{r}/2} + t_2 e^{-i \underline{\sigma} \cdot \underline{r}/2}$$ 2.1

$$t_i = \underline{\sigma}_i \cdot (a \underline{\nabla}_r + b \underline{\nabla}_\pi) \tau_i^{(+)}$$ 2.2

Cheon (CH68) derived a form similar to this, now called the
Galilean invariant form, by doing a Foldy Wouthuysen
transformation on the relativistic pseudoscalar vertex.

The next year Barnhill (BA69) showed how an ambiguity
in the vertex occurs in the reduced Hamiltonian from an
ambiguity in the matrices used in the FW method. Friar
points out that whilst we may do a unitary transformation on
the reduced Hamiltonian

$$H' - i\hbar \frac{\partial}{\partial t'} = e^{i\mu U}\left(H - i\hbar \frac{\partial}{\partial t}\right)e^{-i\mu U} \qquad 2.3$$

(U is any even unitary matrix, μ is arbitrary)
the physics does not change to first order in the coupling
constant g, providing one includes *all* the terms in equation
1.11 and uses plane waves for the pion wave-functions. Many
past analyses have not done this. At the time of Friar's
paper whether the potential was of scalar or vector nature
was unknown. We now know (JA80)(DU56) that to properly
describe the nuclear potential both vector and scalar
potentials must be present. Lee and Pittel (LE76) point out
that since Friar's conclusions depend on having a plane wave
pion, we expect some μ dependence. They also show the
effect of binding the neutron with a (Lorentz) scalar as
opposed to a (Lorentz) vector potential.

Miller (MI74) obtained his own reduction of the vertex
by a high energy approximation (kinetic energies much
greater than the binding energy).

J.V. Noble (NO76) attempted to learn about the vertex
by asking the question; "given that we have a plane wave
Hamiltonian ambiguity of the form

$$\underline{\sigma} \cdot \left(\underline{p}_p - \alpha \, \underline{p}_\pi\right) \qquad 2.4$$

what value of α best explains the energy dependence?" He
finds that the static approximation ($\alpha = 0$) is best,

although still not very good.

In 1980 Greben and Woloshyn (GR80) compared the relativistic vertex (both pseudoscalar and pseudovector types) calculations for the (p,nπ⁺) reaction with the conventional non-relativistic calculations (SH79). They find that the non-relativistic Hamiltonians cannot give the same result as the relativistic ones.

Summing up then, while we now know how to write down a unique non-relativistic Hamiltonian (see Chapter 6) which will exactly mimic the relativistic one; it is not possible to simplify it to the conventional static or Galilean forms, the distorting and binding potentials must always be present.

2.3 Previous ONM calculations

Aside from the special case of production on a hydrogen target, which is discussed in section 1.1, the first calculation of pion production on a nucleus was done by Edwards and Kanaris (ED62). These authors employed 3rd order perturbation theory involving nucleons bound in Gaussian wavefunctions and S-wave pions for the reaction

$$p + {}^3He \rightarrow {}^4He + \pi^+$$

The first modern ONM calculation was by Jones and Eisenberg in 1970 (JO70). These authors did a complete job with the proton distortion coming from an optical potential with real, imaginary and spin-orbit parts. They also

included pion distortion by means of the Kisslinger and Kisslinger-Kroll potentials. They find the (p,π^+) results are increased by a factor of around 200 by turning on the pion optical potentials, taking the theory from below to above the data.

Rost and Kunz (RO73) claimed that (JO70) were overcounting their distortion since the pion production Hamiltonian was also responsible for the OPE potential and hence part of the distorted waves. They scale the coupling constant down and find great sensitivity to the pion distortion potential geometry parameters. Their claim of overcounting is hard to see however.

Eisenberg (EI73) did a ONM calculation using generalised Hulthén wavefunctions for the bound state and eikonal wavefunctions for distortions. The final distortions bring down the cross-section in foreward angles.

Following the lead of Jones and Eisenberg, Keating and Willis (KE73) did a DWBA calculation to explain the 185 MeV data on ^{12}C. Like Jones and Eisenberg they find the pion distortion puts them above the data. They also find great sensitivity to the pion distortion geometry.

In contrast Dahlgren et al (DA73) analysed this same data using a simple square well potential for the pion distortion. These authors found hardly any sensitivity to the pion distortion. They explain this as due to the large off-shell parts of the non-local terms in the Kisslinger-like potentials used by the other authors.

In 1974 Miller (MI74) looked at the effect of using different pion optical potentials and found that he was able to get a pion potential which gave fits to both the elastic scattering and (p,π^+) data for ^{12}C and ^9Be ground and exited states for 185 MeV protons. His pion potential is

$$2E_\pi V_\pi (r) = -b_o k^2 \rho(r) + b_1 \nabla \rho(r) . \nabla \qquad 2.5$$

$$b_o = 5.7 - 1.1 \, i \qquad 2.6$$

$$b_1 = -3.8 + 5 i \qquad 2.7$$

The b_o and b_1 are not obtainable from any microscopic theory in contrast to the Stricker potential (ST78). Miller also looked at the effect of configuration mixing in the final state. He found sensitivity at the level of a factor of 2 the cross-section.

Y. Le Bornec et al. (BO74) performed similar (ONM) calculations for a ^{10}Be target with 185 MeV protons. They found order of magnitude agreement with the data using Miller's pion potentials.

In 1974 Grossman et al. (GR74) did an exhaustive study on the production of pions from 185 MeV protons incident on ^{12}C. They rule out the PWBA ONM as it gives cross section predictions which lie below the experimental data. They consider the effect of N^* and higher order multiple scatterings. This same year, Dahlgren et al (DA74) measured the (p,π^+) differential cross-section on ^{40}Ca, ^{16}O and ^{28}Si

with 185 MeV protons. Later, Le Bornec et al (BO76) found
that, even with a "tame" local square well potential for the
pion distortion, they get, for ^{40}Ca, a DWBA cross section 30
times too high.

Noble (NO75) performed the first analysing power
calculation for (p,π^+) with 185 MeV protons incident on ^{12}C.
He found the analysing power is negative everwhere.

In 1977 Miller and Weber (MI77) tried a relativistic
PWBA calculation. They tried to explain the ^{12}C data at
185 MeV. In plane waves they find overall agreement with the
data, however I believe there was a factor of $\hbar c$ (197.33)
missing in their calculation. Simultaneously Brockman and
Dillig (BR77) tried similar calculations on ^{16}O. They
compare the relativistic to the non-relativistic
calculations at 0° as a function of energy. They find no
value of α (see equation 2.2) can really reproduce the
relativistic results.

An interesting result was obtained by Gibbs and Hess
(GI77) where they relate the (p,π^+) cross-section on various
nuclei to the pion elastic scattering at the same energy.
They used an off shell extrapolation for the pion scattering
amplitude, which they give as

$$ f(\underline{q},\underline{q}') = f_{on\ shell}(\underline{q}-\underline{q}')\left(\frac{1 + \langle r^2 \rangle \underline{q}^2}{1 + \langle r^2 \rangle q'^2}\right) \qquad 2.8 $$

Their success in getting the correct order of magnitude
agreement with the (p,π^+) data indicates why, as we shall

see in Chapter 8, all the structure in the data is lost if we use plane wave pions in the calculations.

Kume and Ohtsubo (KU77) played the same off-shell extrapolation game but in the frame-work of the ONM. In momentum space they multiply the vertex by a factor

$$e^{-\Lambda(q-q')^2}$$

2.9

they find the cross-section is very sensitive to Λ .

In 1978 Auld et al. (AU78) made analysing power measurements on ^{12}C at 200 MeV, the analysing power turned out to be negative as Noble predicted, however Noble did not predict the correct magnitue of the analysing power. Gibbs and Young (GI78) found the consistently negative analysing powers very difficult to obtain from the ONM despite trying many different operators, bound state wavefunctions and off shell behaviours of the π-nucleus scattering amplitude.

Höistad et al. (HO79) published their results for the differential cross-section on ^{40}Ca for various energies from threshold to 185 MeV. They found the PWBA and DWBA ONM results are always 1 to 2 *orders of magnitude* above the data, in stark contrast to the ^{12}C case where approximate order of magnitude agreement can be found.

The (p,π^+) cross-section on Zirconium and Lead were measured by Höistad et al (HO78). These authors also later revisited the ^{40}Ca data (HO79) and found that by using pion potentials with high momentum cut-offs they were able to get approximate agreement with the data. Their plane wave

calculation is now in rough agreement with the data here as opposed to that of Le Bornec et al. (who also may have had the hc discrepancy)

Weber and Eisenberg (WE78) did a calculation of the analysing power of the reaction $^{12}C(p,\pi^+)^{13}C$ at 200 MeV. They find the analysing power comes mainly from the proton distortion. They use partial wave analyses as opposed to the eikonal distorted waves used by Gibbs and Young.

Sicilano and Thaler (SI78) and later Johnson and Ernst (JO79) showed that inclusion of a pion optical potential in either a Klein-Gordon or Schrödinger equation leads to the same phase-shifts but a significantly different pion wave-function, indicating that the ambiguities left in the potential after the elastic scattering data has been fit are quite large at small distances. Very recently Tsangredis has performed an exhaustive study on the non-relativistic ONM (TS80). He found that he was able to get good fits for the (p,π^+) data on oxygen, but was unable to reproduce the energy dependance of the calcium data.

From the work done so far it seems we can expect the relativistic one nucleon model to be sensitive to the way we handle the pion distortion, the proton distortion and the bound state wave function. This turns out to be the case. In the next 3 Chapters we discuss the calculation of these 3 vital ingredients.

3. THE BOUND NEUTRON

In this Chapter we discuss how to describe the interactions
of a valence neutron with a core nucleus. Specifically we
seek a 4-spinor solution to the Dirac Equation which has the
following properties;

1. Exponentially decays with distance as $\exp(-wr)/r$, where
    w is given by the binding energy of the state

$$\hbar^2 c^2 w^2 = m^2 c^4 - \left(mc^2 - |E_B| \right)^2 \qquad 3.1$$

2. Is regular at the origin.

These two requirements give a "handle" on the volume
integral of the binding potential.

To see how to calculate the interaction between the
neutron and the core nucleus, we consider a relativistic
description of nuclei due to Miller and Green (MI72). We
outline their derivation of the single particle wave-
functions in the next section.

3.1 The Relativistic Hartree Fock Model

In this model the nucleons are assumed to interact only
by one Boson exchange potentials. The bosons (mesons) most
likely to contribute (i.e. the lightest) are listed in
table 3.1 (BR78),(JA80), along with their isospins, spins,
parities, masses and coupling constants (with nucleons).

24

Table 3.1 The Mesons which Contribute Significantly to the Nuclear Force

Meson	T	J	P	Mass MeV	$g^2/4\pi$
pi	1	0	-	138.7	14.19
eta	0	0	-	548.5	3.09
sigma	0	0	+	570	6.97
delta	1	0	+	960	0.33
rho	1	1	-	763	0.43
omega	0	1	-	783	9.92
phi	0	1	-	1020	0.86

The N-N potentials arising from these meson exchanges are of the form

$$V_o = -\gamma_1^{\,o}\gamma_2^{\,o}\, J_s(|r_1 - r_2|)$$

$$V_v = -\gamma_1^{\,o}\gamma_2^{\,o}\gamma_1^{\,\mu}\gamma_{2\mu}\, J_v(|r_1 - r_2|)$$

$$V_\rho = \gamma_1^{\,o}\gamma_2^{\,o}\gamma_1^{\,5}\gamma_2^{\,5}\, J_\rho(|r_1 - r_2|) \qquad\qquad 3.2$$

$$\vdots \qquad \vdots$$

The subscripts signify the transformation properties under Lorentz transformations, and the J's are given by

$$J(r) = \hbar c\, g_i^2 \left(\frac{e^{-\mu r}}{r} - \frac{e^{-\Lambda r}}{r} \right)$$

$$\qquad\qquad 3.3$$

$$\mu = mc^2/\hbar c \qquad\qquad 3.4$$

$$F(q^2) = g\,\frac{\Lambda^2 - \mu^2}{\Lambda^2 + q^2} \qquad\qquad 3.5$$

F here is the usual form factor, and Λ is a momentum space cut off taken to be 1414 MeV/c.

Miller and Green construct a potential

$$V = V_o + V_v + V_\rho + \ldots \qquad\qquad 3.6$$

For a system of A nucleons the Dirac Hartree Fock equations are

$$\left(c\, \underline{\alpha}_i \cdot \underline{p}_i + \beta_i\, mc^2 \right) \phi_i(\underline{r}_1) + \sum_{j=1}^{A} \int \phi_j^{\dagger}(\underline{r}_2) V(|\underline{r}_1 - \underline{r}_2|) \phi_j(\underline{r}_2) \phi_i(\underline{r}_1) d^3r_2$$

$$- \sum_{j=1}^{A} \int \phi_j^{\dagger}(\underline{r}_2) V(|\underline{r}_1 - \underline{r}_2|) \phi_i(\underline{r}_2) \phi_j(\underline{r}_1) d^3r_2 \quad . \qquad 3.7$$

This looks very much like the ordinary non-relativistic Hartree-Fock equations. If we define

$$U(\underline{r}_1) = \sum_{j=1}^{A} \int \phi_j^{\dagger}(\underline{r}_2) V(|\underline{r}_1 - \underline{r}_2|) \phi_j(\underline{r}_2) d^3r_2 \qquad 3.8$$

$$K(\underline{r}_1, \underline{r}_2) = - \sum_{j=1}^{A} \phi_j^{\dagger}(\underline{r}_2) V(|\underline{r}_1 - \underline{r}_2|) \phi_j(\underline{r}_1) \qquad 3.9$$

then we have

$$(c\, \underline{\alpha}_i \cdot \underline{p}_i + \beta_i mc^2) \phi_i(\underline{r}_1) + U(\underline{r}_1) \phi_i(\underline{r}_1)$$

$$+ \int K(\underline{r}_1, \underline{r}_2) \phi_i(\underline{r}_2) d^3r_2 = E_i' \phi_i(\underline{r}) \qquad 3.10$$

If we think of a non-local potential as a local *state dependent* potential, then we can write

$$H_i^{(effective)}(\underline{r})\, \phi_i(\underline{r}) = E_i' \phi_i(\underline{r}) \qquad 3.11$$

with

$$H_i^{(effective)}(\underline{r}) = c\, \underline{\alpha}_i \cdot \underline{p}_i + \beta_i (mc^2 + U_S(\underline{r}) + \gamma_\mu U_V^\mu(\underline{r}))$$

$$+ \gamma_5 \gamma_\mu U^\mu(\underline{r}) + \gamma_\mu \gamma_\nu U_T^{\mu\nu}(\underline{r})) \qquad 3.12$$

Now to make the calculation simpler we consider a nucleus which has spin zero (doubly closed shells). This gives the

commutator

$$\left[H_i^{(effective)}(\underline{r}), \underline{J} \right] = \underline{0} \qquad \text{3.13}$$

and it is straightforward to show

$$U_s(\underline{r}) = U_s(r) \qquad \text{3.14}$$

$$U_v^{(o)}(\underline{r}) = U_v^{(o)}(r) \qquad \text{3.15}$$

$$\underline{U}_v(\underline{r}) = \underline{0} \qquad \text{3.16}$$

$$U_\rho(\underline{r}) = 0 \qquad \text{3.17}$$

$$U_A^\mu(\underline{r}) = 0 \qquad \text{3.18}$$

$$U_T^{ij}(\underline{r}) = 0 \qquad \text{3.19}$$

$$U_T^{oj}(\underline{r}) = \left(U_1(r) \right)_j \qquad \text{3.20}$$

$$\underline{U}_1(r) = \hat{r} \left(\hat{r} \cdot \underline{U}_1(r) \right) \qquad \text{3.21}$$

If, finally, the nucleus has zero isospin, one can eliminate the isovector potentials in a similar way. The radial potentials arise only from exchange terms which we can assume to be smaller than the direct terms and so we neglect them. This leaves us with two potentials: one arising from the sigma meson (scalar, attractive) and the other from the omega and phi mesons (vector 4th component,

repulsive), which we put into a Dirac equation.

3.2 Solving for the Bound State

3.2.1 Analytics

The resulting Dirac equation for the bound state looks very similar to that of the incoming proton distorted wave. In Chapter 4 we give a more detailed discussion of the latter. In this Chapter we basically start with the time independent Dirac Equation.

$$\left(-i\hbar c\,\underline{\alpha}\cdot\underline{\nabla} + \beta mc^2 + \beta V_s(r) + U_v(r) - E\right)\psi_B(\underline{r}) = 0$$

<div align="right">3.22</div>

In Chapter 4 we show that the solution to this for a state with quantum numbers L J M is written

$$\psi_B(\underline{r}) = \left\{ \begin{array}{c} f_B(r)\, \mathcal{Y}^M_{L_B \frac{1}{2} J_B}(\Omega) \\ g_B(r)\, \mathcal{Y}^M_{L'_B \frac{1}{2} J_B}(\Omega) \end{array} \right\}$$

<div align="right">3.23</div>

The equations satisfied by f and g are;

$$\left(U_v(r) + U_s(r) + E + mc^2 \right) f_B(r) = i\hbar c \left(g'_B(r) - g_B(r)\left(\frac{2\mu(J_B+1)-1}{r}\right)\right)$$

<div align="right">3.24</div>

$$\left(U_v(r) - U_s(r) + E - mc^2 \right) g_B(r) = i\hbar c \left(f'_B(r) + f_B(r)\left(\frac{2\mu(J_B+1)-1}{r}\right)\right)$$

<div align="right">3.25</div>

where

$$\mu = L_\beta - J_\beta$$

3.26

It should be noted that if f is purely real, g is purely imaginary. Complex arithmetic can be avoided by defining g' = ig.

Only the normalisation remains unspecified. We require that

$$\int \psi^+_\beta (\tau) \, \psi_\beta (\tau) \, d^3\tau = \int_0^\infty \left(|f_\beta (r)|^2 + |g_\beta (r)|^2 \right) r^2 \, dr = 1$$

3.27

As in the proton distorted wave we solve the differential equations by eliminating g, then transforming away the first derivative terms to get:

$$y''(\tau) + Ker(\tau) \, y(\tau) = 0$$

3.28

where

$$Ker(r) = A - \tfrac{1}{2} B' - \tfrac{1}{4} B^2$$

3.29

$$f_\beta (r) = y(r) \, e^{-\tfrac{1}{2} \int^r B(r') dr'}$$

3.30

$$B(r) = \frac{V_2'(\tau)}{V_2(\tau)} - \frac{2}{\tau}$$

3.31

$$A(r) = \frac{V_1(r)V_2(r)}{(\hbar c)^2} - \frac{(1 + 2\mu (J_\beta + 1))}{r^2} \left(\frac{r V_2'(r)}{V_2(\tau)} + 2\mu (J_\beta + 1) \right)$$

3.32

$$V_1(r) = U_v(r) + U_s(r) + E + mc^2 \qquad 3.33$$

$$V_2(r) = U_v(r) - U_s(r) + E - mc^2 \qquad 3.34$$

We integrate equations 3.28 using the Numerov method (see Appendix A) once we have set up "Ker" as an array of points.

A typical solution to 3.28 looks like Fig 3.1.
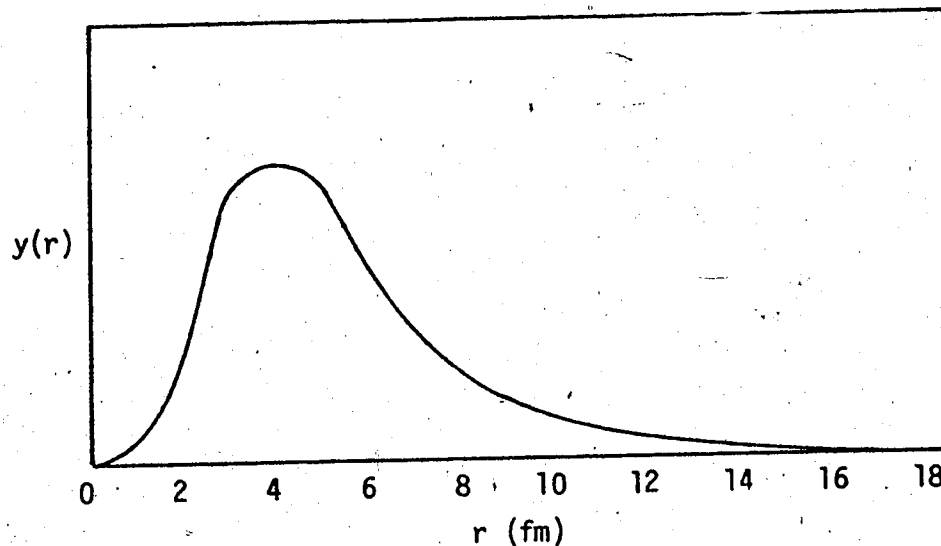
Figure 3.1 A typical bound state solution.

3.2.2 Numerics

Numerical integration of a curve is of course only an approximate method, and at each step errors may occur. For a second order differential equation these errors have the

effect of adding some of the 'other' (irregular) solution to the one we want. Suppose we were integrating outwards from B to C: at the first step then we have our required regular solution $y(r)$. At the second step we have $y(r) + \epsilon z(r)$, where z is the irregular solution and where ϵ may be very small. Then as we continue, $y(r)$ exponentially decays whilst $z(r)$ exponentially increases. Clearly no matter how small we make our step size (and therefore ϵ), the second term will eventually dominate leading to a curve as shown in Figure 3.2
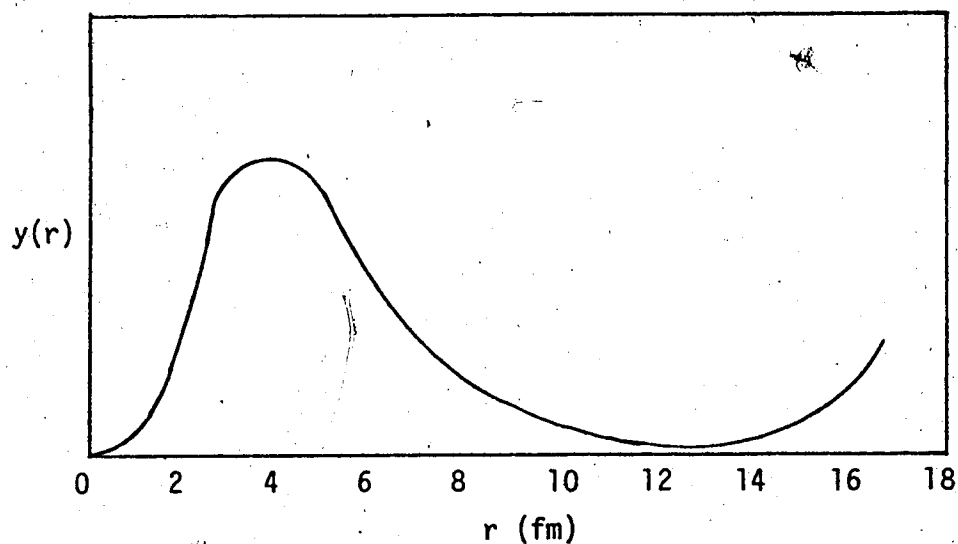
Figure 3.2 The numerical instability of integrating outwards.

This "instability" can be put to good use however, since if we integrate backwards from C to B then the errors

we introduce at each step are exponentially damped. If we start off at C with totally the wrong solution, our calculation will correct itself.

Using similar arguments for the range A to B, we see we must start at A and integrate outwards; the other solution, being irregular at the origin, damps out quickly. Thus for a given arbitrary potential we must estimate where the wave function peaks and integrate to that spot from both sides. If we miss by a little it is not too serious. The curve resulting from this procedure will typically look like the one shown in figure 3.3[1].
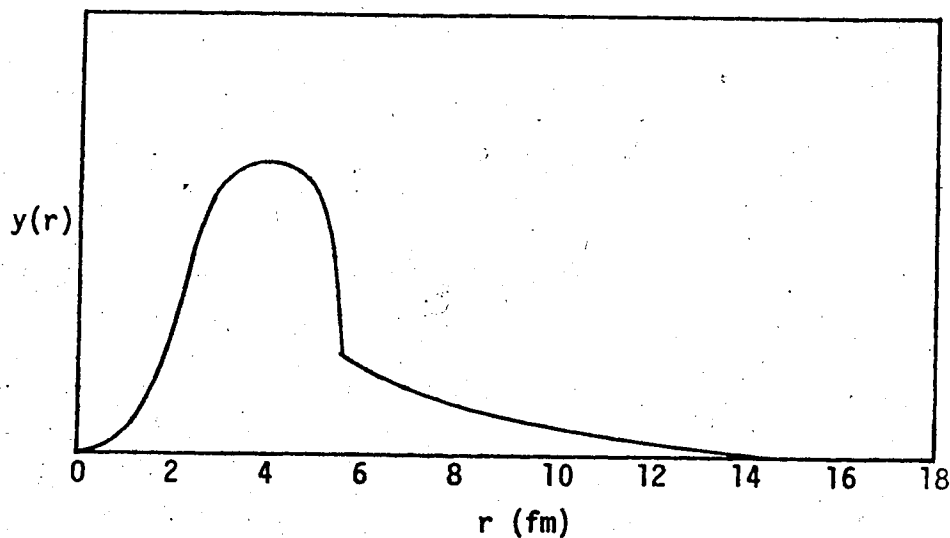
Figure 3.3 The binding potential being too strong causes a derivative mismatch.

_____

[1](after suitably normalising one side so that they meet)

At the matching point the (log) derivatives do not match. This is a symptom of having the wrong potential strength; in Fig 3.3 the potential is too strong. If we call the difference in (log) derivatives at B, θ, then the problem is summarised as finding a potential strength V such that θ(V) = 0. We therefore have to solve a non-linear equation in one variable.

3.3 Determining the potentials

The vague term "potential strength" must now be explained. We parameterise the vector and scalar potentials as,

$$U_v(r) = \frac{V_v}{1 + e^{\frac{r - R_v}{a_v}}} \qquad U_s = \frac{V_s}{1 + e^{\frac{r - R_s}{a_s}}} \qquad 3.35$$

For light nuclei, relativistic Hartree Fock calculations (JA80) show a dip in the potential near the origin; we thus expect to have a parabolic term in the numerator. However, we ignore such a possibility here in an attempt to limit the number of parameters.

The geometry parameters in these potentials can be taken to be the same as those obtained from fitting the proton nucleus elastic scattering data. Typical values are a ~ 0.65 fm and r ~ 1 fm.

To get the potential strengths we can do one of two things:

1. The mean field theory of nuclear matter (WA74) indicates the volume integrals are in the ratio $Jv/Js = -.81$ and so fixing Vs by this we vary Vv to fit the binding energy. Moreover Arnold et al.'s (AR79) phenomenological analysis of proton-nucleon elastic scattering gives Jv/Js as a function of energy which extrapolates to -0.81 at zero energy.

2. Following the analogy with the scattering states, one knows that Uv-Us is in some way proportional to the spin orbit potential, and so if the associated spin orbit split state is known to be bound we can vary Vv and Vs independently to fit both states.

For the (p,π^+) calculations we will require the single particle wavefunctions of ^{41}Ca and ^{13}C. Since for both of these nuclei the spin-orbit split state is not well defined in energy we adopt the first criterion.

Of interest in DWBA calculations (see Chapter 6) are the bound state wavefunctions in momentum space. Figures 3.4 and 3.5 show the momentum space single particle wavefunctions for the 1f7/2 state in ^{41}Ca for two different geometries. The geometry we shall be using for the (p,n^+) calculations is the one in which $a = 0.65$ fm. In Chapter 8 we show the effect of using $a = 0.5$ fm.

The feature which is immediately apparent is that for momentum transfers typical of the (p,π^+) reaction (shown in the figures by the arrowed lines for 160 meV incident protons) it is no longer correct to think of the lower
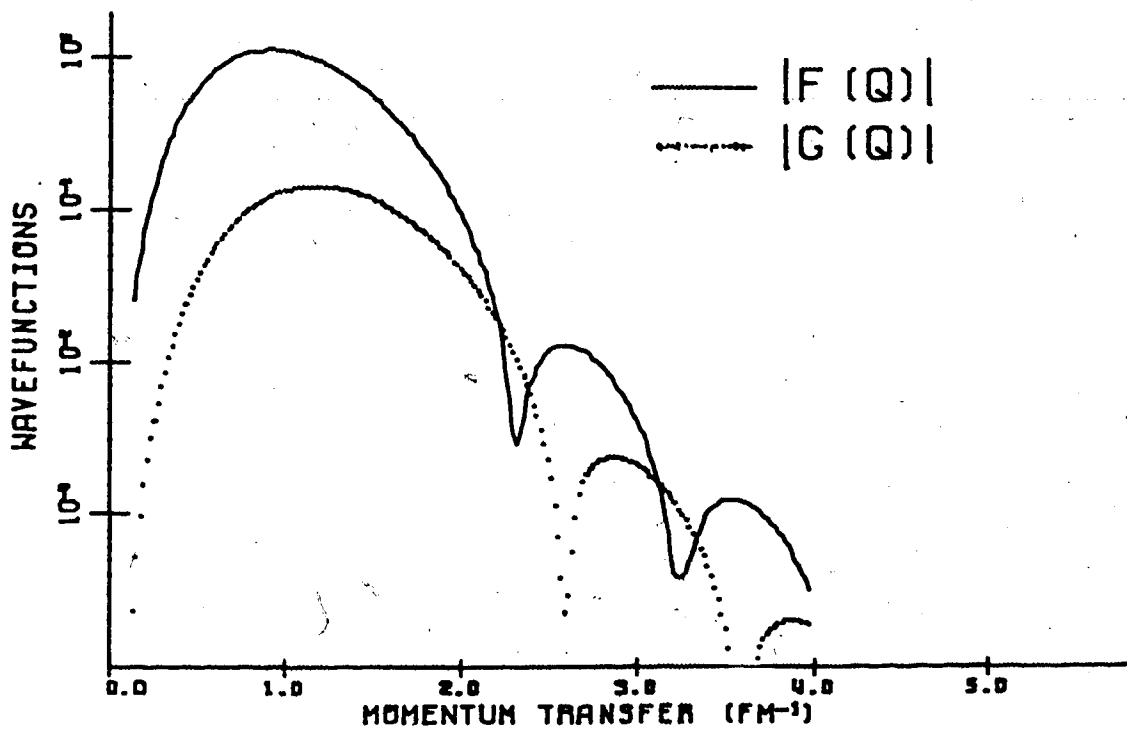
Figure 3.4 The 1f7/2 bound state wavefunctions in momentum space for ^{41}Ca with r=1.0 fm and a=0.65 fm.
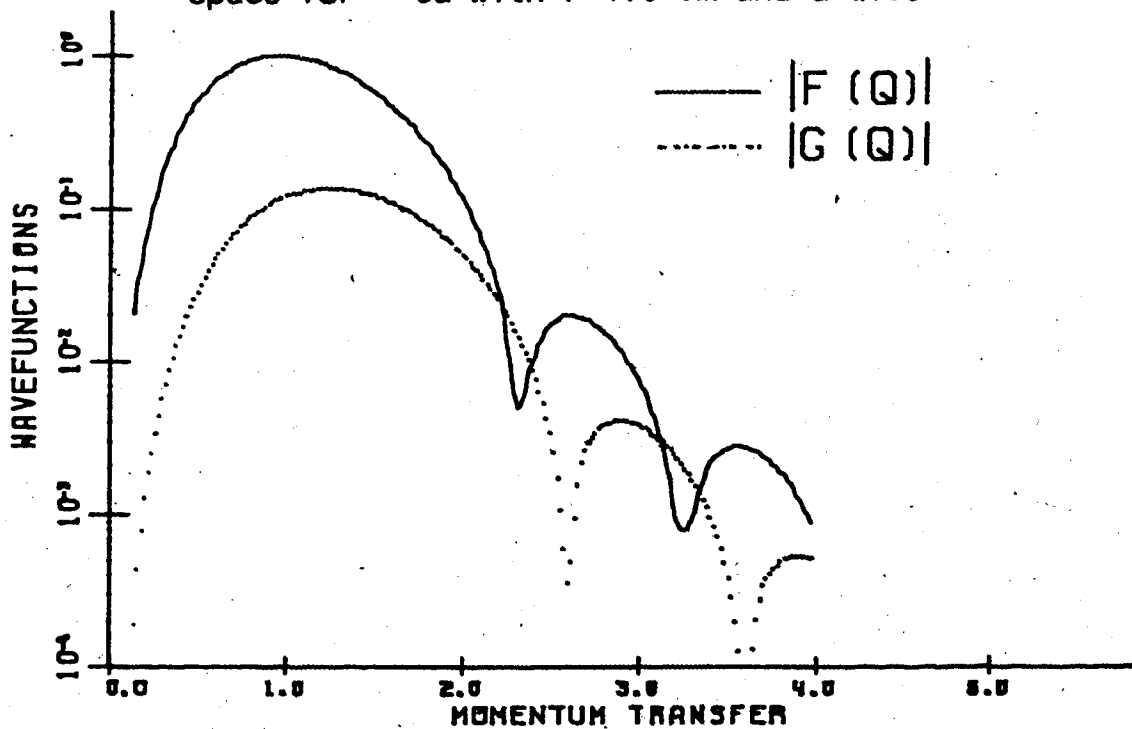
Figure 3.5 The 1f7/2 bound state wavefunctions in momentum space for ^{41}Ca with r=1.0 fm and a=0.5 fm.
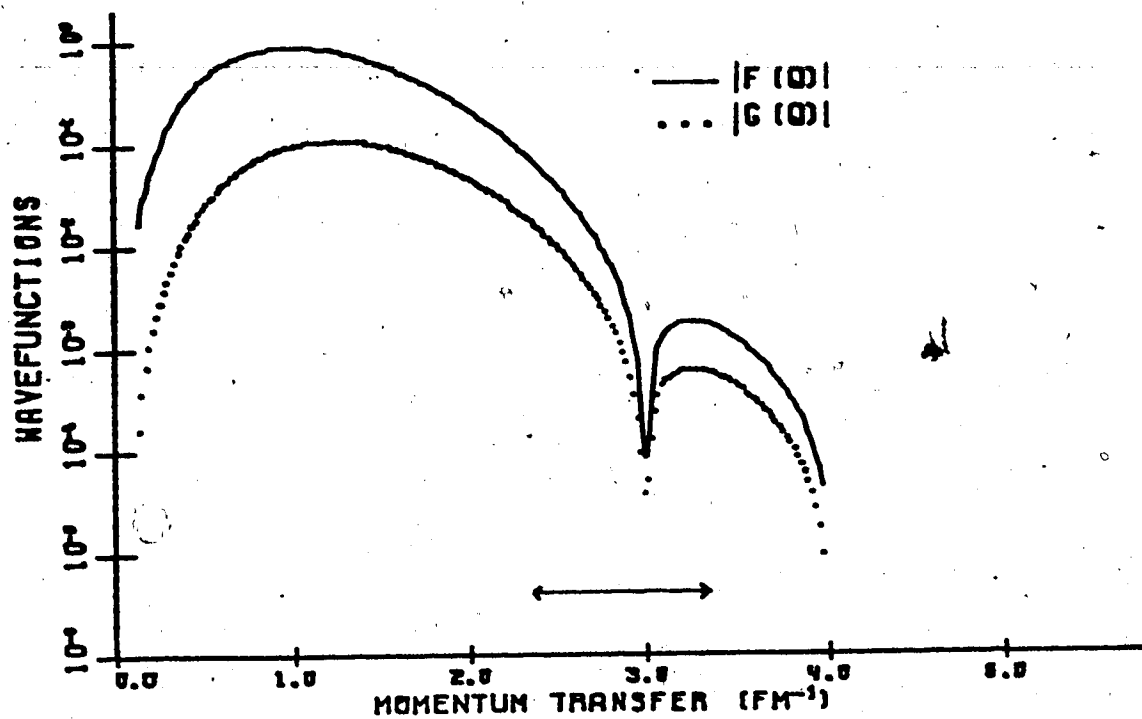
Figure 3.6 The bound state wavefunctions in momentum space for ^{41}Ca with r=1.0 fm and a=0.65 fm generated from a pure vector potential.
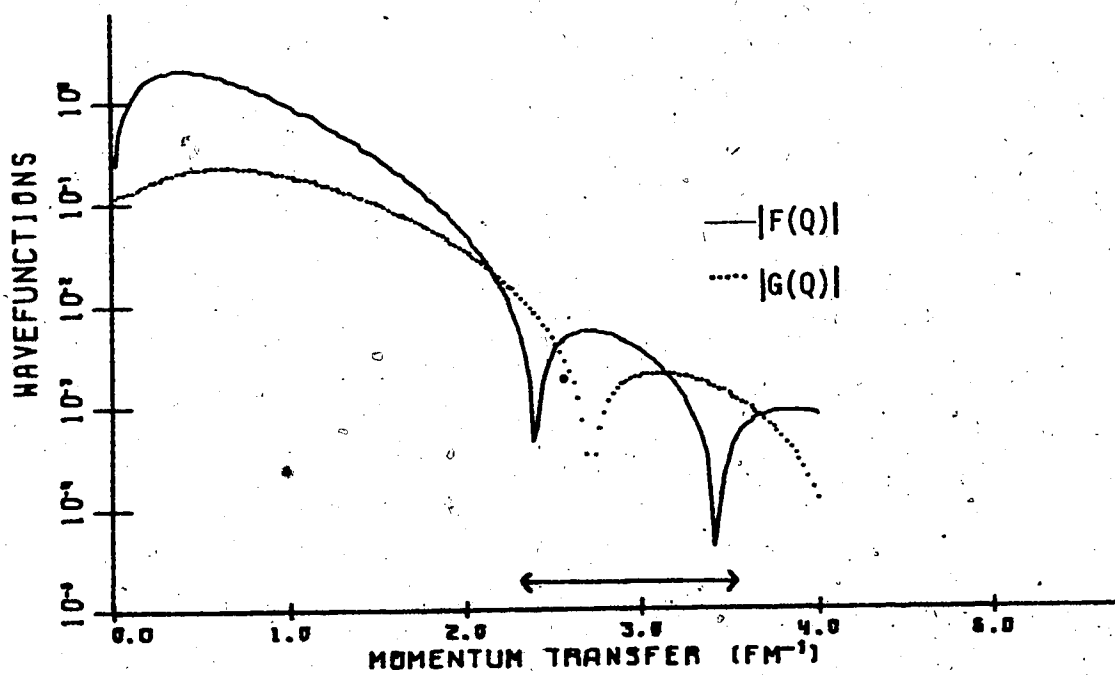
Figure 3.7 The 1p1/2 bound state wavefunctions in momentum space for ^{13}C, r=1.0 fm and a=0.4 fm.

component (g) as the *small* component. This is a feature of using the strong oppositely signed scalar and vector potentials.

If we use the Schrödinger equation to get a bound state with the correct binding energy, then we need a potential of about 50 MeV. In the hydrogen atom the Coulomb potential is put into the Dirac equation as the 4th component of a four-vector; this yields the correct hyperfine splitting (spin-orbit force). By analogy we can put the 50 MeV Schrödinger potential into the Dirac equation in the same way, thus generating a bound state. The results of doing this are shown in figure 3.6. It turns out that we do not have to adjust the strength more than a few MeV to get the correct binding energy. The resulting spin-orbit strength is about ten times smaller than that observed from nuclear spectroscopy; since the Dirac equation has no explicit way of 'putting in' an extra spin orbit potential, we can expect this simple approach to fail. The most striking feature shown in figure 3.6 is that the f and g have their zero's at the same value of momentum transfer and so we always have f >> g. The 'large g' is then a consequence not so much of using the Dirac equation but of using the strong oppositely signed potentials.

Lastly, figure 3.7 shows the momentum space wave-functions for the 1p1/2 (ground) state in ^{13}C. The feature of g being large at high momentum transfers is still apparent.

4. THE PROTON NUCLEUS INTERACTION

The second ingredient that enters into the calculation of
the (p,π^+) amplitude is the distorted wave describing the
motion of the incoming proton. To obtain this we need to
solve the time-independent Dirac equation in the presence of
the two potentials: scalar and vector. The arguments for
using these potentials are the same as for the bound state;
we must however account for the inelastic channels. This is
done in the same way as in the conventional optical model by
giving the potentials imaginary parts. There is no simple
way of knowing the order of magnitude of these imaginary
potentials; however, we expect them to be absorptive and
thus negative. The potential parameters are ultimately tied
down by fitting the elastic scattering data as decribed in
Chapter 7; the success with which the data can be fitted
justifies the assumptions a postiori (AR79). In this section
there is necessarily a lot of algebra. Not all the steps are
included however; the interested reader may find some of the
missing details in the thesis of Mercer (ME72). We assume,
initially, that there is no Coulomb interaction present; we
later show how it can be incorporated into the formalism.

4.1 Separating the Dirac Equation

The Dirac equation is:

39

$$(-i\hbar c\,\underline{\alpha}\cdot\underline{\nabla} + \beta mc^2 + \beta U_s(r) + U_v(r) - E)\,\psi(\underline{r},t) = 0$$

<div align="right">4.1</div>

$$\underline{\alpha} = \begin{pmatrix} 0 & \underline{\sigma} \\ \underline{\sigma} & 0 \end{pmatrix} \qquad \beta = \begin{pmatrix} I & 0 \\ 0 & -I \end{pmatrix}$$

<div align="right">4.2</div>

where $\psi(r)$ is a 4-vector (actually a 4-spinor), α and are the 4 by 4 Dirac matrices and I is the 2 by 2 unit matrix.

The upper two components of ψ may be expanded in a complete set. In analogy with the spin 1/2 non-relativistic case we write (RO57)

$$\psi_i^{m_s}(\underline{r},t) = \frac{e^{-iEt}}{\pi}\sqrt{\frac{E+mc^2}{2mc^2}}\sum_{\substack{LJM \\ m_L}} i^L Y_L^{m_L*}(\hat{k}_i)(L\,\tfrac{1}{2}\,m_L\,m_s|JM)\left\{ f_{LJ}(r)\,Y_{L\,\frac{1}{2}\,J}^M(\Omega) \right\}$$

<div align="right">4.3</div>

We wish to find two lower components (to fit into the curly bracket in 4.3), which yield a solution to the Dirac equation for each LJM partial wave. To do this we define

$$\phi_i(\underline{r}) = f_{LJ}(r)\,Y_{L\,\frac{1}{2}\,J}^M(\Omega)$$

<div align="right">4.4</div>

and use the Dirac Equation

$$\left[-i\hbar c \begin{pmatrix} 0 & \underline{\sigma} \cdot \underline{\nabla} \\ \underline{\sigma} \cdot \underline{\nabla} & 0 \end{pmatrix} + \begin{pmatrix} mc^2 + U_s(r) & 0 \\ 0 & -mc^2 - U_s(r) \end{pmatrix} + \begin{pmatrix} U_v(r) - E & 0 \\ 0 & U_v(r) - E \end{pmatrix} \right] \begin{bmatrix} \phi_1(r) \\ \phi_2(r) \end{bmatrix} = \begin{bmatrix} 0 \\ 0 \end{bmatrix}$$

$$4.5$$

which gives, for the two component equations

$$-i\hbar c \, \underline{\sigma} \cdot \underline{\nabla} \, \phi_2(\underline{r}) + \left(mc^2 + U_s(r) + U_v(r) - E \right) \phi_1(\underline{r}) = 0$$

$$4.6$$

$$-i\hbar c \, \underline{\sigma} \cdot \underline{\nabla} \, \phi_1(r) + \left(U_v(r) - mc^2 - E - U_s(r) \right) \phi_2(\underline{r}) = 0$$

$$4.7$$

Equation 4.7 gives us the lower component as required

$$\phi_2(\underline{r}) = \frac{-i\hbar c \, \underline{\sigma} \cdot \underline{\nabla} \, \phi_1(r)}{U_v(r) - E - mc^2 - U_s(r)}$$

$$4.8$$

We need to evaluate the expression

$$\underline{\sigma} \cdot \underline{\nabla} \, \phi_1(\underline{r}) = \underline{\sigma} \cdot \underline{\nabla} \, f_{\ell j}(r) \, y^M_{\ell \frac{1}{2} J}(\underline{\Omega})$$

$$4.9$$

We can use the identity

$$\underline{\sigma} \cdot \underline{\nabla} = \underline{\sigma} \cdot \hat{r} \left(\frac{\partial}{\partial r} - \frac{\underline{\sigma} \cdot \underline{L}}{r} \right)$$

$$4.10$$

which gives us

$$\underline{\sigma} \cdot \nabla \, \phi_1(\underline{r}) = f_{LJ}'(r) \, \underline{\sigma} \cdot \hat{\underline{r}} \, \mathcal{Y}_{L^{1/2}J}^{M}(\Omega) - \frac{f_{LJ}(r)}{r} \, (\underline{\sigma} \cdot \hat{\underline{r}})(\underline{\sigma} \cdot \underline{L}) \, \mathcal{Y}_{L^{1/2}J}^{M}(\Omega)$$

4.11

using

$$\underline{\sigma} \cdot \underline{L} = 2 \underline{S} \cdot \underline{L} = J^2 - L^2 - S^2$$

4.12

which, since the generalised spherical harmonic is an eigenfunction of all the operators in 4.12 gives us

$$\underline{\sigma} \cdot \underline{L} \, \mathcal{Y}_{L^{1/2}J}^{M}(\Omega) = \left(J(J+1) - L(L+1) - 3/4 \right) \mathcal{Y}_{L^{1/2}J}^{M}(\Omega)$$

4.13

$$\Rightarrow \underline{\sigma} \cdot \nabla \, \phi_1(\underline{r}) = \left\{ f_{LJ}'(r) - \frac{f_{LJ}(r)}{r} \left(J(J+1) - L(L+1) - 3/4 \right) \right\} \underline{\sigma} \cdot \hat{\underline{r}} \, \mathcal{Y}_{L^{1/2}J}^{M}(\Omega)$$

4.14

This expression can be simplified if we notice that

$$J(J+1) - L(L+1) - 3/4 = - \left(1 + (L-J)(2J+1) \right)$$

4.15

and introduce a useful quantity when dealing with the Dirac Equation.

$$K \equiv (L - J)(2J + 1)$$

4.16

Finally we use equation 9.12b of Rose (RO57)

$$\sigma \cdot \hat{\underline{r}} \; \mathcal{Y}^{M}_{L\,\frac{1}{2}\,J}(\Omega) \;=\; -\; \mathcal{Y}^{M}_{L'\,\frac{1}{2}\,J}(\Omega) \qquad , \quad L' = 2J - L \tag{4.17}$$

Therefore

$$\sigma \cdot \nabla \, f_{LJ}(r)\, \mathcal{Y}^{M}_{L\,\frac{1}{2}\,J}(\Omega) \;=\; -\left(\frac{\partial}{\partial r} + \frac{1+K}{r}\right) f_{LJ}(r)\, \mathcal{Y}^{M}_{L'\,\frac{1}{2}\,J}(\Omega) \tag{4.18}$$

The full 4 component wave function can now be written as

$$\psi(r,t) = \frac{e^{iEt}}{\pi}\sqrt{\frac{E + mc^2}{2mc^2}} \sum_{\substack{LJM \\ m_L}} i^{L}\, \mathcal{Y}^{*\,m_L}_{L}(\hat{R}_i)\,(L\,\tfrac{1}{2}\,m_L\,m_s\,|\,JM)$$

$$\times \begin{bmatrix} f_{LJ}(r)\, \mathcal{Y}^{M}_{L\,\frac{1}{2}\,J}(\Omega) \\[2mm] g_{LJ}(r)\, \mathcal{Y}^{M}_{L'\,\frac{1}{2}\,J}(\Omega) \end{bmatrix} \tag{4.19}$$

where the lower component is give in terms of the upper one by

$$g_{LJ}(r) = \frac{i\hbar c}{E + mc^2 + U_s(r) - U_v(r)}\left(\frac{\partial}{\partial r} + \frac{1+K}{r}\right) f_{LJ}(r) \tag{4.20}$$

Proceeding form 4.7 in a manner completely analogous to that where 4.20 is derived from 4.6, the second differential equation is

$$f(r) = \frac{i\hbar c}{E - U_v(r) - U_s(r) + mc^2} \left(\frac{\partial}{\partial r} + \frac{1-K}{r} \right) g_{LJ}(r)$$

4.21

4.2 Setting up the Radial Equation

It now remains to solve the coupled differential equations 4.20 and 4.21 subject to the boundary conditions of an elastic scattering state. In order to do this eq 4.20 is substituted into 4.21, thereby eliminating the lower component. A few new symbols can be introduced for convenience of notation.

$$f(r) = r f_{LJ}(r)$$

4.22

$$g(r) = r g_{LJ}(r)$$

4.23

$$d(r) = \frac{-i}{\hbar c} \left(U_v(r) - E - U_s(r) - mc^2 \right)$$

4.24

$$s(r) = \frac{-i}{\hbar c} \left(U_v(r) - E + U_s(r) + mc^2 \right)$$

4.25

Our differential eqn for f(r) can be written as

$$f''(r) - \frac{\mathcal{l}'(r)}{\mathcal{l}(r)} f'(r) - \left[\mathcal{l}(r)s(r) + \frac{K\mathcal{l}'(r)}{r \cdot \mathcal{l}(r)} + \frac{K(K+1)}{r^2} \right] f(r) = 0$$

4.26

As in the bound state calculation, the first derivative term can easily be transformed away by defining

$$y(r) = f(r)\left[\mathcal{l}(r) \right]^{1/2}$$

4.27

which gives us the following result

$$y''(r) + \left[ker(r) - \frac{K\mathcal{l}'(r)}{r \, \mathcal{l}(r)} - \frac{K(K+1)}{r^2} \right] y(r) = 0$$

4.28

where the function ker has been introduced.

$$ker(r) = \frac{\mathcal{l}''(r)}{2\mathcal{l}(r)} - \frac{3}{4}\left| \frac{\mathcal{l}'(r)}{\mathcal{l}(r)} \right|^2 - \mathcal{l}(r)s(r)$$

4.29

4.3 Comparison to the Non-Relativistic Case

The structure of equation 4.28 is rather enlightening when compared to the corresponding non-relativistic equation. The non-relativistic equation for spin-1/2 scattering is

$$y''(r) + \left(k^2 - \frac{2m}{\hbar^2} U(r) + \frac{m}{\hbar^2} (1+K) U_{s.o.}(r) - \frac{L(L+1)}{r^2} \right) y(r) = 0$$

4.30

We can clearly identify the term in the Dirac Equation which corresponds to the Spin Orbit potential as the one proportional to K.

$$V_{s.o.}(r) = -\frac{\hbar^2}{mr} \frac{d'(r)}{d(r)}$$

4.31

Assuming for the moment that

$$E + mc^2 \gg |Us(r) - Uv(r)| \text{ and } E \sim mc^2$$

we can obtain the rather nice result that

$$U_{s.o.}(r) = -\frac{\hbar^2}{mr} \frac{U_v'(r) - U_s'(r)}{U_v(r) - U_s(r) - E - mc^2}$$

4.32

$$\approx \frac{\hbar^2 c^2}{2m^2 c^4} \frac{1}{r} \frac{d}{dr} \left[U_v(r) - U_s(r) \right]$$

4.33

It should be noted how the 'Thomas' form of the spin orbit force appears naturally from the formalism. Not only the spin orbit force, but also the equivalent non-relativistic central one can be obtained from a comparison of equations 4.28 and 4.30.

$$\hbar^2 - \frac{2m}{\hbar^2} U(r) \equiv k_{eff}(r) + \frac{1}{r} \frac{d'(r)}{d(r)}$$

$$\Rightarrow U(r) \simeq \frac{1}{2mc^2} \left[\left(U_s(r) + mc^2 \right)^2 - \left(U_v(r) - E \right)^2 \right] + \frac{p^2 c^2}{2mc^2}$$

4.34

So if we have

$$2mc^2 \gg U_v(r) , U_s(r)$$

then

$$U(r) \approx U_s(r) + U_v(r) \qquad 4.35$$

Thus, loosely, we can say that the central potential depends on the *sum* of the potentials and that the spin-orbit potential depends on the *difference* . It should be emphasized that this is not a very good approximation at intermediate energies, only a rule of thumb. If we use this simple approximation for the class A fits shown in Table 7.1, then we get the wrong sign for the imaginary potential. If, however, we use the more exact expression for the non-relativistic correspondence, we obtain the correct sign.

4.4 The Born Approximation

We can learn something of the relationship between potentials and observables from the closed analytic forms obtainable from the Born Approximation.

We assume there are no Coulomb terms present in the

potentials. After the usual process of obtaining a Green function to turn the differential equation into an integral equation, we get for the differential cross-section

$$\frac{d\sigma}{d\Omega} = (E + mc^2)^2 |A(\mathbf{q})|^2 + p^2 c^2 \frac{E - mc^2}{E + mc^2} |B(\mathbf{q})|^2$$

$$+ 2 p^2 c^2 Re \left(A^*(\mathbf{q}) B(\mathbf{q}) \right)$$

$$\hspace{10cm} 4.36$$

where

$$A(\mathbf{q}) = \frac{1}{4\pi (\hbar c)^2} \int e^{i\mathbf{q}\cdot\mathbf{r}} (U_v(r) + U_s(r)) \, d^3r \hspace{2cm} 4.37$$

$$B(\mathbf{q}) = \frac{1}{4\pi (\hbar c)^2} \int e^{i\mathbf{q}\cdot\mathbf{r}} (U_v(r) - U_s(r)) \, d^3r$$

$$\hspace{10cm} 4.38$$

For the analysing power we get

$$A = 2 p^2 c^2 \sin\theta \, Im \left(A^*(\mathbf{q}) B(\mathbf{q}) \right) \Big/ \frac{d\sigma}{d\Omega} \hspace{2cm} 4.39$$

We can make the following observations:

1. In the non-relativistic limit

$$\frac{d\sigma}{d\Omega} = 4 m^2 c^2 |A(\mathbf{q})| \hspace{5cm} 4.40$$

We thus have Uv + Us as our effective central potential.

2. Also the analysing power vanishes:

   a. If Uv=Us showing a difference in potentials is necessary.

   b. In the formal limit of c tending to infinity, thus showing that the analysing power is a relativistic

effect.

c. If Uv = 0 or Us = 0 , so both potentials are necessary.

d. If both potentials are *real*, so absorption is necessary.

4.5 Obtaining Phase Shi̶̶̶ervables

We numerically̶̶̶28, by a marching method described in appendix A. Up to a pre-determined matching radius Rmax, chosen so that the potentials have become vanishing small.

At this point (Rmax), we know y and y' and so we can calculate f and f' from equations 4.27. To extract the correct normalisation for the f(r) and also the phase-shift for use in elastic scattering, it is necessary to match to the solutions to the Dirac equation with no potentials present. With the conventions of Bjorken and Drell (BJ64) such a solution looks like

$$\psi_o^{m_s}(r,t) \longrightarrow \frac{e^{i(kz-Et)}}{(2\pi)^{\frac{3}{2}}} \sqrt{\frac{E+mc^2}{2mc^2}} \begin{pmatrix} 1 \\ \dfrac{\sigma \cdot p\, c}{E+mc^2} \end{pmatrix} \chi(m_s)$$

4.41

where $\chi(m_s)$ is the usual Pauli 2-Spinor. We write

$$N_K f(r) = e^{i\delta_K}(\cos\delta_K f^R_{pw}(r) + \sin\delta_K f^I_{pw}(r))$$

4.42

$$N_K f'(r) = e^{i\delta_K}(\cos\delta_K f'^R_{pw}(r) + \sin\delta_K f'^I_{pw}(r))$$

4.43

where the superscripts R and I refer to, respectively, the regular and irregular behaviour of the solution at the origin.

From the above two simultaneous equations we can extract both the phase shift δ_K and the normalisation N_K. We choose the normalisation by requiring the following boundary condition

$$\psi^{m_s}(\underline{r},t) \longrightarrow e^{i(kz-Et)} \sqrt{\frac{E+mc^2}{2mc^2}} \begin{pmatrix} 1 \\ \frac{\underline{\sigma}\cdot\underline{p}c}{E+mc^2} \end{pmatrix} \chi(m_s) + \frac{e^{ikr}}{r} \sum_{m_s'} \begin{pmatrix} f^{m_s m_s'}_1(\Omega) \\ f^{m_s m_s'}_2(\Omega) \\ f^{m_s m_s'}_3(\Omega) \\ f^{m_s m_s'}_4(\Omega) \end{pmatrix}$$

4.44

If we are interested only in elastic scattering, then all the relevant physics is contained in the phase-shifts. This means we only ever need f and f' just at Rmax, rather than every point; this can lead to a major saving in calculations (about a factor of 4). Whilst from eqn 4.44 it would appear that there are 4 amplitudes to be evaluated, it turns out that the lower two are expressible in terms of the upper two and that all observables can be conveniently expressed in terms of multiples of the upper two amplitudes, namely

$$F_1 = \sum_{L=0}^{\infty} \left((L+1) \eta_L^{(+)} + L \eta_L^{(-)} \right) P_L(\cos\theta)$$

4.45

$$F_2 = \sum_{L=1}^{\infty} \left(\eta_L^{(-)} - \eta_L^{(+)} \right) P_L'(\cos\theta)$$

4.46

where

$$\eta^{(\pm)} = \frac{e^{2i\delta_{L, J = L \pm \frac{1}{2}}} - 1}{2ik}$$

4.47

We can now write the cross-section as

$$\frac{d\sigma}{d\Omega} = |F_1|^2 + |F_2|^2$$

4.48

and the analysing power as

$$A = \frac{2 \operatorname{Im} F_1^* F_2}{|F_1|^2 + |F_2|^2}$$

4.49

Also, for completeness we include another independent quantity (GL78),

$$Q = \frac{2 \operatorname{Re} F_1 F_2^*}{|F_1|^2 + |F_2|^2}$$

4.50

Clearly, we have skipped many lines in turning the phase-shifts into observables. The missing steps, however, are more or less identical with those of the corresponding non-relativistic theory which is very well documented in the

text books on elementary scattering theory, as for example,
in (RO67). In the next Chapter we discuss the results of
fitting the elastic data and present there the parameters of
the potentials.

4.6 The Coulomb Interaction

4.6.1 The Meaning of the Phase Shift

So far nothing has been said about the delicate
question of the Coulomb interaction. We can be guided by
analogy with the non-relativistic case (ME58). Messiah shows
that for the case of pure Coulomb, the scattering solution
to the Schrödinger equation has the property

$$\psi(r) \longrightarrow \frac{e^{i(kz - \gamma/k \, k(r-z))}}{(2\pi)^2} + \frac{f_c(\theta)}{(2\pi)^2} \frac{e^{i(kr - \gamma/k \, 2kr)}}{r}$$

$$4.51$$

where $f_c(\theta)$ is the standard Coulomb amplitude given by

$$f_c(\theta) = \frac{\gamma e^{i(2\sigma_0 - \gamma/k \sin^2 \theta/2)}}{2k \sin^2 \theta/2}$$

$$4.52$$

Comparing 4.51 with 4.44, we see that since the Coulomb
parameter (γ) is non-zero we have a fundamental difference
in boundary conditions between the two equations.
Nevertheless, if we think in terms of *flux* then the
logarithmic term in the argument produces no observable
effect. To see this one must consider the flux operator

$$J = \frac{\hbar}{m} \, Im \left(\psi^*(r) \nabla \, \psi(r) \right)$$

4.53

Putting

$$\psi(r) = e^{i(kz - \gamma \ln k(r-z))}$$

4.54

we get

$$J = \frac{\hbar k}{m} \hat{z} - \frac{\hbar \gamma}{m} \frac{\hat{r} - \hat{z}}{(r-z)}$$

4.55

and putting

$$\psi(r) = \frac{e^{i(kr - \gamma \ln 2kr)}}{r}$$

4.56

we get (ignoring a $1/r^3$ term)

$$J = \frac{\hbar}{m t^2 r^2} \left(k - \frac{\gamma}{r} \right) \hat{r}$$

4.57

Since the pieces which depend on the Coulomb parameter vanish at infinity we can still interpret the individual pieces as an incoming flux along the z-direction and an outgoing radial flux.

Instead of using plane waves in equations 4.42 and 4.43, we now can define Coulomb waves which are the solutions to the Dirac equation with a 1/r term as the time-like component of a 4-vector potential.

If we expand the Coulomb wavefunctions in terms of the generalised spherical harmonics, then the *radial* components of the wavefunctions corresponding to the solution which has

the asymptotic form 4.51 themselves have the asymptotic forms

$$f_c^R(r) \longrightarrow \frac{1}{k}\sqrt{\frac{E+mc^2}{\pi mc^2}}\cos\left(kr - \gamma \ln 2kr - \frac{\ell\pi}{2} + \Sigma_K\right)$$

4.58

$$f_c^I(r) \longrightarrow \frac{-1}{k}\sqrt{\frac{E+mc^2}{\pi mc^2}}\sin\left(kr - \gamma \ln 2kr - \frac{\ell\pi}{2} + \Sigma_K\right)$$

4.59

Here Σ_K is the relativistic Coulomb phase-shift discussed in Appendix B.

We introduce the phase-shifts in exactly the same way as for the plane wave case: that is to say in the presence of a (short range) additional potential, the regular solution asymptotically goes like

$$f_{cN}^R(r) \longrightarrow \frac{1}{k}\sqrt{\frac{E+mc^2}{\pi mc^2}}\cos\left(kr - \gamma \ln kr - \frac{\ell\pi}{2} + \Sigma_K + \delta_K\right)$$

4.60

We can extract from this, again in analogy with the non-relativistic case, the *total* phase shift for the scattering as

$$\Delta_K = \Sigma_K + \delta_K$$

4.61

This Δ_K is the quantity we insert into equation 4.47.

4.6.2 Summing the Partial Wave Series

Now we have one more problem, namely

$$\lim_{|K| \to \infty} \delta_K = 0 \qquad but \lim_{|K| \to \infty} \langle \Delta_K = \Sigma_K + \delta_K \rangle \neq 0$$

$$4.62$$

The sums in eqns 4.45 do not in fact converge.[1]

In order to get around this problem, we will have to understand the nature of the function to which we would like the sum to converge. The non-relativistic case suffers from the same malady, although in this case we do know the analytic solution for a point charge to be

$$f_c(\theta) = \frac{-\gamma e^{i(2\sigma_0 + \gamma \ln(1-x)/2)}}{k(1-x)}, \qquad x = \cos\theta$$

$$4.63$$

In figure 4.1 we show, qualitatively, the real part of the Coulomb amplitude (equation 4.63) plotted against the centre of mass scattering angle (θ). There is a singularity in both amplitude and phase; clearly there is *no way* the Legendre polynomial expansion can converge in the normal sense. We can, however, use a transformation (YE54) to hide the singularity. If

---

[1] In practice we may argue that the electron clouds shield the charge and so at values of $\ell \sim 10^4$ the terms go rapidly to zero. The problem may be interpreted as *speeding up* the convergence of the series rather than *making* the convergence.
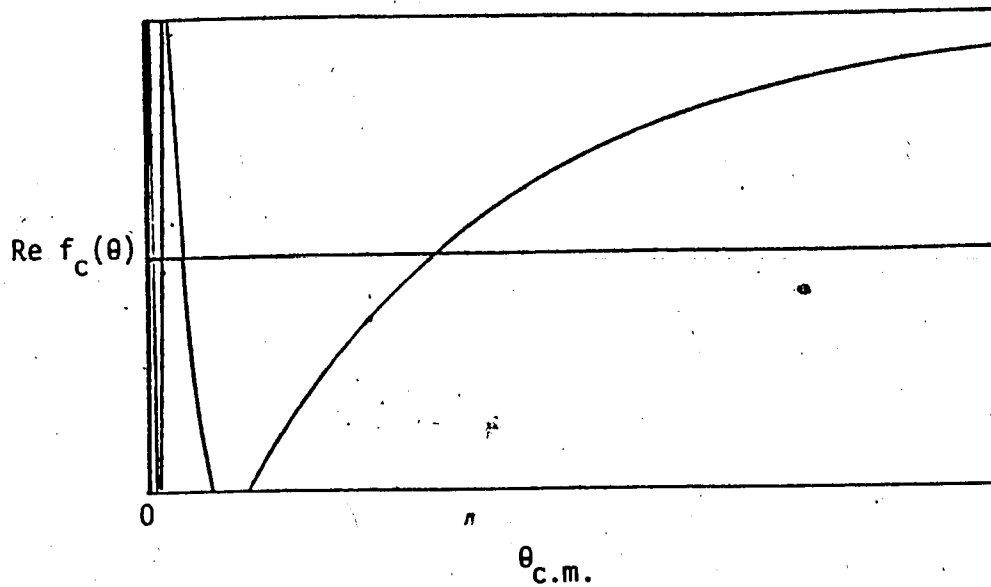
Figure 4.1 The non-relativistic point coulomb amplitude.

$$f_c^{(o)}(x) = \sum_{l=o}^{\infty} a_l^{(o)} P_l(x)$$

4.64

then we can multiply by $(1 - x)$ to get

$$f_c^{(r)}(x) = (1-x) f_c^{(o)}(x) = \sum_{l=o}^{\infty} a_l^{(l)} P_l(x)$$

4.65

where the a_l's are related by

$$a_l^{(l)} = a_l^{(o)} - \frac{l+1}{2l+3} a_{l+1}^{(o)} - \frac{l}{2l-1} a_{l-1}^{(o)}$$

4.66

The function to which we want this series to converge is shown in figure 4.2 We have eliminated the amplitude
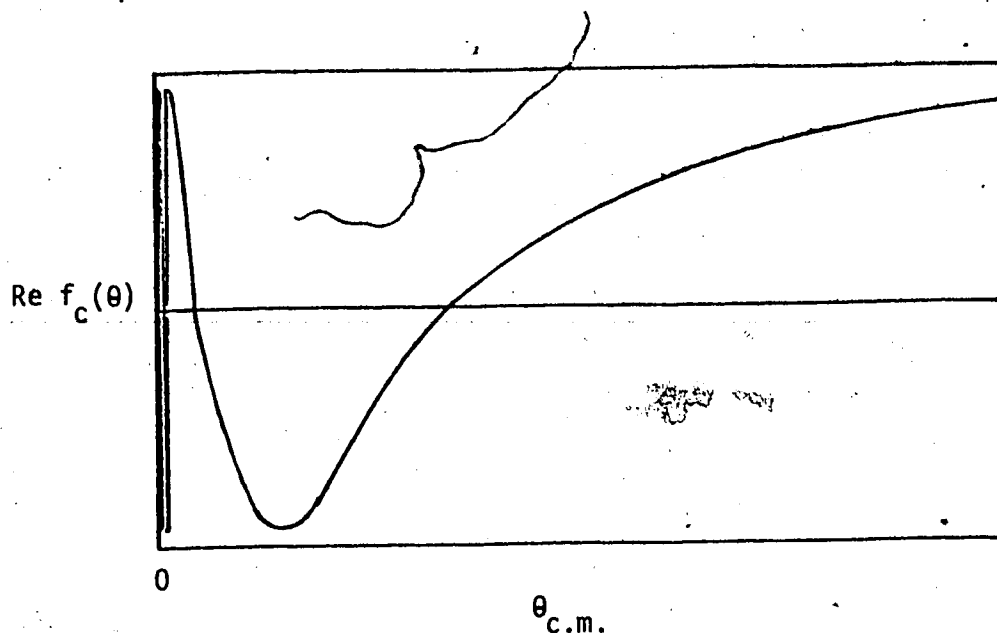
Figure 4.2 The removal of the amplitude singularity.

singularity but the phase singularity remains. Mercer (ME72)

suggests an elegant way of doing a transformation similar to

this one to remove both amplitude and phase singularities.

However, in the experience of this author, the series he

finally obtains still diverges. We can 'hide' the

singularity by repeating the transformation of series

(eqn 4.66) to get

$$f_c^{(3)}(x) = (1 - x)^3 f_c^{(0)}(x) = \sum_{l=0}^{\infty} a_l^{(3)} P_l(x)$$

4.67

Then we have a situation as in figure 4.3

The phase singularity is now under the parabolic

envelope and so the Legendre polynomial expansion of this

function can be expected now to converge uniformly. In fact

the higher the power of (1 - x) we multiply by, the more hidden the singularity is and the faster the series converges.
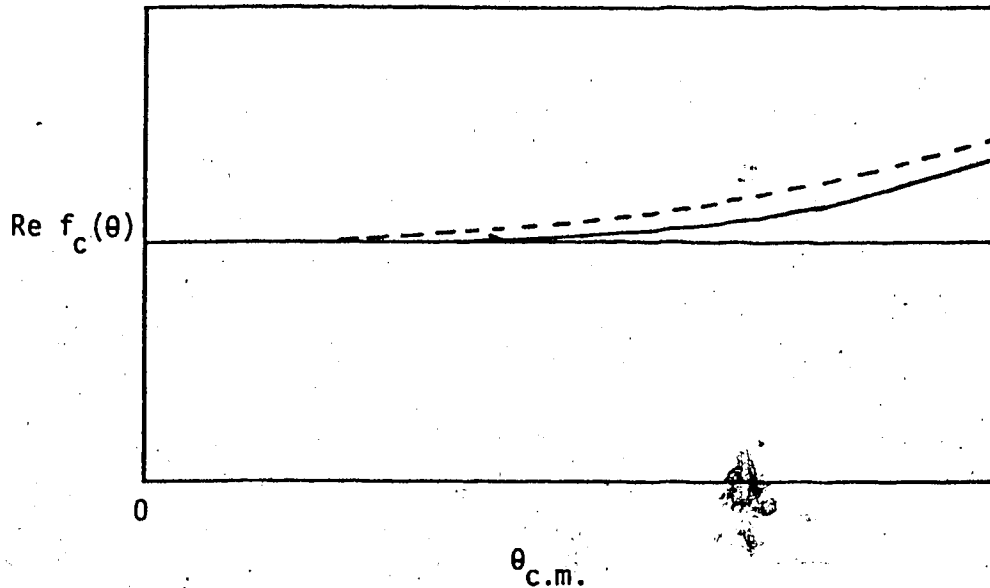
Figure 4.3 The Phase singularity is hidden under the parabolic envelope

If we perform n such transformations, the series will converge like

$$\sum_{l} 1/l^{(2n-1)}$$ 4.68

What then is the optimum value of n?

If n is too high, we have another problem. Once we have done the sum to, say, 15 figures of accuracy for $\theta = 5°$ and n=10, we then multiply it by

$$\frac{1}{\left(1 - \cos 5°\right)^{10}} \simeq (70)^{20} \gg 10^{17}$$

4.69

Thus the series would have to sum to a number much less than 10^{-17} with terms of order 10^0; clearly this is not possible with the limited precision (17 figures) available on a computer.

It seems then that n = 3,4,5 or perhaps 6 are all about as good as each other. We follow the lead of (YE54) and take n=3; this requires typically about 150 terms in the sums 4.45 and 4.46.

5. THE PION DISTORTED WAVE

In the final state of the (p, π^+) reaction we have an outgoing pion. As we shall see in Chapter 8, the final state interactions of the pion with the final nucleus are vital to explaining the (p, π^+) data. To describe this final state interaction we employ a potential due to Stricker, McManus and Carr (SMC) (ST78), which provides good fits not only to the pionic atom shifts and widths but also to the pion elastic scattering in the energy range 0→50 MeV.

The derivation of the potential form used by SMC is outlined below.

5.1 Potential Derivation

Starting form the Klein-Gordon equation, but neglecting terms which are quadratic in the potential, gives an equation which resembles a Schrödinger equation

$$\left(\nabla^2 + k^2 - 2 \bar{\omega} \, U_{opt}(r) \right) \phi(r) = 0$$

5.1

where $\bar{\omega}$ is the reduced centre of mass energy.

5.1.1 First Order Terms

In the centre of mass frame, the pion nucleon scattering amplitude is;

$$f_{\pi N} = b_0 + b_1 \underline{\tau} \cdot \underline{t} + (c_0 + c_1 \underline{\tau} \cdot \underline{t}) \underline{k} \cdot \underline{k}'$$

$$+ i(d_0 + d_1 \underline{\tau} \cdot \underline{t}) \underline{\sigma} \cdot \underline{k}' \times \underline{k} \qquad 5.2$$

where $\underline{\sigma}$ and $\underline{\tau}$ are the spin and isospin opoerators for the nucleon and t is the isospin operator for the pion.

If we transform equation 5.2 from the c.m. of the pion-nucleon system to that of the pion-nucleus system (the so-called angle transformation) and fold in the nuclear density, we get the first order potential

$$2 \bar{\omega} U(r) = -4\pi \left[(1+\epsilon) b_0 \rho(r) - \frac{c_0}{\pi^2} \underline{\nabla} \cdot \rho(r) \underline{\nabla} + \frac{\epsilon C_0 \nabla^2 \rho(r)}{2(1+\epsilon)} \right]$$

$$5.3$$

where

$$\epsilon = E_\pi / m_\pi c^2 \qquad 5.4$$

5.1.2 Second Order Terms

Since pion absorption cannot take place on a single nucleon (conservation of energy and momentum); at least 2 nucleons must contribute. A phenomenological amplitude for this process can be written

$$f_{(2)} = B_0 + C_0 \underline{k} \cdot \underline{k}' \qquad 5.5$$

where Im B_0 and Im C_0 can be calculated from a microscopic model involving graphs such as figure 5.1
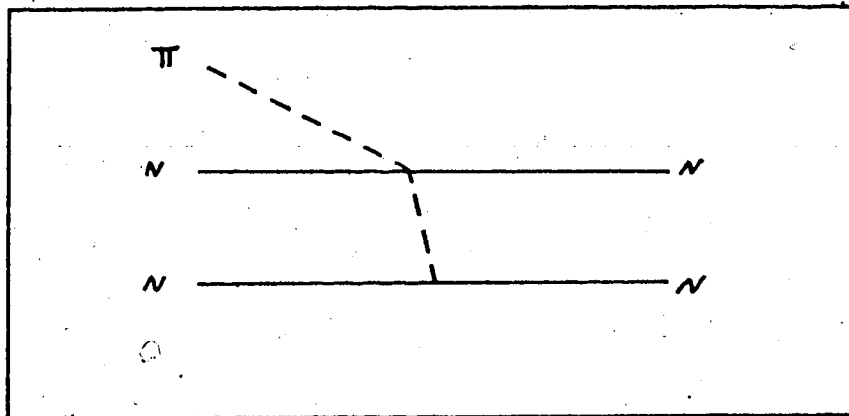
Figure 5.4 The source of imaginary terms in the potential.

The real parts of B and C are not determined by this model and are taken[1] as the negative of their imaginary counterparts (ST78). At energies above 50 MeV they are set to zero (ST79).

Since we have a 2 nucleon amplifude, we get terms proportional to the density squareo in the potential, namely

$$2\bar{\omega}\, U_{abs}(r) = -4\pi \left\{ (1 + \epsilon/2) B_0 \rho^2(r) - \frac{2C_0}{2+\epsilon} \nabla \cdot \rho^2(r) \nabla + \frac{\epsilon C_0 \nabla^2 \rho^2(r)}{4+2\epsilon} \right\}$$

5.6

5.1.3 Higher order terms

The multiple scattering series for the potential operator $\tilde{U}$

---

[1] quite arbitrarily

$$\langle \, o \mid \tilde{U} \mid o \rangle \; = \; U(r) \tag{5.7}$$

is given as

$$\tilde{U} \; = \; \sum_{\alpha} t_{\alpha} \; + \; \sum_{\beta \neq \alpha} t_{\alpha} G Q t_{\alpha} \; + \; \ldots \tag{5.8}$$

where G is the pion propagator, t is the pion-nucleon 2-body T-matrix and Q is a projection operator which projects off the ground state. Ericson and Ericson (ER66) have shown that if short range correlation effects are included, the P-wave piece of the multiple scattering series is summable, providing we assume the pion wavelength is much greater than the average correlation length between the nucleons. This results in the modification

$$4\pi b_0 \rho(r) \longrightarrow \frac{4\pi b_0 \rho(r)}{1 + (\xi/\lambda') 4\pi b_0 \rho(r)} \tag{5.9}$$

where ξ is the average correlation length between nucleons in the nucleus. At present

$$\lambda' = \frac{A}{A-1} \cdot \frac{3\xi^2}{2} \tag{5.10}$$

is taken as a free parameter and adjusted to fit the elastic scattering data.

The S-wave part can be summed to second order, which results in the replacement

$$b_o \longrightarrow \bar{b}_o = b_o - (b_o^2 + 2b_1^2) \frac{3k_f}{2\pi}$$

<div align="right">5.11</div>

with the Fermi wavevector, $k_f = 1.4$ fm^{-1}.

5.2 The Stricker McManus Carr Potential

Summing up we obtain

$$2\bar{\omega} U_{opt}(r) = -4\pi \left[b(r) + P_2 p^2(r) + \frac{P_1 - 1}{2} \nabla^2 c(r) + C_o \frac{(P_2 - 1)}{2P_2} \nabla^2 p^2(r) \right]$$

$$+ 4\pi \left[\underline{\nabla} \cdot \mathcal{L}(r) c(r) \underline{\nabla} + \frac{C_o}{P_2} \underline{\nabla} \cdot p^2(r) \underline{\nabla} \right] + 2\bar{\omega} V_c(r)$$

<div align="right">5.12</div>

where

$$b(r) = P_1 \left(\bar{b}_o p(r) - b_1 \delta p(r) \right)$$

<div align="right">5.13</div>

$$c(r) = P_1^{-1} \left(c_o p(r) - c_1 \delta p(r) \right)$$

<div align="right">5.14</div>

$$\delta p(r) = \frac{N - Z}{A} p(r)$$

<div align="right">5.15</div>

$$\mathcal{L}(r) = \left(1 + \frac{4\pi\lambda}{3} \left(\frac{A-1}{A} \right) c(r) \right)^{-1}$$

<div align="right">5.16</div>

$$P_1 = \frac{1 + \varepsilon}{1 + \varepsilon/A} \qquad P_2 = \frac{1 + \varepsilon/2}{1 + \varepsilon/A}$$

<div align="right">5.17</div>

5.3 Numerical solution

From 5.12 we see that we can write the potential in the form

$$2\bar{\omega}\, U_{opc}(r) \;=\; -\, g_4(r) \;-\; \underline{\nabla}\cdot g_3(r)\,\underline{\nabla}$$

5.18

where

$$g_4(r) \;=\; -\, g_1(r) \;-\; \nabla^2 g_2(r)$$

5.19

$$g_1(r) \;=\; 4\pi\Big(b(r) + \rho_2 B_0 \rho^2(r) - \tfrac{2\bar{\omega}}{4\pi} V_c(r)\Big)$$

5.20

$$g_2(r) \;=\; \frac{C_0(\rho_2-1)4\pi\rho^2(r)}{2\rho_2} \;+\; \frac{(\rho_1-1)}{2}\,4\pi c(r)$$

5.21

$$g_3(r) \;=\; -4\pi\Big(\mathcal{L}(r)c(r) + \frac{C_0}{\rho_2}\rho^2(r)\Big)$$

5.22

$$g_0(r) \;=\; g_1(r) \;+\; \frac{1}{r^2}\frac{d}{dr}\Big(r^2\frac{d}{dr}g_2(r)\Big)$$

5.23

$$g_5(r) \;=\; g_0(r) \;+\; k^2$$

5.24

Equation 5.1 can be written in the form

$$\Big(\nabla^2 + g_5(r) + \underline{\nabla}\cdot g_3(r)\underline{\nabla}\Big)\phi(r)$$

5.25

Using

$$\underline{\nabla}\cdot g_3(r)\underline{\nabla}\,\phi(r) \;=\; g_3'(r)\frac{\partial}{\partial r}\phi(r) + g_3(r)\nabla^2\phi(r)$$

5.26

we get

$$\left[\left(1 + g_3(r)\right)\nabla^2 + g_6(r) + g_3'(r)\frac{\partial}{\partial r}\right]\phi(r) = 0 \tag{5.27}$$

As usual we expand the wavefunction in partial waves

$$\phi(r) = \sum_{\ell=0}^{\infty}\sum_{m=-\ell}^{\ell}(-i)^\ell Y_\ell^m(\hat{k}_n)\frac{u_\ell(r)}{r}Y_\ell^m(\Omega) \tag{5.28}$$

We get the radial equation to be

$$\left(1 + g_3(r)\right)u_\ell''(r) + g_3'(r)u_\ell'(r) +$$

$$+ u_\ell(r)\left[g_6(r) + \frac{g_3'(r)}{r} - \left(1 + g_3(r)\right)\frac{\ell(\ell+1)}{r^2}\right] \tag{5.29}$$

Just as in the Dirac case (see Chapters 3 and 4), we transform away the first derivative terms. Defining

$$R^2(r) = 1 + g_3(r) \tag{5.30}$$

and

$$y(r) = R(r)u_\ell(r) \tag{5.31}$$

we obtain

$$y''(r) + y(r)\left[\frac{g_6(r)}{R^2(r)} - \frac{R''(r)}{R(r)} - \frac{\ell(\ell+1)}{r^2}\right] \tag{5.32}$$

We can now finally define the ℓ-independent part as

$$B u \ell k(r) = \frac{g_6(r)}{R^2(r)} - \frac{R''(r)}{R(r)} \tag{5.33}$$

equation

$$y''(r) + y(r)\left[B v_0 k(r) - \frac{\ell(\ell+1)}{r^2} \right]$$

5.34

which is suitable for solving with the Cowell Method (C010).

6. THE RELATIVISTIC DWBA T-MATRIX FOR (P,PI) REACTIONS.

In this Chapter we show how to put together the results of the previous three Chapters, thereby obtaining a DWBA expression for the T-matrix elements. The main results of this section are given by equations 6.19, 6.20 and 6.21. A brief glimpse at these equations will convince the reader that the *structure* of the T-matrix is not apparently very simple. It turns out (as mentioned in Chapter 4) that the T-matrix does have a rather nice structure however and this structure becomes transparent if we do not include initial and final state interactions (i.e. do a plane wave Born approximation). This section then is started with a derivation of the PWBA T-matrix elements. There are two types of vertex we consider, namely the pseudo-scalar and pseudo-vector vertices. We derive all our results for the pseudo-scalar vertex and then show how to modify them for the pseudo-vector vertex.

6.1 The Pseudo-Scalar Vertex

6.1.1 The Plane Wave Born Approximation

In the PWBA model for the (p,π^+) reaction the interactions of the incident proton with the target and the outgoing pion with the residual nucleus are not taken into account. The process is depicted in figure 6.1. In this approximation, the T-matrix element can be written as:
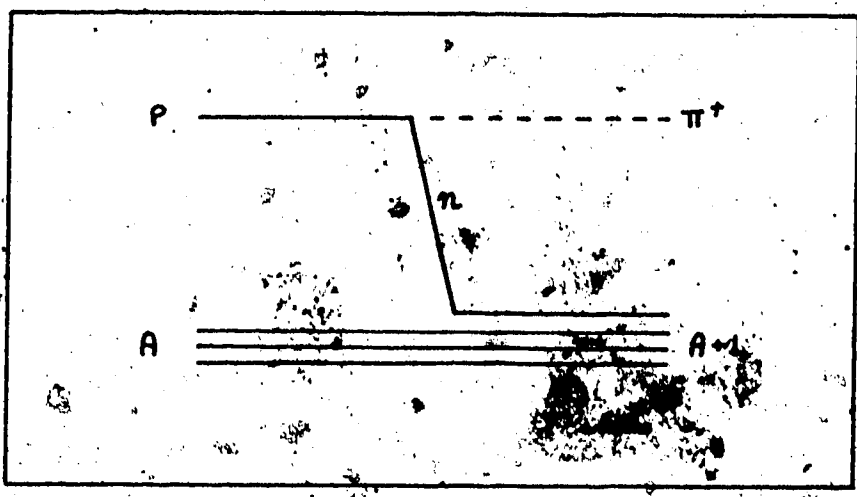
Figure 6.1 The plane wave one nucleon model.

$$T_{\mu_i M_a}(k_p, k_\pi) = \int \bar{\psi}_\beta^{M_\beta}(x) H_{int}(x) \psi_{\mu_i}^{(+)}(x) d^4 x$$

6.1

where

$$H_{int}(x) = i\sqrt{2} g_\pi \gamma_5 \phi_\pi^{(-)}(x)$$

6.2

This expression is given in Miller and Weber's paper (MI76). The motions of the outgoing pion and that of the incident proton are described by plane waves (with 4-delta function normalisation).

$$\psi_{\mu_i}^{(+)}(x) = \frac{e^{-ik_p \cdot x}}{(2\pi)^2} \begin{pmatrix} 1 \\ \frac{\vec{\sigma} \cdot \vec{p} c}{E + mc^2} \end{pmatrix} \chi(\mu_i)$$

6.4

where k_p and k_π are the proton and pion 4-vectors. The bound state wavefunction is, as discussed in Chapter 3,

$$\psi_\beta^{M_\beta}(x) = \frac{e^{-iEt}}{\sqrt{2\pi}} \begin{pmatrix} f_\beta(r)\, \mathcal{Y}_{L_\beta\,\frac{1}{2}\,J_\beta}^{M_\beta}(\Omega) \\ g_\beta(r)\, \mathcal{Y}_{L_\beta'\,\frac{1}{2}\,J_\beta}^{M_\beta}(\Omega) \end{pmatrix} \qquad L_\beta' = 2J_\beta - L_\beta$$

6.5

where

$$\mathcal{Y}_{L\,\frac{1}{2}\,J}^{M}(\Omega) = \sum_{m_L, m_s} (L\,\tfrac{1}{2}\,m_L\,m_s | J\,M)\, Y_L^{m_L}(\Omega)\chi(m_s)$$

6.6

We make the plane wave expansions:

$$e^{-i\vec{q}\cdot\vec{r}} = 4\pi \sum_{\ell=0}^{\infty} \sum_{m=-\ell}^{\ell} (-i)^\ell j_\ell(qr)\, Y_\ell^{*m}(\hat{q})\, Y_\ell^m(\Omega)$$

6.7

where $j_\ell(x)$ is a spherical Bessel function (ME58) and

$$q = |\vec{k}_\pi - \vec{k}|$$

6.8

If these forms of the wave functions are used in equation 6.1, the following expression for the T-matrix results.

$$T_{\mu_i M_a}(k_p, k_\pi) = \frac{2\sqrt{4\pi}\, g_\pi}{(2\pi)^2} \sqrt{\frac{E+mc^2}{2mc^2}}\ \delta(E_f + E_\pi - E_p)$$

$$\times \left\{ \begin{array}{c} (L_a'\ {}^{1\!/\!_2}\ M_a^- \mu_i;\ \mu_i | J_a M_a)\ Y_{L_a}^{*M_a}(\hat{q})\ G_{L_a'}(q) \\[4mm] \frac{2\mu_i\, p_i c}{E+mc^2} (L_a\ {}^{1\!/\!_2}\ M_a - \mu_i;\ \mu_i | J_a M_a) Y_{L_a}^{M_a}(\hat{q})\ F_{L_a}(q) \end{array} \right\}$$

$$6.9$$

where we have introduced

$$F_{L_a}(q) = i^{-L_a} \int_0^\infty r^2 f_a(r) j_{L_a}(qr)\, dr$$

$$6.10$$

and

$$G_{L_a'}(q) = i^{-(L_a'+1)} \int_0^\infty r^2 g_a(r) j_{L_a'}(qr)\, dr$$

$$6.11$$

This result is the same as that obtained by Miller and Weber (MI76) (although the notation is different). We can see from these equations the structure as mentioned in Chapter 1, namely that the T-matrix depends on the lower component of the wavefunctions to *first* order, i.e.

$$T \sim f_\pi g_p + f_p g_\pi$$

$$6.12$$

where f and g are the upper and lower components of the Dirac spinor and the subscripts n and p refer to the neutron and proton.

If the lower component of the bound-state wavefunction

is neglected, we get[1]

$$T_{\mu_i M_s}(k_p, k_\pi) \sim Y_{L_s}^{*M_s}(\hat{q}) F_{L_s}(q)$$

6.13

showing that the T-matrix depends on the product of the bound state in momentum space and a spherical harmonic. It was this result (albeit the non-relativistic one) which lead to the hopes years ago (Chapter 2) that the (p,π^+) reaction would give us *directly* the high momentum components of the nuclear wavefunctions.

6.1.2 The Distorted Wave Born Approximation

If we want to include the possibilities of the proton interacting with the target nucleus before emitting the pion and also the emitted pion interacting with the final nucleus before leaving the nucleus we get a situation as depicted in figure 6.2. There are 3 inputs to the calculation, depicted by the three shaded areas in the figure; the proton distortion potentials, the pion distortion potentials and the neutron binding potentials.

As in the PWBA we write down from the diagram,

$$T_{\mu_i M_s}(k_p, k_\pi) = \int \bar{\psi}_\beta^{M_s}(x) \Gamma \psi_{\mu_i}^{(+)}(x) \phi_\pi^{(-)}(x) dx$$

6.14

Where we now write the 3 parts

---

[1] not, it turns out such a good approximation at these momentum transfers
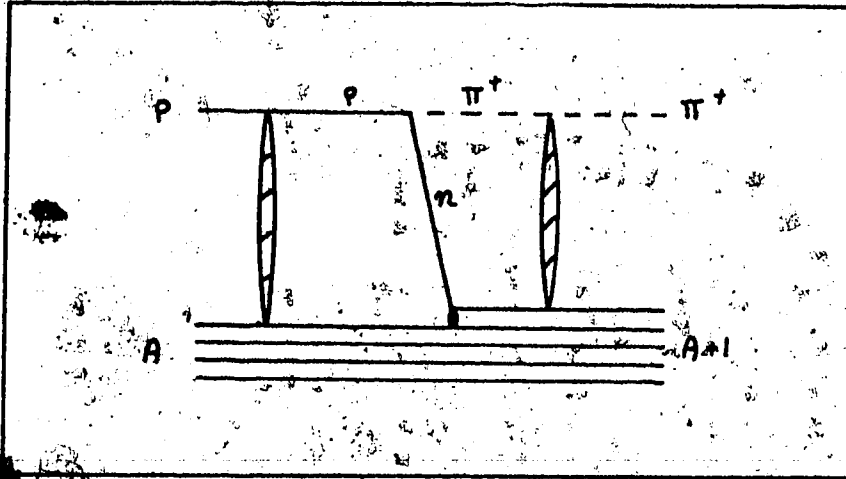
Figure 6.2 The distorted wave one nucleon model

$$\psi(x) = \frac{e^{-iEt}}{\sqrt{2\pi}}\begin{pmatrix} f_0(r) \, Y^{m_0}_{L_0 \, \frac{1}{2} \, J_0}(\Omega) \\ -i g_0(r) \, Y^{m_0}_{L_0' \, \frac{1}{2} \, J_0}(\Omega) \end{pmatrix}$$

6.15

$$\psi(x) = \frac{e^{-iE_n t}}{\sqrt{2\pi}} \sum_{\ell m} (-i)^{\ell} \, Y^{m}_{\ell}(\hat{k}_n) \, e^{i\sigma_{\ell}} f_{\ell}(k_n r) \, Y^{*m}_{\ell}(\Omega)$$

6.16

$$\psi_{\mu_i}^{(+)}(x) = \frac{e^{-iE_p t}}{\sqrt{2\pi}} \sum_{JLM} i^L e^{i\Sigma_K} Y_L^{*(M-\mu_i)}(\hat{k}_i)(L \, M-\mu_i, \tfrac{1}{2}\mu_i; \tfrac{1}{2} J M)$$

$$\times \left(\begin{matrix} F_{LJ}(r) \, Y_{L\,\frac{1}{2}J}^{M}(\Omega) \\ G_{LJ}(r) \, Y_{\bar{L}\,\frac{1}{2}J}^{M}(\Omega) \end{matrix} \right) \tag{6.17}$$

$$L_\beta' = 2J_\alpha - L_\beta \, , \qquad\qquad L' = 2J - L \tag{6.18}$$

It is straightforward to put all these together. We need to use the result

$$\int Y_{L_1\frac{1}{2}J_1}^{+M_1}(\Omega) \, Y_{L_2\frac{1}{2}J_2}^{M_2}(\Omega) \, Y_{L_3}^{*M_3}(\Omega) \, d\Omega$$

$$= (J, J_2; -M_1 M_2 | L_3 M_3)(L_1 L_2; 0 \, 0 | L_3 0) \left\{ \begin{matrix} J_2 & L_3 & J_1 \\ L_1 & \frac{1}{2} & L_2 \end{matrix} \right\}$$

$$\times (-)^{L_2 + J_1 - J_2 - M_2 + M_3 - \frac{1}{2}L} \left[\frac{(2L_1+1)(2J_1+1)(2J_2+1)}{4\pi} \right]^{1/2} \tag{6.19}$$

where the curly brackets indicate a Wigner 6J symbol and the round bracketed expressions are Clebsh-Gordon coefficients in the Condon-Shortly phase convention. We choose the x axis parallel to k and choose k to lie in the x-y plane. Whilst this is not the most elegant choice of axis, it makes the expressions for the cross-section and especially analysing power transparent. We ultimately end up with the expression for the T-matrix element;

$$T_{\mu_i M_6}(k_p, k_\pi) = \frac{-i g_\pi \sqrt{2J_6+1}}{2\pi} \delta(E_f + E_\pi - E_i)$$

$$\times \sum_{\ell=0}^{\infty} (-i)^\ell e^{i\sigma_\ell} \sum_{J=|\ell-J_6|}^{|\ell+J_6|} (2J+1) \sum_{L=J-\frac{1}{2}}^{J+\frac{1}{2}} i^L e^{i\Sigma_{K_\pi}}$$

$$\times \left\{ \begin{array}{l} I_A^{\ell J L}(L_6 \ell; 0\, 0 | L' 0) \left\{ \begin{array}{ccc} J & \ell & J_6 \\ L_6 & \frac{1}{2} & L' \end{array} \right\} \sqrt{2L_6+1} \\ - \tilde{I}_B^{\ell J L}(L_6' \ell; 0\, 0 | L\, 0) \left\{ \begin{array}{ccc} J & \ell & J_6 \\ L_6' & \frac{1}{2} & L \end{array} \right\} \sqrt{2L_6'+1} \end{array} \right\}$$

$$\times \sum_{m=-\ell}^{+\ell} \begin{pmatrix} L & \frac{1}{2} & J \\ m+M_6-\mu_i & \mu_i & -(m+M_6) \end{pmatrix} \begin{pmatrix} J_6 & J & L \\ -M_6 & M_6+m & -m \end{pmatrix} Y_\ell^m(\frac{\pi}{2}, \phi)\, Y_L^{m+M_6-\mu_i}(\frac{\pi}{2}, 0)$$

<div align="right">6.20</div>

Here we have introduced the two overlap integrals

$$I_A^{\ell J L} = \int_0^\infty f_6(r)\, G_{LJ}(r)\, f_\ell(r)\, r^2 dr$$

<div align="right">6.21</div>

$$I_B^{\ell J L} = -i \int_0^\infty g_6(r)\, F_{LJ}(r)\, f_\ell(r)\, r^2 dr$$

<div align="right">6.22</div>

The cross-section and analysing power are now given by

$$\frac{d\sigma}{d\Omega} = \frac{(2\pi)^2 m_p c^2 \, p_\pi}{2\hbar c} \frac{\overline{p_\pi}}{p_i} \sum_{\mu_i M_6} \left| T_{\mu_i M_6} \right|^2$$

<div align="right">6.23</div>

$$A = \frac{\sum_{M_6} |T_{\frac{1}{2} M_6}|^2 - |T_{-\frac{1}{2} M_6}|^2}{\sum_{M_6} |T_{\frac{1}{2} M_6}|^2 + |T_{-\frac{1}{2} M_6}|^2}$$

<div align="right">6.24</div>

6.2 The Pseudo-Vector Vertex

To get the T-Matrix for the pseudo-vector vertex (PVV) from that of the pseudo-scalar vertex (PSV) we have to make the replacement

$$\gamma_5 \longrightarrow \frac{\gamma_5 \not{p}_\pi c}{2 m_N c^2}$$

6.25

where

$$\not{p}_\pi = -i \hbar \gamma^\mu \partial_\mu^{(\pi)}$$

6.26

The T-matrix looks like

$$T_{PV} = \frac{i \sqrt{2} \, g_\pi \hbar c}{2 m_N c^2} \int \bar{\psi}_6(x) \gamma_5 \gamma_\mu \psi_i^{(+)}(x) \partial_\mu^{(-)} \phi_\pi^{(-)}(x) d^4 x$$

6.27

If we integrate by parts we can turn the $\gamma^\mu \partial_\mu$ onto the nucleon spinors. Instead of carrying out the differentiation we can use the Dirac Equation for the proton,

$$i \hbar c \, \gamma^\mu \partial_\mu \psi_i(x) = (m c^2 + U_s^i(r) - \gamma_0 U_V^i(r)) \psi_i(x)$$

6.28

and the Hermitian conjugate of this equation for the neutron wavefunction to get

$$T_{\mu_i M_6} = i \sqrt{2} \, g_\pi \int \bar{\psi}_N^{m_6}(x) \gamma_5 \Gamma(r) \psi_{\mu_i}^{(+)}(x) \phi_\pi^{(-)}(x) d^4 x$$

6.29

where for the PSV

$$\Gamma(r) = 1$$

6.30

and for the PVV

$$\Gamma(r) = 1 + \frac{U_s^B + U_s^i}{2 m_N c^2} + \frac{\gamma^\circ}{2 m_N c^2}\left(E_T + E_B - E_i - U_v^B(r) - U_v^i(r) \right)$$

6.31

Thus to include the PVV as an option in our calculations the I_A and I_B of equation 6.20 and 6.21 are simply modified by the inclusion of the potential terms, no numerical differentiation of the pion wavefunction is necessary.

6.3 The Non-Relativistic Hamiltonian

As promised in Chapter 2 we outline how to obtain a Hamiltonian for use in a Schrödinger equation, which will give the same results as the PS or PV vertex used in a Dirac equation. First we notice that equations 6.20 and 6.21 are where the "physics" is put into the formalism. Our pion wavefunction already satisfies a Schrödinger equation, and so we need not change its wavefunction, all we have to do is (formally) replace the f and g for the nucleons by their Schrödinger equivalent forms. We eliminate f in terms of 'y' using equation 4.27 and eliminate g similarly using 4.20. This will give us an expression of the form

$$T_{\mu;M_\beta} \sim \sum_{\substack{\ell JM \\ L M_L}} \left\{ \int \mathcal{Y}^*_{L_\beta S_\beta}{}_{(r)} O \mathcal{Y}_{\ell j}(r) d^3r \right\} C_{L_\beta J_\beta M_\beta}^{\ell J \ell\, m_\ell M \mu_i}$$

6.32

where O is the non-relativistic operator we seek, and $\mathcal{C}$ is a function which depends on the angular momentum quantum numbers. O will contain the binding and distorting potentials as well as their derivatives and derivative operators. Due to the complexity of the expression we do not attempt a derivation here since we do not need the result. In order to derive the same results as the relativistic formalism we must, of course, use potentials of the form 4.32 and 4.34 in the Schrödinger equations.

7. ELASTIC SCATTERING FITS

The generation of the proton-distorted wave functions necessary for the calculation of the (p,π^+) amplitude of equation 6.19 necessitated the development of a computer program based on the formalism of Chapter 4. The program, called *RUNT* is described in Appendix D. Essentially *RUNT* varies the potential parameters to fit the calculated proton elastic scattering cross-section and analysing power to the data. This is achieved through an automatic search routine using a chi-squared minimisation technique.

From the RHF arguments presented in Chapter 3 we expect to be able to get a fit only for spin-zero isospin-zero nuclei. We are primarily interested in using our potentials to get distorted waves for use in the (p,π^+) reaction and so have concentrated on the two nuclei ^{12}C and ^{40}Ca. For eteness, we show also a fit to some recent ^9Be and ^4He scattering data.

The vector and scalar potentials are parameterised as

$$U_v(r) = \frac{V_v}{1 + e^{\frac{r - R_{v1}}{a_{v1}}}} + \frac{iW_v}{1 + e^{\frac{r - R_{v2}}{a_{v2}}}}$$

7.1

$$U_s(r) = \frac{V_s}{1 + e^{\frac{r - R_{s1}}{a_{s1}}}} + \frac{i W_s}{1 + e^{\frac{r - R_{s2}}{a_{s2}}}}$$

7.2

which gives 12 parameters to search on. In addition to these nuclear potentials, a Coulomb potential due to a uniform charge density of radius R_c is added to the vector term. In general R_c is not searched on (since the fit is fairly insensitive to it) and is taken to be some number between 1.0 and 1.2, in accordance with the known charge distributions.

The parameters obtained, which give fits to the elastic scattering data, are shown in tables 7.1,7.2 and 7.3.

There are two *classes* of potential: those that have large imaginary parts of opposite sign (which we shall call class A) and those which have small imaginary parts, both absorptive (which we shall call class B).

The search code *RUNT* has turned up many solutions for the potential parameters. It turns out that, with a few exceptions, they can be divided into the two above classes. One consistent feature for all fits is the sign and magnitude of the real potentials.

Class A type solutions are of the type that has been used by L.G. Arnold et al. (AR78), in their analysis of p + ^{4}He scattering and recently on ^{40}Ca at 181 MeV. The class B solutions are new.

Table 7.1 The Optical Potential Strengths (MeV)

Nucleus	Energy	Vv	Wv	Vs	Ws
Class A					
^{4}He	500 MeV	274.4	-138.5	-464.1	215.7
^{9}Be	225 MeV	140.0	-248.0	-185.1	271.2
^{12}C	185 MeV	241.4	-111.3	-332.1	137.9
^{40}Ca	155 MeV	285.2	-129.4	-369.57	136.5
^{40}Ca	160 MeV	315.9	-157.1	-422.0	180.6
^{40}Ca	181 MeV	312.9	-117.6	-426.9	128.0
^{40}Ca	200 MeV	177.3	-119.5	-238.0	159.8
^{40}Ca	400 MeV	187.8	-331.3	-199.8	472.0
^{40}Ca	500 MeV	122.6	-228.0	-226.09	359.6
Class B					
^{12}C	150 MeV	270.3	-11.85	-364.7	-19.58
^{12}C	185 MeV	289.6	-12.74	-361.0	-48.8
^{40}Ca	155 MeV	346.6	-16.55	-436.9	-41.46
^{40}Ca	160 MeV	388.6	-12.75	-504.9	-55.79
^{40}Ca	181 MeV	363.8	-10.18	-486.0	-52.29
^{40}Ca	200 MeV	379.4	-16.51	-489.1	-28.89
^{40}Ca	200 MeV	260.3	-14.87	-349.4	0.0
^{40}Ca	400 MeV	173.0	-22.62	-264.8	0.0

Table 7.2 The Optical Potential Radial Parameters (fm)

Nucleus	Energy	Rv_1	Rv_2	Rs_1	Rs_2
Class A					
^{4}He	500 MeV	0.8832	1.0936	0.8502	1.0362
^{9}Be	225 MeV	0.8575	0.8106	0.889	0.8713
^{12}C	185 MeV	0.9688	1.0924	0.9492	1.032
^{40}Ca	155 MeV	1.0	1.0599	0.9985	1.042
^{40}Ca	160 MeV	1.006	1.0467	0.9969	1.0126
^{0}Ca	181 MeV	1.0233	1.0697	1.0107	1.0477
^{40}Ca	200 MeV	1.056	1.018	1.053	0.8936
^{40}Ca	400 MeV	0.9362	1.0441	1.0387	1.0244
^{40}Ca	500 MeV	0.9266	0.9848	0.9492	0.9124
Class B					
^{12}C	150 MeV	0.9880	1.2587	0.9812	0.5147
^{12}C	185 MeV	0.9827	1.3043	0.9925	0.4482
^{40}Ca	155 MeV	0.9885	1.1703	0.9924	0.7512
^{40}Ca	160 MeV	0.9870	1.241	0.9823	0.7480
^{40}Ca	181 MeV	1.0255	1.3176	1.0156	0.7747
^{40}Ca	200 MeV	1.0083	1.2651	1.0066	0.8241
^{40}Ca	200 MeV	1.063	1.2151	1.0571	
^{40}Ca	400 MeV	1.029	1.2071	1.001	

Table 7.3 The Optical Potential Diffusenesses (fm)

Nucleus	Energy	Av_1	Av_2	As_1	As_2
Class A					
^{4}He	500 MeV	0.2972	0.3203	0.3149	0.3036
^{9}Be	225 MeV	0.6541	0.6953	0.6782	0.6489
^{12}C	185 MeV	0.4551	0.5669	0.4978	0.5755
^{40}Ca	155 MeV	0.6181	0.8266	0.6641	0.8195
^{40}Ca	160 MeV	0.6202	0.7570	0.6500	0.7492
^{40}Ca	181 MeV	0.6181	0.6709	0.6470	0.6462
^{40}Ca	200 MeV	0.5494	0.8009	0.5963	0.8783
^{40}Ca	400 MeV	0.7038	0.6189	0.7078	0.6184
^{40}Ca	500 MeV	0.8094	0.6754	0.8593	0.7303
Class B					
^{12}C	150 MeV	0.5211	0.543	0.5523	0.3069
^{12}C	185 MeV	0.5779	0.4325	0.6064	0.4829
^{40}Ca	155 MeV	0.6764	0.7053	0.6977	0.5906
^{40}Ca	160 MeV	0.6757	0.6194	0.7004	0.6227
^{40}Ca	181 MeV	0.6721	0.5641	0.6988	0.5989
^{40}Ca	200 MeV	0.7121	0.5560	0.7400	0.5022
^{40}Ca	200 MeV	0.5857	0.6018	0.6109	
^{40}Ca	400 MeV	0.5935	0.4875	0.6898	

Elastic scattering data alone are not enough to choose between these two classes- interestingly they both predict similar reaction cross-sections which are in rough agreement with the data.

In the non-relativistic limit, class A potentials give rise to an imaginary spin-orbit potential of about the same magnitude as the phenomenological non-relativistic one. This non-relativistic strength was, however, derived by fitting the elastic scattering data and assuming a Woods-Saxon shape for the real potential. The real central potential obtained from the relativistic formalism has a repulsive core, so it is not obvious to equate imaginary spin-orbit potentials under these conditions.

The class A potentials give rise to a serious problem with *interpretation*. Physically they tell us that the coupling of the incident proton to the omega field removes a *vast* quantity of flux from the elastic channel, whereas the coupling to the sigma field returns most of this flux to the elastic channel. There is no physical justification for this rather bizarre state of affairs. It turns out that both class A and class B potentials predict a repulsive core in the real central potential, the evidence for which is now accumulating.

Class B potentials predict almost zero for the imaginary part of the equivalent non-relativistic spin-orbit potential. However, they afford good fits to the elastic scattering data indicating that the repulsive core in the

real central potential makes up for the absence of the imaginary spin-orbit potential. These potentials have the more reasonable property that they are both absorptive; indicating that both sigma and omega fields remove flux from the elastic channel. This absorption by both potentials is more acceptable, from a physics point of view, than the situation with the class A potentials. One feature of the class B potentials is that, whilst the geometries of the two real potentials are roughly equal to the expected nuclear geometry, the imaginary vector potential extends something like 20% beyond the nucleus and the imaginary scalar potential tends to lie inside, its radius being about 20% less than that of the nucleus.

Below we show fits of both classes and discuss them in order of increasing target weight.

7.1 ⁴He

Figures 7.1 and 7.2 show a class A fit at 500 MeV; the data are from Moss et al. (MO80). The fit cannot be described as a good one, the cross-section deteriorates rapidly, for larger angles and the analysing power is too high at foreward angles. The cross-section failure at larger angles can perhaps be understood as due to exchange effects (LE78),(AR80),(SH81a). The analysing power failure is probably a symptom of ⁴He being so small; consequently the coupling to the inelastic channels is not described well by

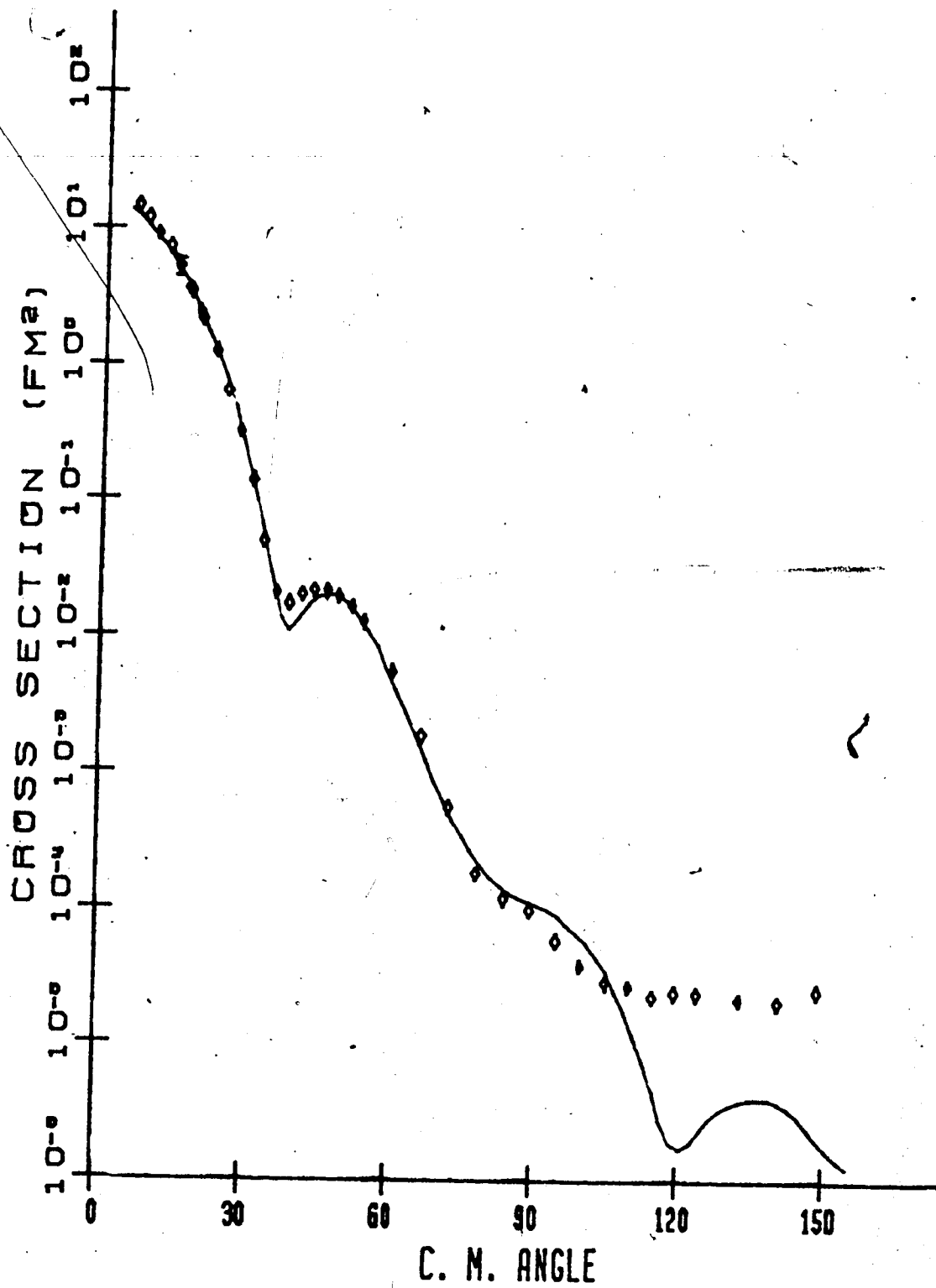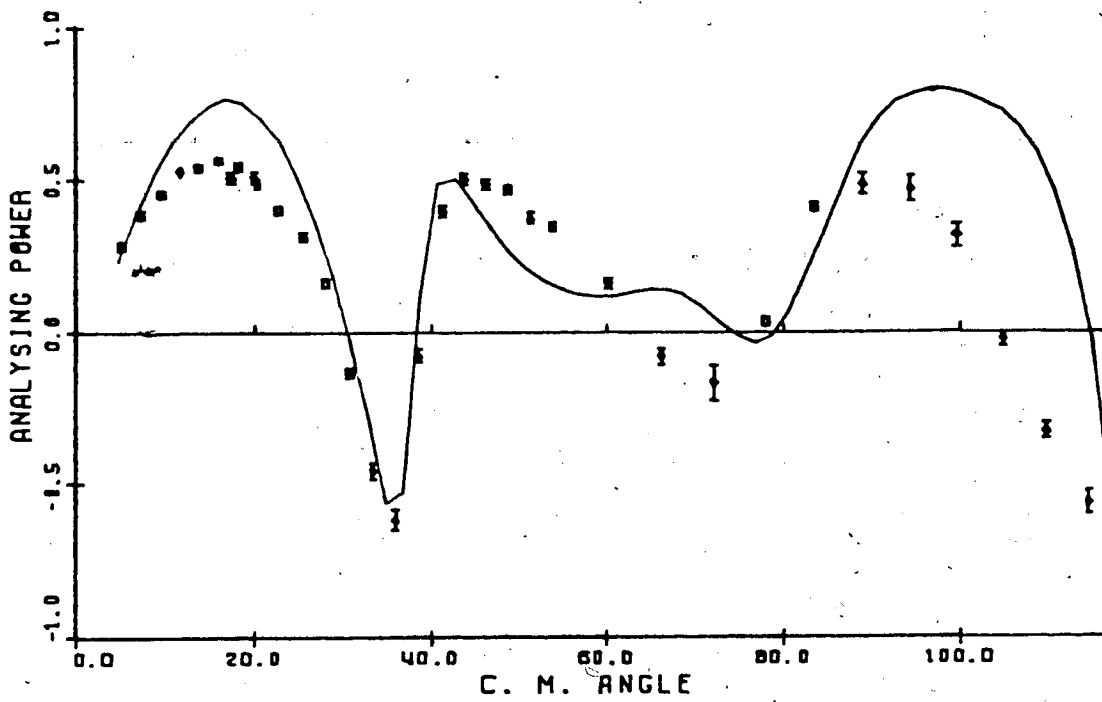Figure 7.1 Fit to 500 Mev p-⁴He elastic scattering cross section data.

Figure 7.2 Fit to 500 Mev p-⁴He elastic scattering analysing power data.
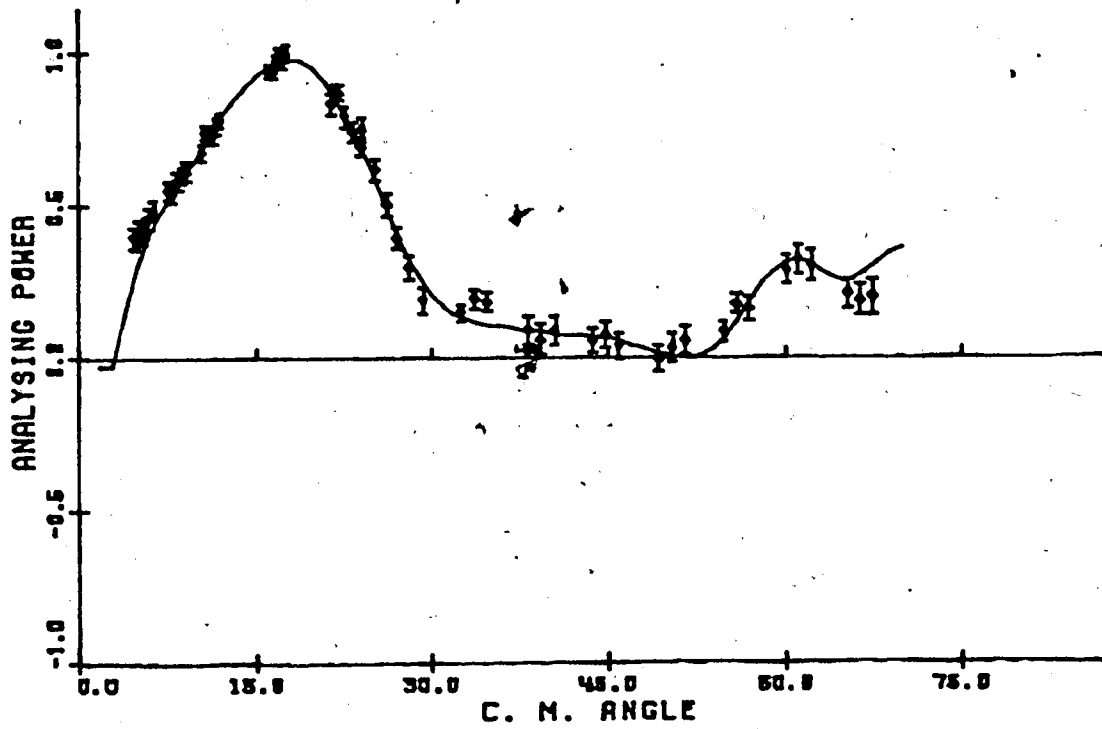
Figure 7.3 Fit to 225 Mev p-⁹Be elastic scattering analysing power data.

a smooth imaginary potential as is required in the optical model. The non-relativistic optical model has the same difficulties. Arnold et al. (AR79) have found reasonably good fits on ^{4}He at higher energies.

7.2 ^{9}Be

Figures 7.3 and 7.4 show a class A fit to the 225 MeV proton elastic scattering data from Roy et al. (RO81). The fit here is embarrassingly good since we have not only assumed a spin and isospin zero nucleus in eliminating all but scalar and vector potentials, but also since the nucleus is light, we expect to experience problems as in the case of ^{4}He. It turns out (RO81) that this fit is better than that obtainable from a non-relativistic model, even when an explicit coupled channel calculation is done on a prominent exited state.

Non-relativistically the coupled channels approach is necessary since there is one (collective) state which strongly couples to the ground state. The effect of this state is to remove a lot of flux from the elastic channel, thereby exiting the nucleus, and then replace the flux as the nucleus de-exites. This is similar to the physics associated with the class A potentials and was the reason we earlier said they were unrealistic for ordinary scattering. It turns out that the class B fit to this data is of a similar quality as the non-relativistic fits; indicating
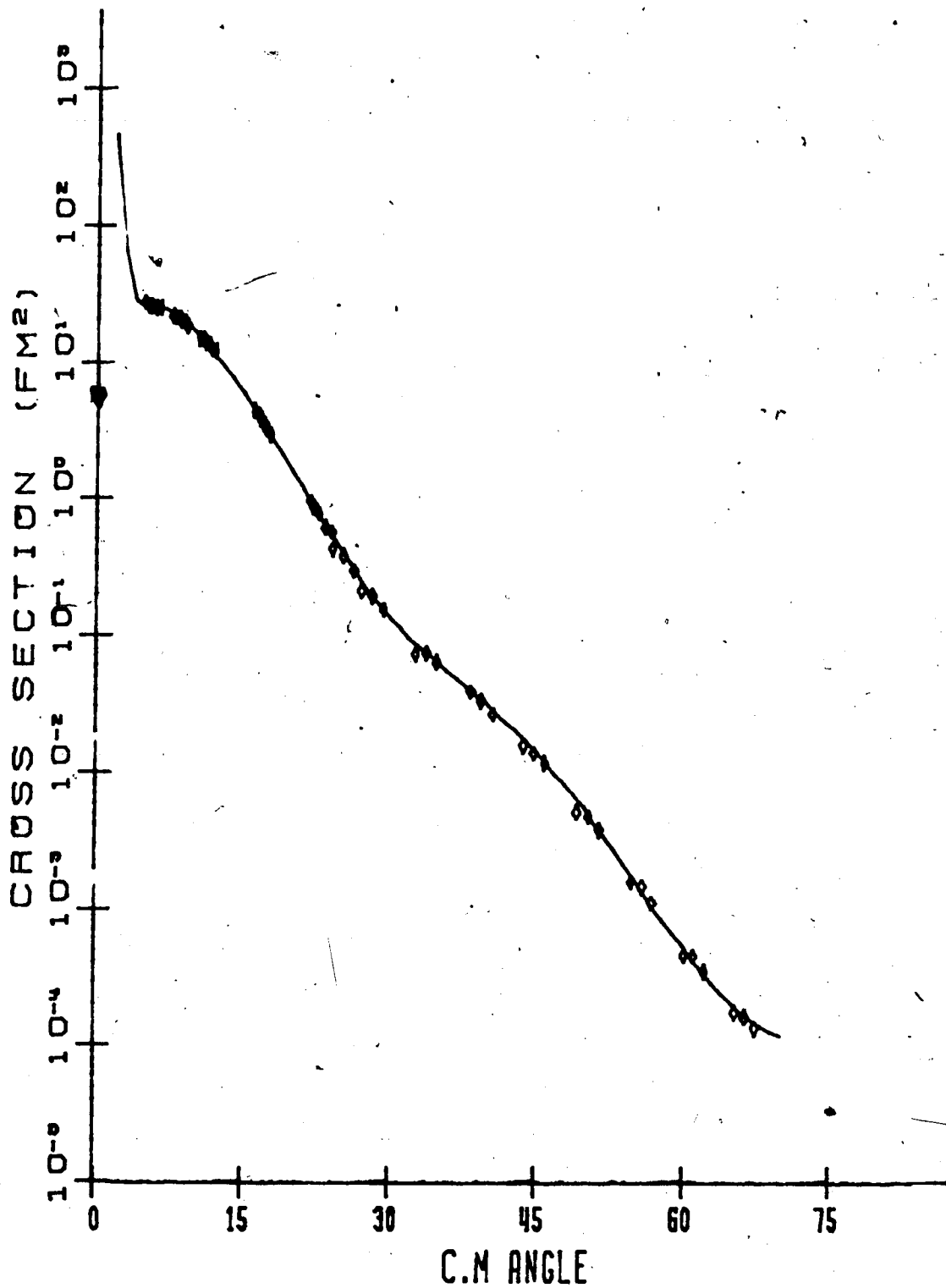
Figure 7.4 Fit to 225 Mev p-⁹Be elastic scattering cross section data.

that somehow the class A fits are behaving like a coupled channel calculation.

7.3 ^{12}C

Figures 7.5 and 7.6 show the fits to the elastic scattering cross-section and analysing power data at 200 MeV. The data are from Meyer et al. (ME81). It turns out that if we take the potentials obtained from fitting the 181 MeV calcium data and just scale the radial parameters, we can get a good fit to this data. The figures show the result of further refining the fits; the parameters in the tables are therefore not quite the same as their starting values.

7.4 ^{40}Ca

For calcium we have analysed the data from the five energies, 155 MeV, 160 MeV, 181 MeV, 200 MeV and 400 MeV. We show the fits at 160,181 and 400 MeV in figures 7.7 to 7.12 the data shown are from (RO65),(NA81) and (HU81).

As the figures show, the fits here are better than those on the lighter nuclei ^{4}He and ^{12}C. This is to be expected since calcium is a larger nucleus; meaning that the inelastic channels present are better represented by imaginary potentials. As can be seen from the tables the optical potential parameters move slowly with increasing energy, especially for the class B fits. Whilst we do not show them, it is quite possible to obtain reasonable fits to

Figure 7.5 Fit to 200 Mev p-^{12}C elastic scattering cross section data.
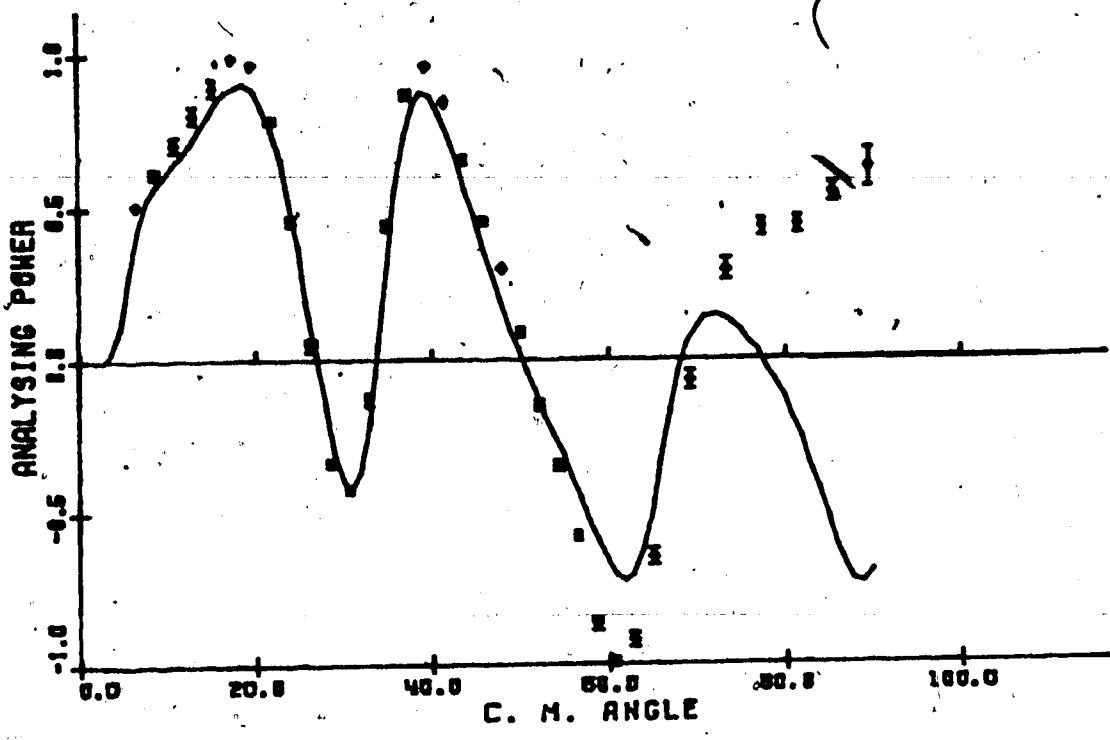
Figure 7.6 Fit to 200 Mev p-^{12}C elastic scattering analysing power data.
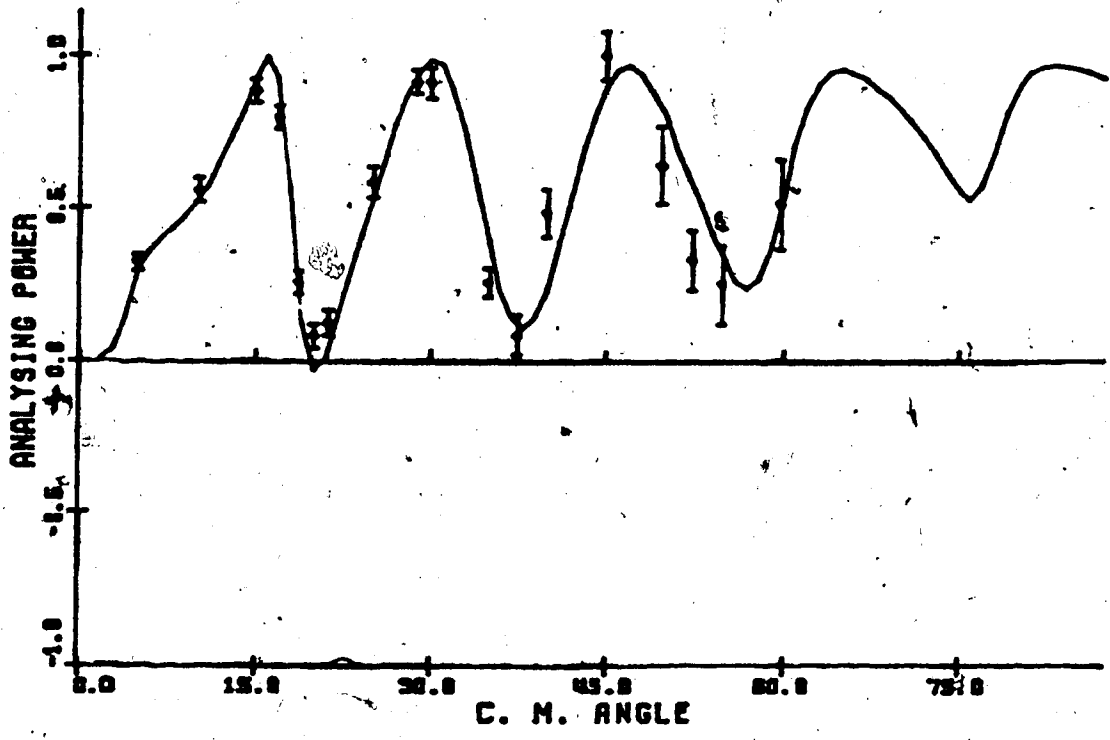
Figure 7.7 Fit to 160 Mev p-^{40}Ca elastic scattering analysing power data.
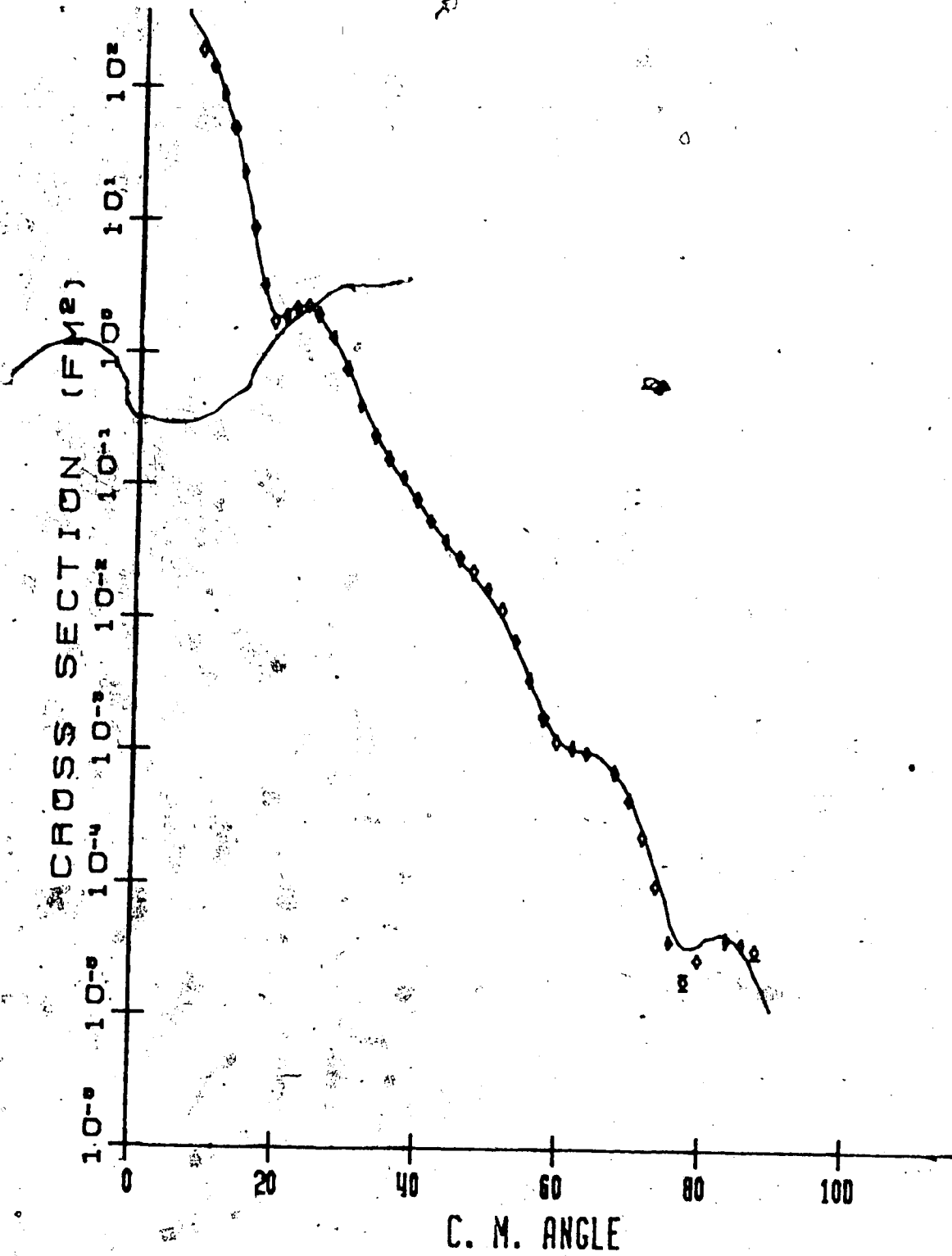
Figure 7.8 Fit to 160 MeV p-⁴⁰Ca elastic scattering
cross-section data.
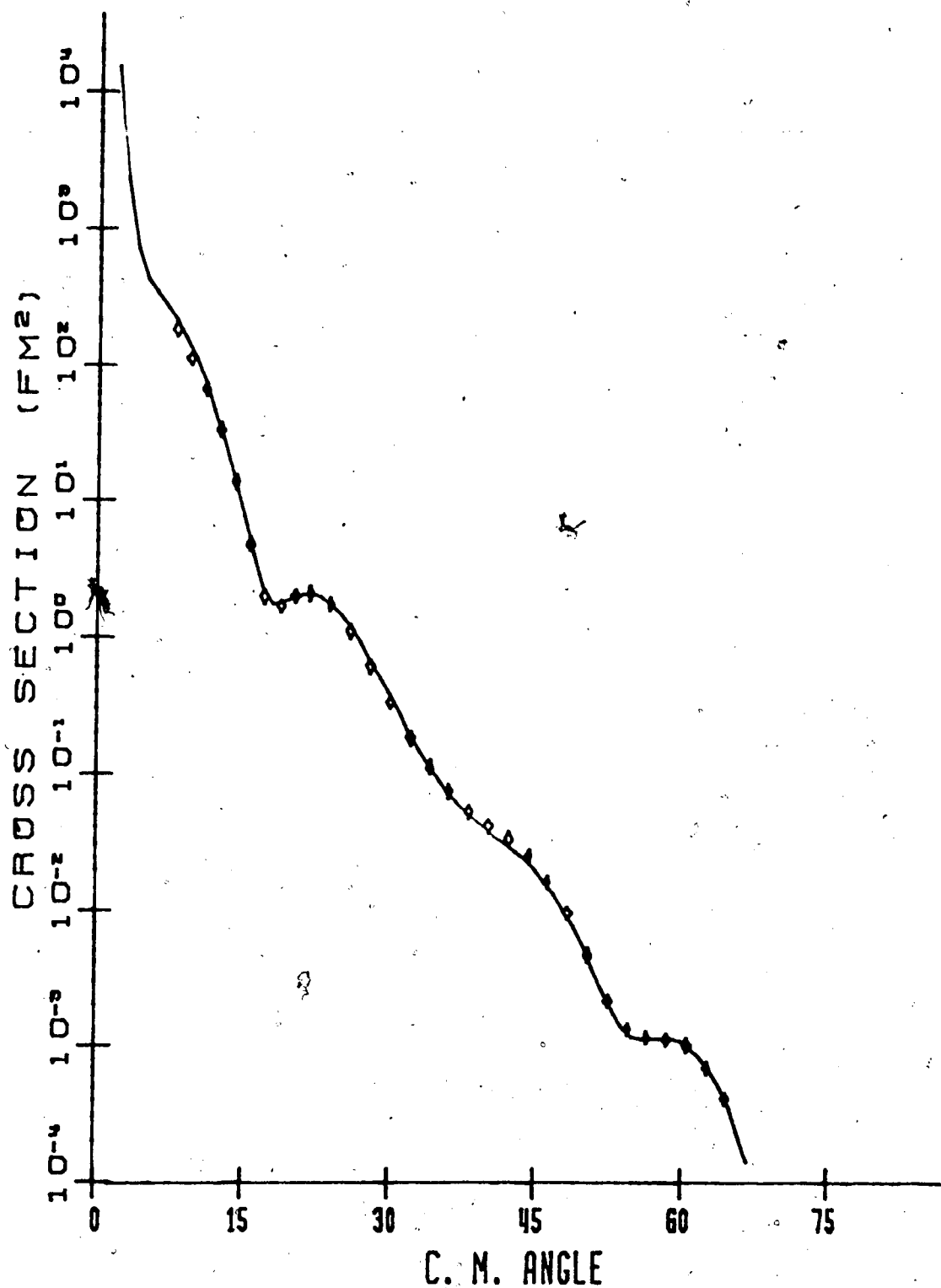
Figure 7.9 Fit to 181 MeV p-⁴⁰Ca elastic scattering
cross-section data.
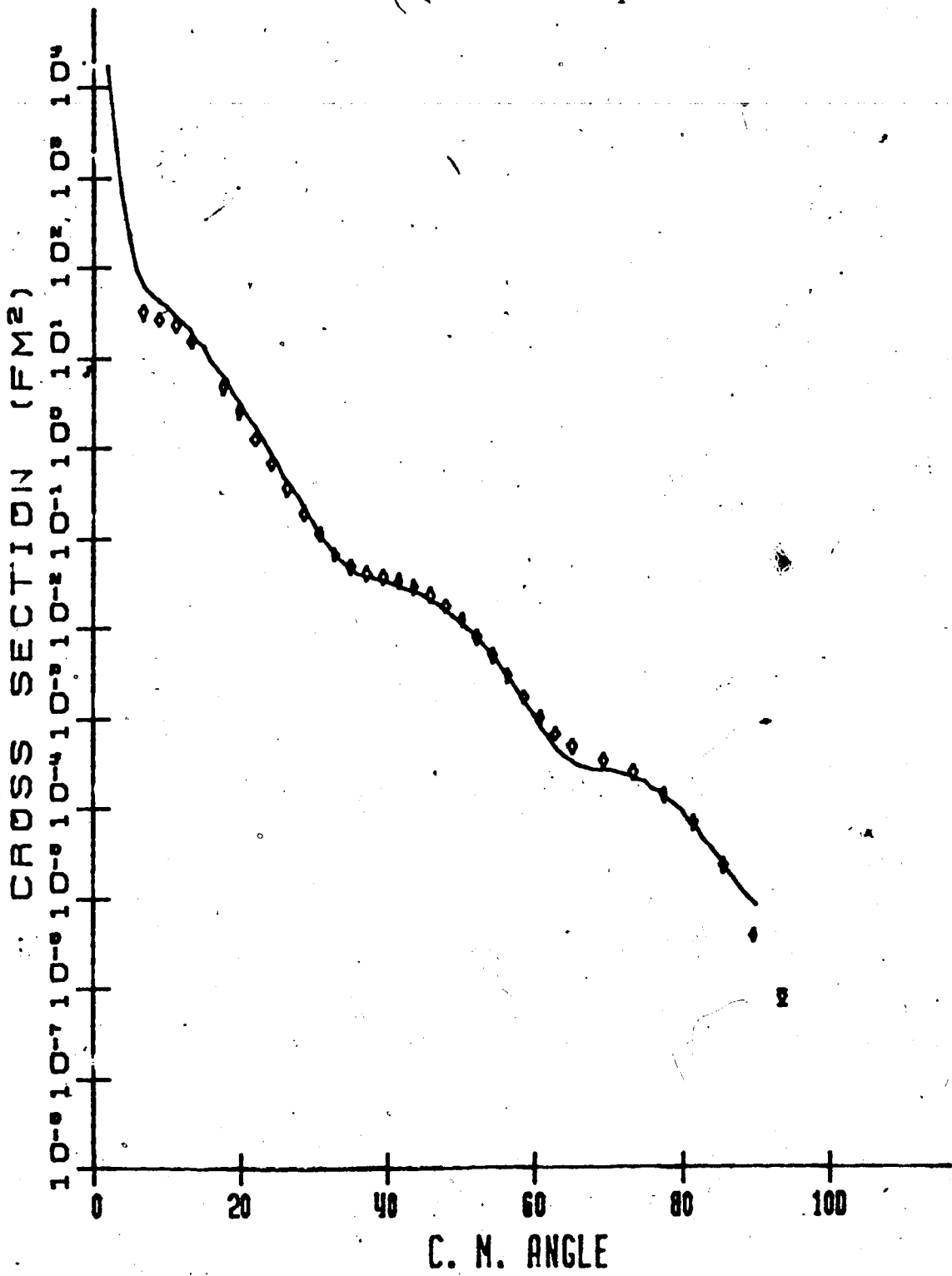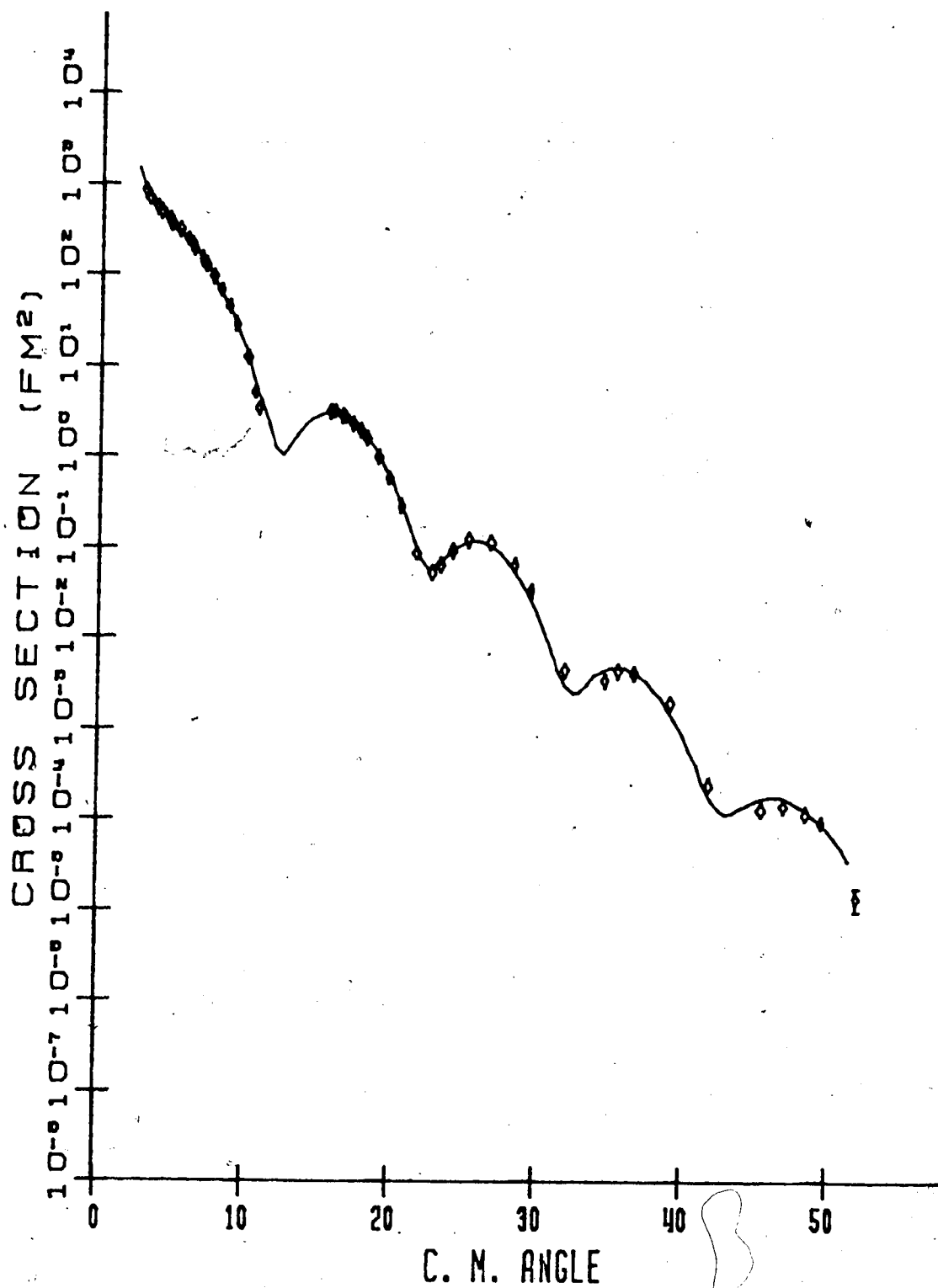
Figure 7.10 Fit to 400 MeV p-^{40}Ca elastic scattering
cross-section data.
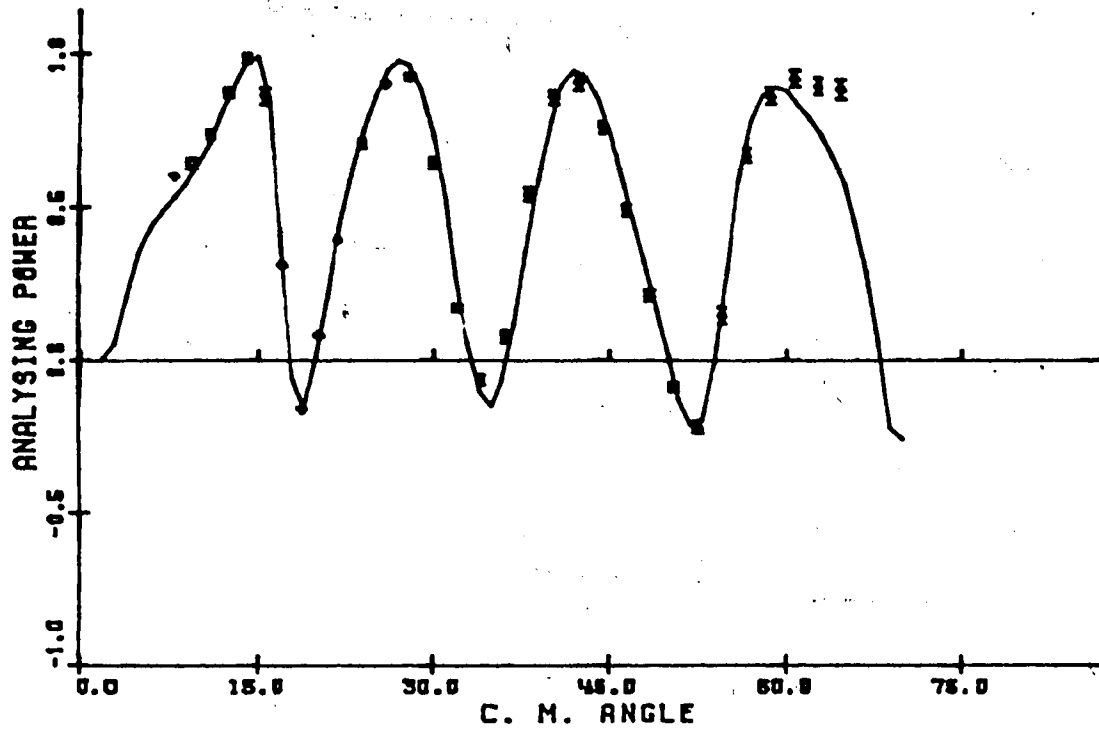
Figure 7.11 Fit to 181 Mev p-⁴⁰Ca elastic scattering analysing power data.
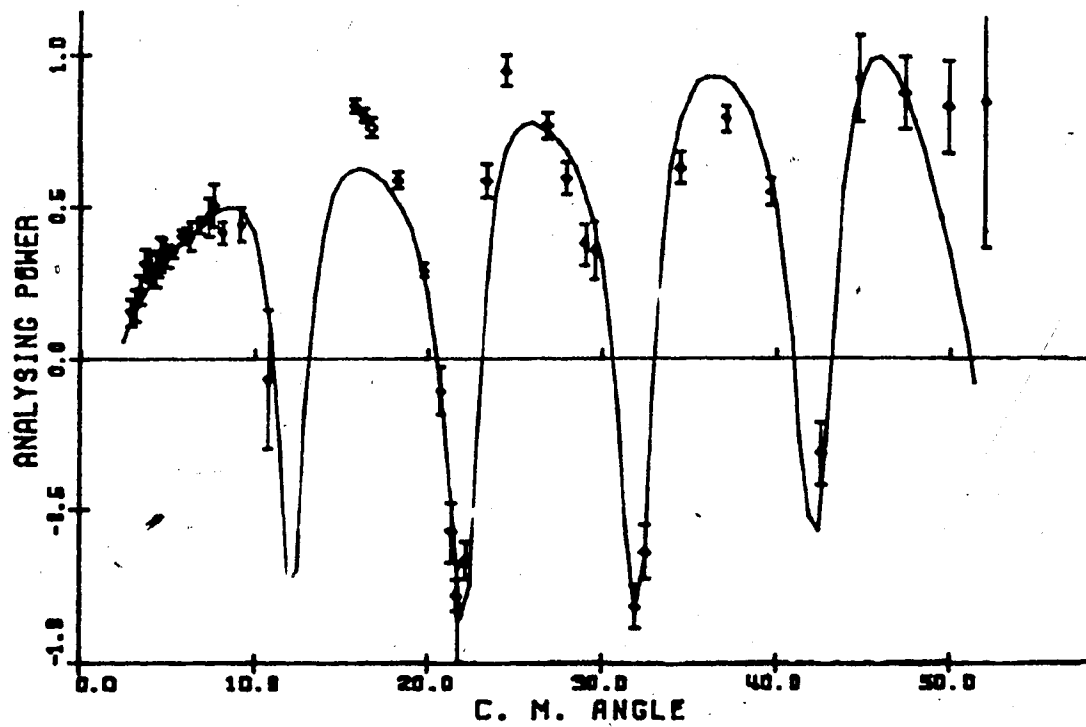
Figure 7.12 Fit to 400 Mev p-⁴⁰Ca elastic scattering analysing power data.

the data at 200 MeV and 400 MeV by arbitrarily setting Ws to zero. While there is no physical justification for this it demonstrates how *ambiguous* the parameters are. It will take a lot more than a few isolated elastic scattering measurements to limit the number of parameter sets. At 200 MeV is was not possible to get a good fit with the same sort of parameters which worked so well at 155 MeV, 160 MeV and 181 MeV. The reason for this is that while all 3 of these data sets give much the same cross-section and analysing powers when plotted against momentum transfer, the 200 MeV set shows a 30% normalisation difference in the cross-section for angles less than 18°. The class B parameter set given in the table was obtained by dropping such points from the search.

7.5 Non-Relativisic Equivalence

One nice feature of the model is that we know that the non-relativistic optical potentials are energy dependent; this feature comes out explicitly in the relativistic model, as can be seen in equations 4.32 and 4.34. This energy dependence is illustrated in figures 7.13 and 7.14, where the potentials obtained from fitting the 181 MeV data are extrapolated to other energies. The energies shown are 80 MeV, 130 MeV, 180 MeV, 230 MeV and 280 MeV. With increasing energy the imaginary potential gets deeper and the real potential goes from an attractive potential to a

potential with a large repulsive core. The spin orbit potentials also have an energy dependence, but it is a much smaller effect, as can be seen if one considers the large energy-independent terms in the denominator of equation 4.32.

It turns out that the 160 MeV parameters give good fits at 181 MeV and 200 MeV; this illustrates that the energy dependence is approximately correct.

It is tempting to look for a set of potential parameters which give good fits over a large energy range. However, from equation 4.34, we can see that the Volume integrals of the real and imaginary potentials depend linearly on energy. We know from non-relativistic analyses (LE78) that this is not the case, and therefore expect some energy dependence in our relativistic parameters.
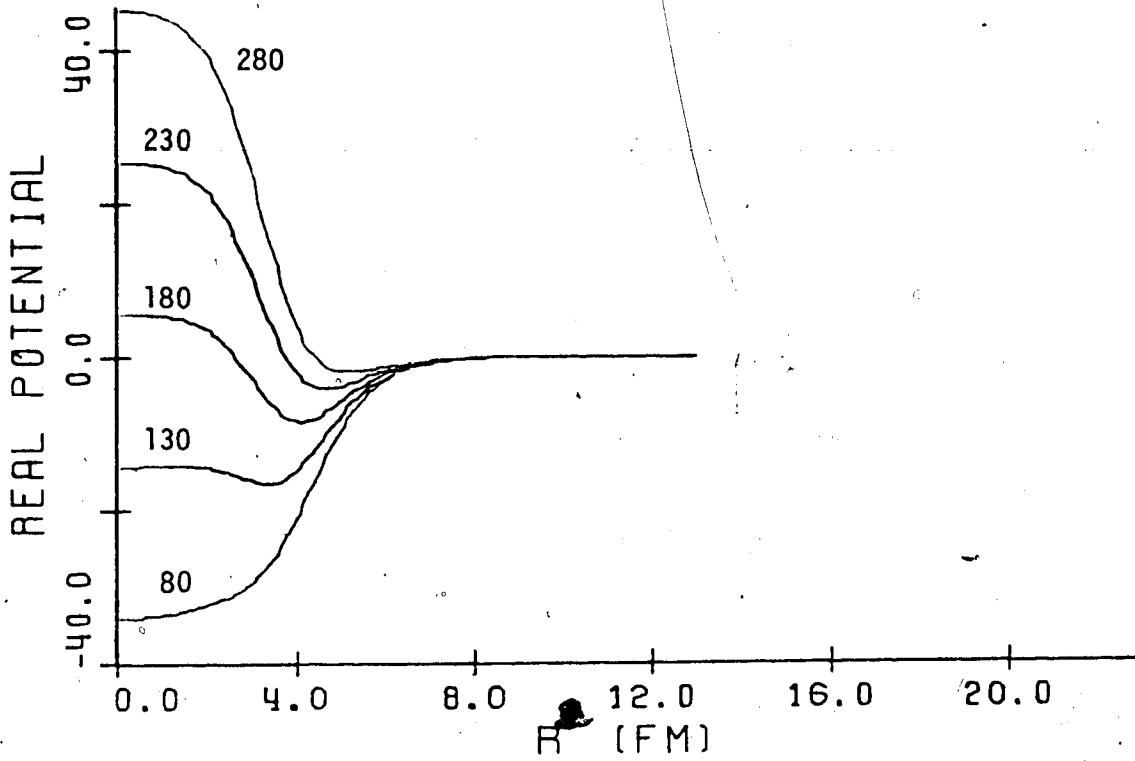
Figure 7.13 The energy dependence of the real central potential based on 181 MeV fit.
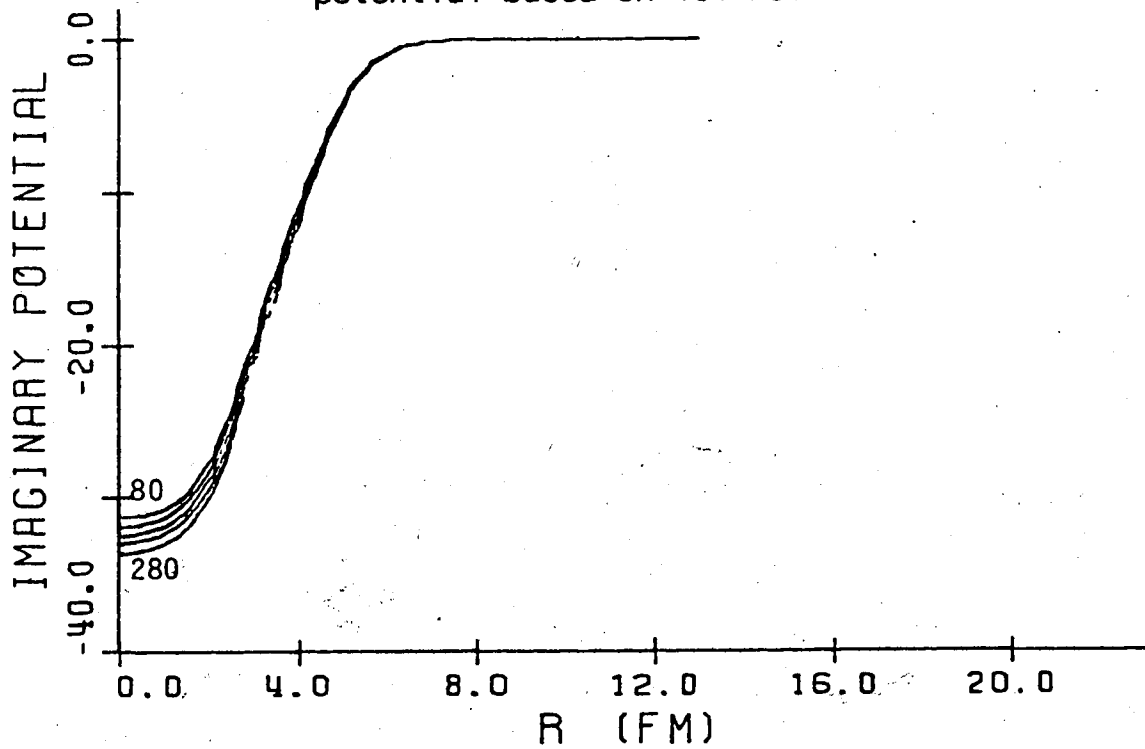
Figure 7.14 The energy dependence of the imaginary central potential based on 181 MeV fit.

99

8. RESULTS OF THE (P,PI) CALCULATIONS

From the literature (Chapter 2) on the non-relativistic ONM we see that the calculations exhibit great sensitivity to the proton and pion distortions and also to the bound state wavefunction used (NO76). We can, it seems, by doing suitable mischief on the bound state potential parameters always get a fit to the (p,π^+) data. This, however, does not mean that the model can be called a success. To illustrate this point we demonstrate how even though we expect the non-relativistic PWBA not to reproduce the data, we can always make it do so.

Consider the simple T-matrix for pionic stripping where the neutron goes into an S-state

$$T_{\mu_i M_6} = \int \psi_6^{+M_6}(r) H_I(r) \psi_{\mu_i}^{(-)}(r) \phi_\pi^{*(-)}(r) d^3r$$

$$8.1$$

If we take the Hamiltonian to be a constant (for the sake of argument as unity) and $\psi_{\mu_i}^{(-)}$ and $\phi_\pi^{*(-)}$ as plane waves,

$$T_{\mu_i M_6} = \int \psi_6^{+M_6}(r) e^{i\underline{q}\cdot\underline{r}} = \phi_6(\underline{q}) \quad , \quad \underline{q} = \underline{k}_p - \underline{k}_\pi$$

$$8.2$$

then given a $T_{\mu_i M_6}(q)$ we can always find a $\phi_6(q)$ to generate it. Because the range of q we want to fit is *finite* and the data has *finite* error bars, once we have $\phi_6(q)$ we can always find a $\psi_6^{M_6}(r)$ which decays exponentially with the correct binding energy. If we define a function $\tilde{T}(q)$ which agrees

with T(q) only for those values of q probed by the (p,π^+) data, then we can find a $\psi_B^{M_\phi}(r)$ given by

$$\psi_B^{M_\phi}(r) = \frac{1}{(2\pi)^3} \int e^{-i\underline{q}\cdot\underline{r}} \tilde{T}_{\mu_i M_B}(\underline{q}) d^3q \qquad 8.3$$

We can then obtain a potential for the bound state given by

$$U_B(r) = \frac{\hbar^2 (\nabla^2 + k^2) \psi_B^{M_\phi}(r)}{2m \, \psi_B^{M_\phi}(r)} \qquad 8.4$$

So the plane wave ONM *can always* explain the data if we allow enough freedom in the binding potential.

Now we expect the binding potential to resemble the nuclear shape in some sense. If we cannot find a potential which gives fits to the (p,π^+) data at several energies and looks 'reasonable', then we must conclude there is in the (p,π^+) reaction, some physics which the model is not describing. In the non-relativistic PWBA, the V(r) given by 8.4 will be a strange shape and will not work at any other energy, this failure tells us that the model is not realistic.

The effective pion nucleus potential is an example of a potential shape which does not follow the nuclear density. The effective potential is derived by starting from a nuclear density, but then non-local and correlation effects change its shape significantly.[1] In evaluating DWBA models for the (p,π^+) reaction, the pertinent question to ask becomes the following:

----

[1] Dahlgren et al. (DA73) give the effective potential shapes.

given that the proton and pion distortions are described correctly by the potentials given in Chapters 4, 5 and 7, is it possible to find neutron binding potentials which look like the nuclear density and give reasonable fits to the (p,π^+) cross-section and analysing power at several energies? For the non-relativistic ONM (and DWBA) the answer is clearly in the negative. It is the purpose of this section to answer the same question for the relativistic ONM (and DWBA) using both pseudoscalar (PS) and pseudovector (PV) coupling for the πNN vertex.

We chose initially for this purpose the nucleus ^{40}Ca as a target for the following reasons:

1. The nucleus is heavy enough to render centre of mass ambiguities unimportant (see appendix C).

2. The ground state in ^{41}Ca is very close to a one particle state (its spectroscopic factor is given by Seth et al. (SE74) as 0.80).

3. Good data exist from threshold up to 200 MeV incident proton energy (PI79b).

Since the analysing power has been measured on ^{12}C at 200 MeV we examine this nucleus as well. Whilst we do not expect treating ^{13}C as an inert ^{12}C core and a 1p1/2 neutron to be a good approximation, our simple model has no way of introducing configuration mixing.

For all the figures in this section we shall denote the pseudoscalar (PS) curves by dashed lines and the curves calculated using pseudovector (PV) coupling as solid curves.

We start by showing in figure 8.1 the results of a PWBA calculation for the cross-section on ^{40}Ca at 160 MeV; the data are from Pile et al. (PI79b). Here, the proton and pion wavefunctions are taken as plane waves, and the vertex is taken to be of pseudoscalar or pseudovector type and the bound state potential geometry is taken to be the same as that obtained in fitting the proton elastic scattering data.

We can see immediately that the pure one nucleon (exchange) mechanism is not in accord with the data. Either we must allow the proton to interact with the target nucleons before emitting the pion, and/or the pion must be allowed to re-scatter from other nucleons.

Let us consider the first possibility, namely that the proton interacts with the target nucleus before emitting the pion; this allows the proton to be off shell when the pion is emitted. We represent an initial proton scattering by means of the optical potential described in Chapter 4. This allows the proton to undergo multiple collisions involving all A target nucleons, possibly entering into various reactions and thereby removing flux from the elastic channel. Strictly speaking we have now a (A+1) nucleon model. However, since A of them are not treated *explicitly* but used as a source of potential and an absorber of energy and momentum, we follow the conventions of the literature and retain the ONM label.

The results of allowing this initial scattering, whilst still using a plane wave for the pion wavefunction, are
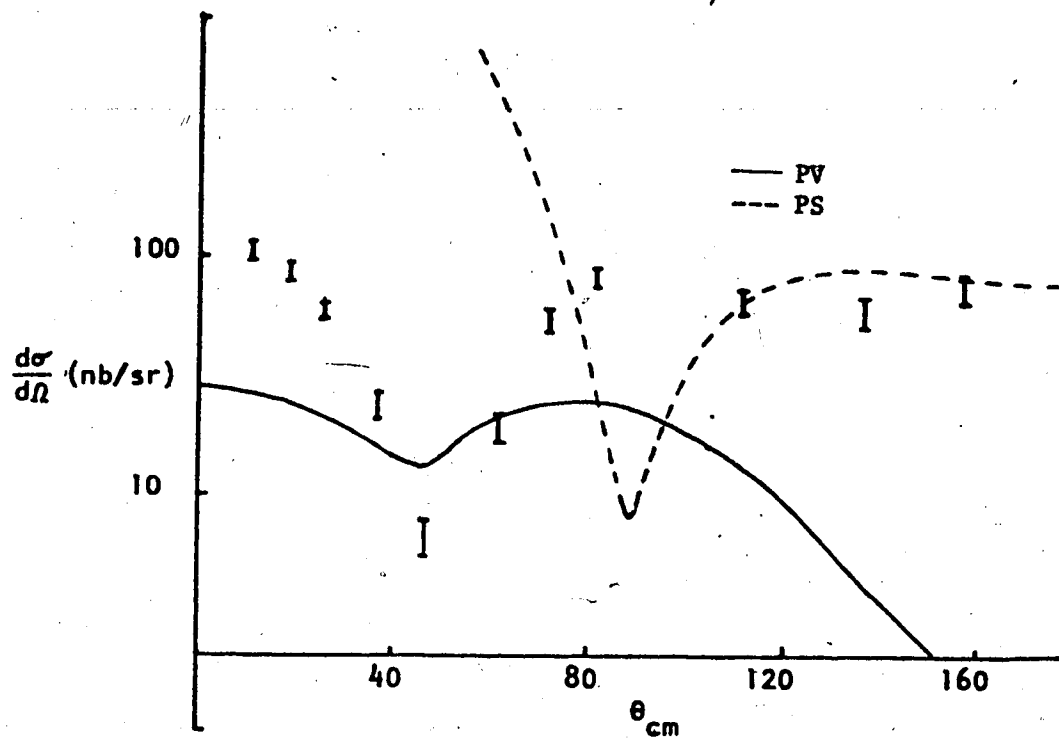
Figure 8.1 PWBA results on ^{40}Ca at 160 MeV.
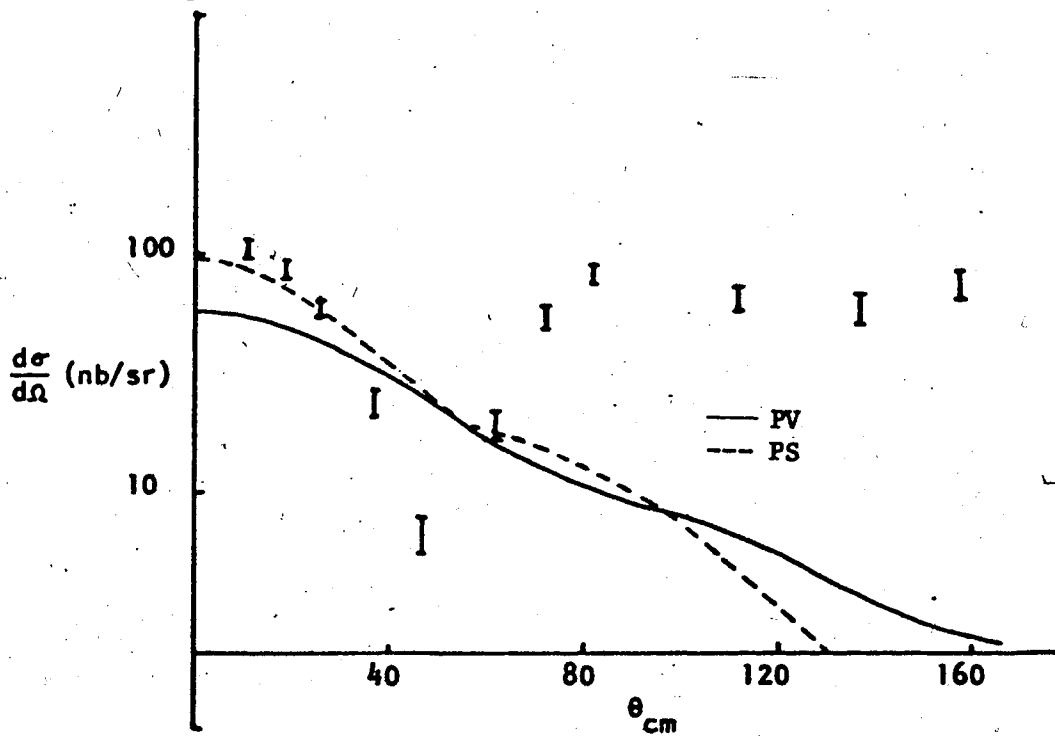
Figure 8.2 The effect of the proton distortion.

shown in figure 8.2. Comparing 8.1 and 8.2, we can see that the curves, especially the PS one, have moved substantially. It is interesting to see that the PV and PS curves are close together and that at 0° they have approximately the correct normalisation. However, the cross-section now lacks the structure seen in the data.

Perhaps the feature missing from the model is that the pion, a strongly interacting particle, will elastically scatter from the nucleons in the final nucleus. This allows now for the possibility that the pion is created (at the πNN vertex) off shell. The results of allowing the pion to re-scatter, whilst not allowing any distortion of the incoming proton, are shown in figure 8.3. The theoretical curves are again very different from the PWBA curves, but still not in agreement with the data. Both curves are well above the data, thus showing that the momentum sharing now allowed by the pion rescattering by far outweighs the flux loss due to pion absorption.

Since we have seen that both proton and pion distortions by themselves are very important, it seems logical to allow not only the incident proton to scatter before emitting the pion, but also to allow the pion to rescatter before leaving the nucleus. In the full DWBA calculation where both pre and post scattering effects are included, none of the "legs" of the vertex needs to be on shell. We show the result of the DWBA calculation in figure 8.4.
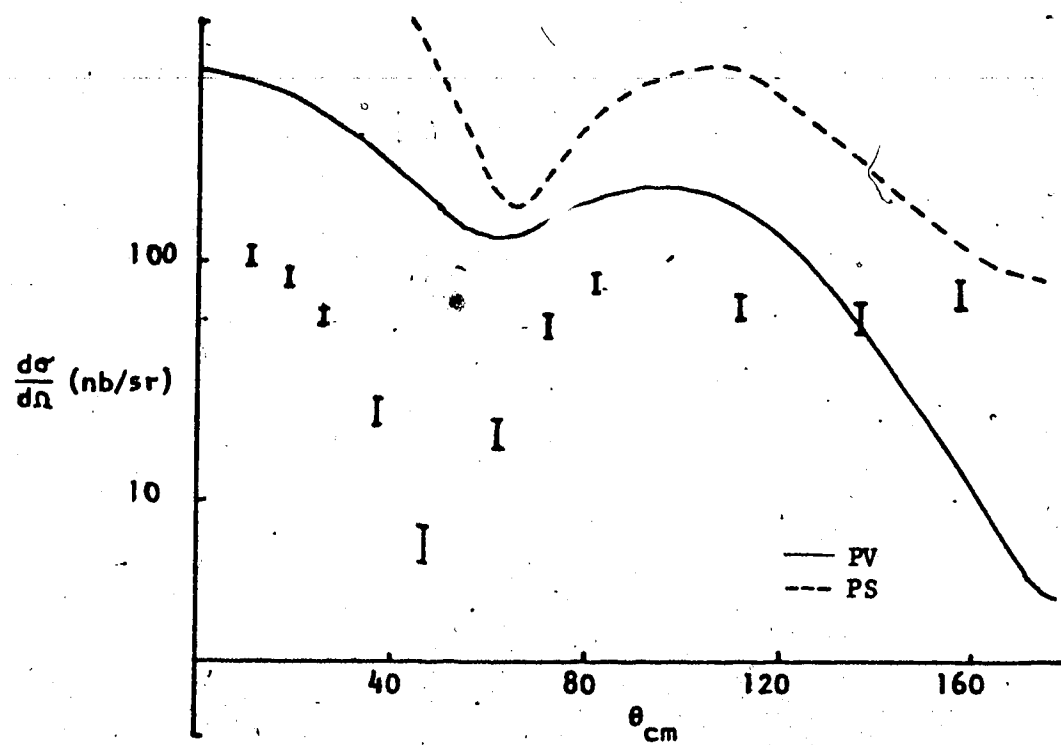
Figure 8.3 The effect of the pion distortion.
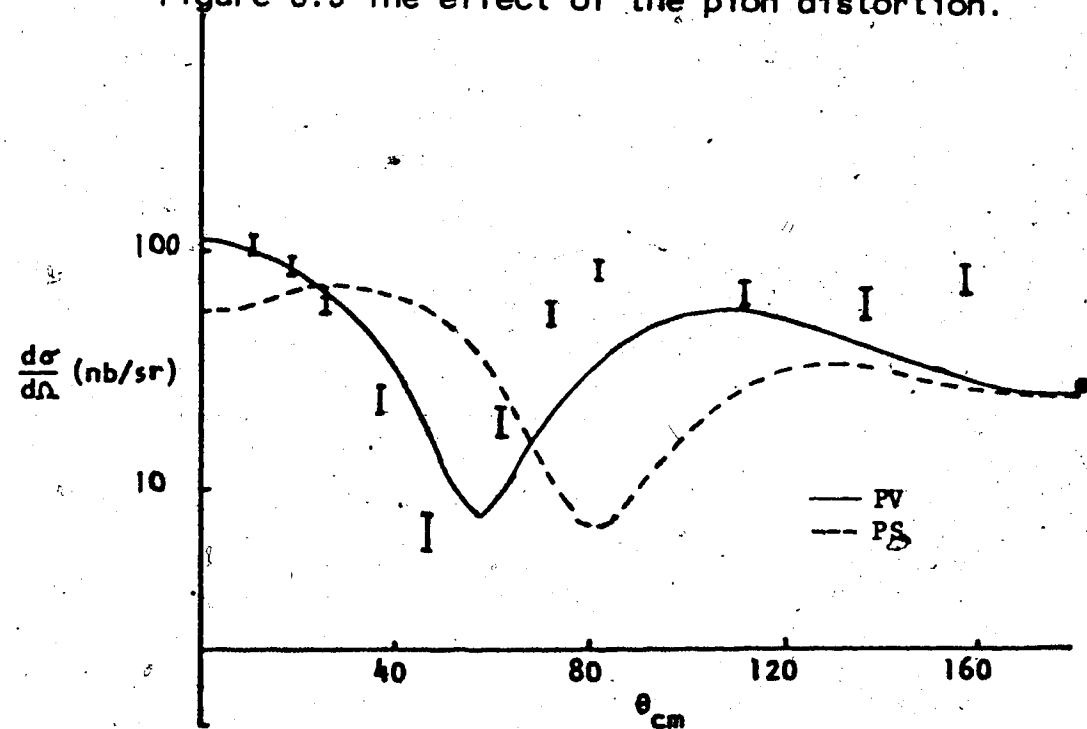
Figure 8.4 The full DWBA calculation.

At present we have not adjusted any parameters except
to fit the elastic scattering data and the binding energy;
and yet the curve calculated from using PV coupling is in
relatively good agreement with the data, whilst the curve
generated from PS coupling is not. It turns out to be
impossible to make the PS curve agree with the data, even if
we allow for small changes in the distorting and binding
potentials. It would entail a rather long sequence of graphs
to demonstrate this here, and so we merely state the main
results which are as follows:

1. Adjusting the bound state potentials appears merely to
   lift or depress the theoretical curve, not change its
   shape.

2. Using class A potentials moves the minimum in to about
   72° but drops the curve so that after 100° it is a
   factor of 7 lower than the data.

   It seems then that a full DWBA calculation involving PV
coupling can explain the (p,π^+) data. In figure 8.5 we show
the results of using class A potentials with PV coupling.
The fit is not as good as with class B potentials but still
the general features of the curve are there; in particular
the minimum has moved forward in angle and agrees exactly
with the data.

   At the beginning of the Chapter we made the comment
that reproduction of the data at one energy is not a
sufficient qualification for the model to be called a
success. In figure 8.7 we show the PV and PS class B
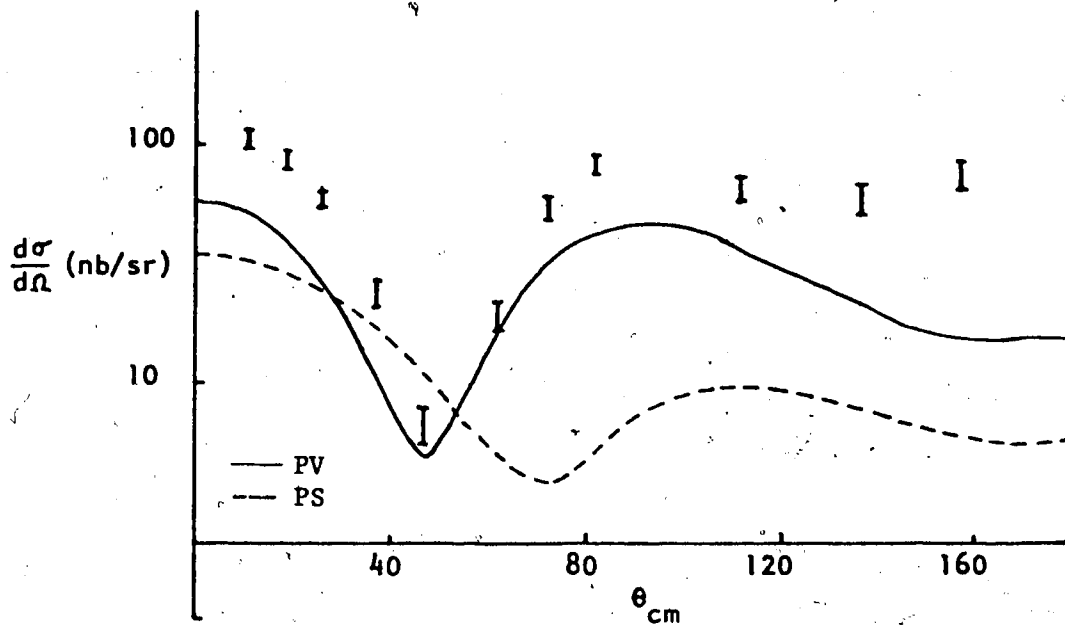
Figure 8.5 The effect of using class A potentials.
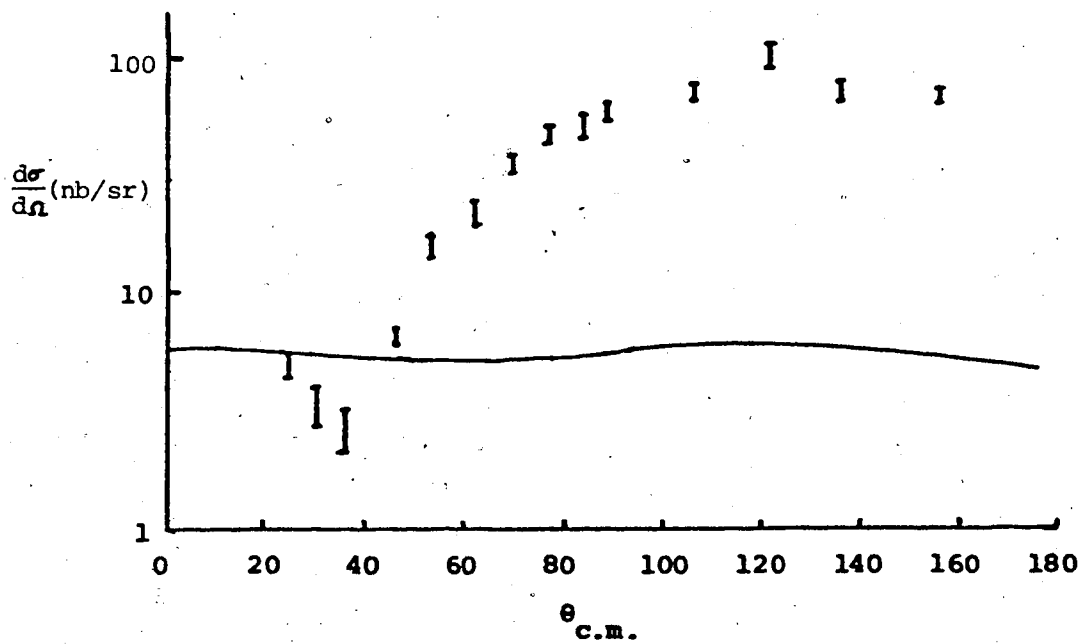
Figure 8.6 146 MeV prediction with no pion distortion and PV coupling.

predictions for 3 energies on ^{40}Ca, the 146 MeV data are from Pile et al. (PI79c) and the 185 MeV data are from Dahlgren et al. (DA74). At 146 MeV we have the problem that no proton elastic scattering data exist; we therefore use the parameters obtained from fitting the 160 MeV data. It is interesting to see that the position of the minimum is the same as at 160 MeV, indicating, perhaps, that the proton distortion is very important in determining the position of the minimum.

In all cases the shape of the data is well reproduced. At 146 MeV the magnitude is rather low. This could be due to the proton absorption called for by fitting the 160 MeV data being too high for the 146 MeV data (as we have seen the (p,π^+) cross-section is very sensitive to the proton distortion). At 185 MeV the momentum transfer at back angles is very large. For example at 180° it is 3.7 fm^{-1}. This means that the (p,π^+) observables are going to be very sensitive to the off shell behaviour of the distorting potentials. There are several reasons for believing the Stricker potential does not extrapolate well off shell (DA73), therefore the deterioration of the DWBA calculations at the larger angles for the 185 MeV and 160 MeV cases can, perhaps, be attributed to this extrapolation becoming unphysical. It is possible to perform phase-shift equivalent transformations on the potential and, whilst maintaining the same fit to the pion elastic scattering, significantly change the (p,π^+) results. Keister (KE80) has shown this can
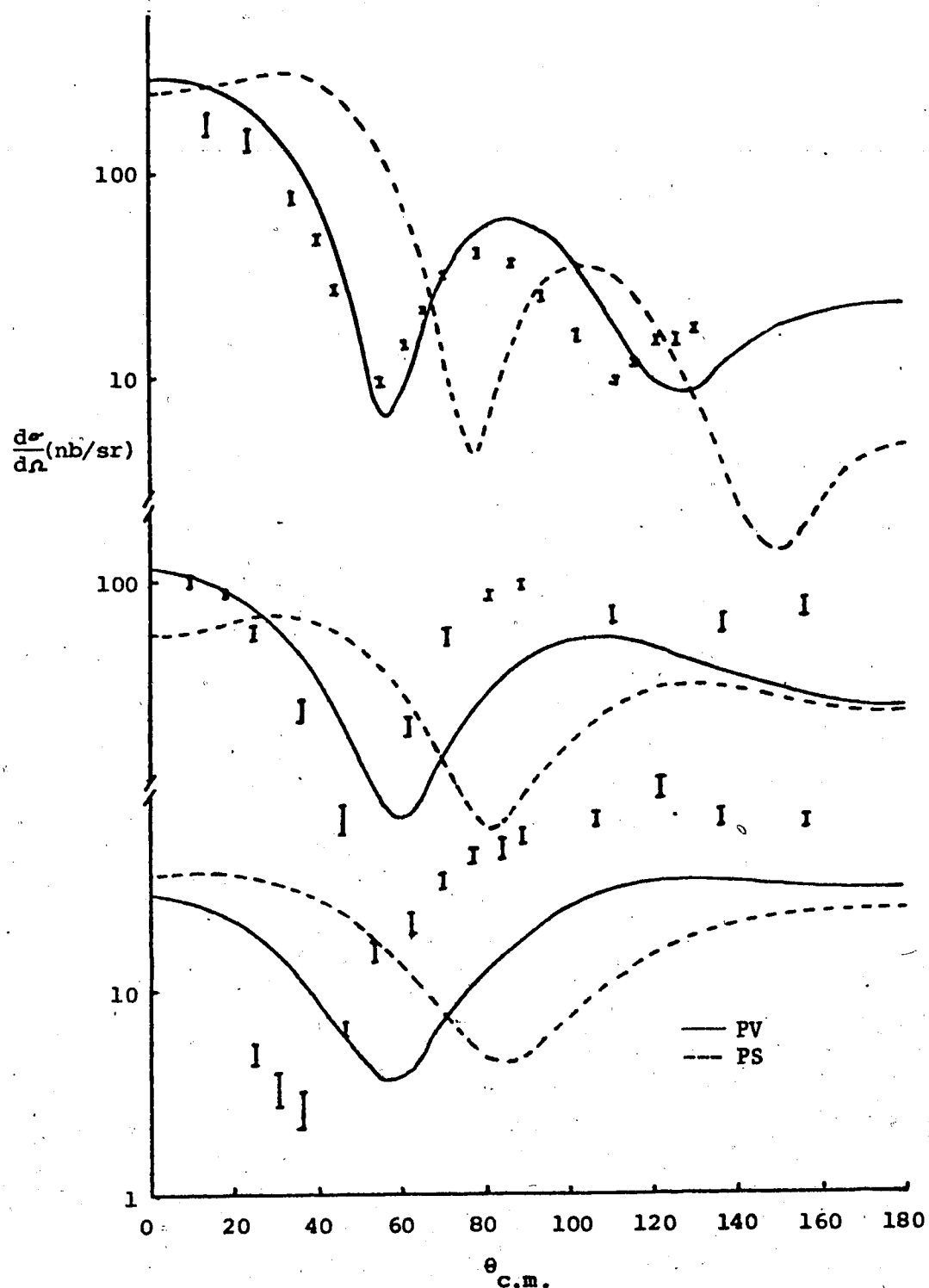
Figure 8.7 DWBA predictions for the $^{40}Ca(p,\pi^+)^{41}Ca$ differential cross-sections using PV and PS vertices, class B proton distortion potentials and bound state potential geometry parameters r=1.0 fm and a=0.65 fm.

lead to differences of around a factor of 2 in the non-relativistic (p,π^+) cross-sections. The effect of a phase-shift equivalent transformation of the kind that Keister suggests (TH81) was investigated for calcium with 146 MeV incident protons. The effects were limited to the back angles where the cross-section was depressed by a factor of 2 and the analysing power was made to go slightly negative after 120°.

One general trend which is most striking is that the PV coupling gives much better agreement with the data than PS coupling. We can say with some confidence that the πNN vertex must involve derivative coupling. This agrees nicely with the constraints imposed on the vertex by PCAC (WO80).

Having concluded that the pion vertex is well described by PV coupling, is it possible to ascertain further information about the two classes of potentials used in the proton distortion? It turns out that the class A potentials give predictions below the experimental data at 146 MeV and 160 MeV. This is not grounds for expulsion, however, since we really cannot say with any confidence that the Woods-Saxon geometry of the bound state potential is well determined by fitting the proton elastic scattering data. It turns out that if we shrink the diffuseness of the binding potential from 0.65 fm to 0.5 fm, then this lifts the curves up to the data. Figure 8.8 shows the result of doing just this for the 3 energies considered in figure 8.7. The PS curves are now in violent disagreement with the data. At 146
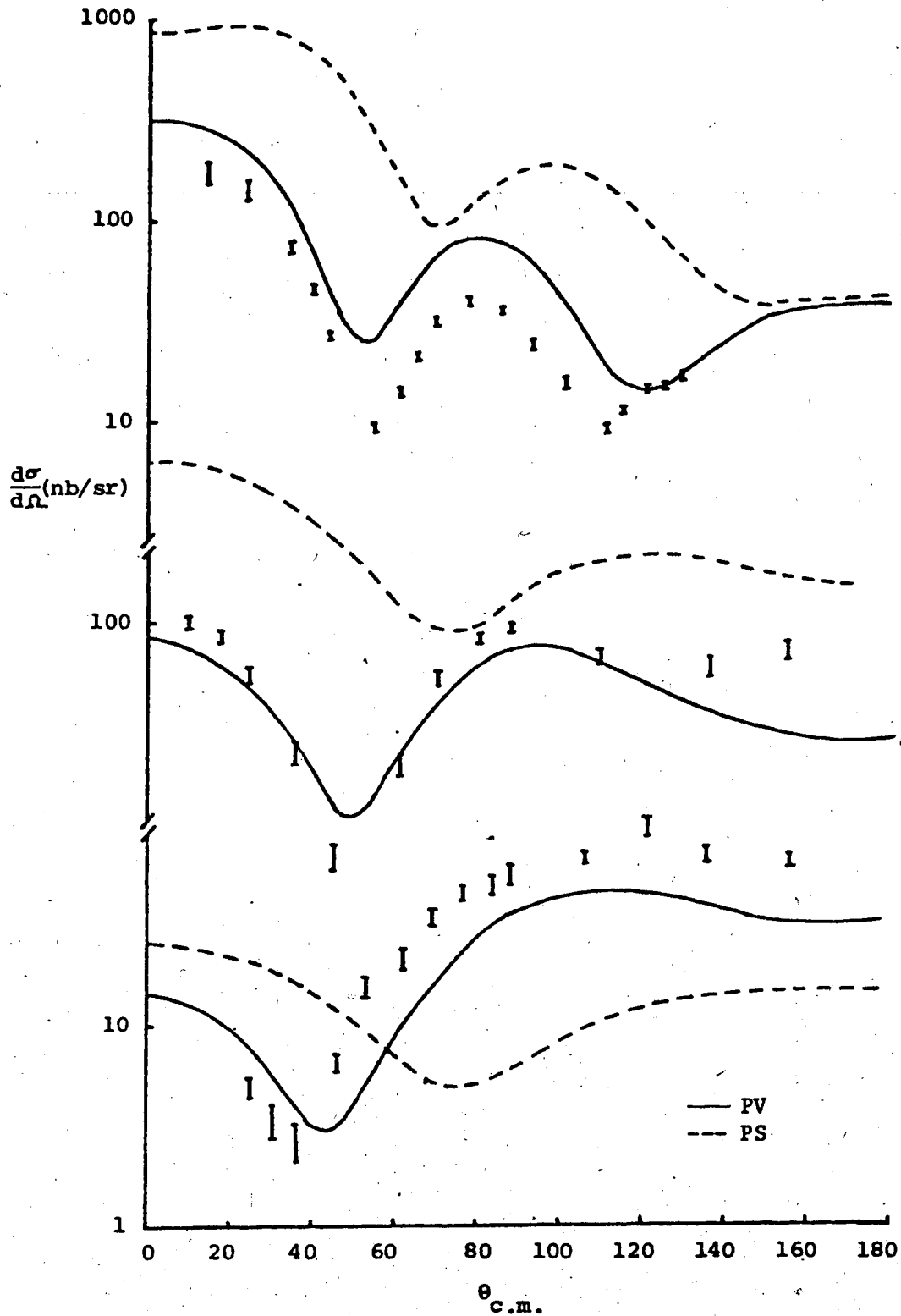
Figure 8.8 DWBA predictions for the $^{40}Ca(p,\pi^+)^{41}Ca$ differential cross-sections using PV and PS vertices, class A proton distortion potentials and bound state potential geometry parameters r=1.0 fm and a=0.5 fm.

and 160 MeV the PV agreement is quite good, even though at
146 we have used the 'wrong' proton distortion obtained from
fitting the 160 MeV data. At 185 MeV, the shrinking of the
diffuseness from 0.65 fm to 0.5 fm has now lifted the curve
above the data, destroying what otherwise was an excellent
fit. Comparison of figures 8.7 and 8.8 gives us an insight
into how poorly determined the proton potential parameters
are. We can, within the constraints of fitting the elastic
scattering data, move the (p,π^+) curves up and down and move
the minima in and out by as much as $10°$. However, we still
cannot get the minima calculated from PS coupling to agree
with the data.

It seems, from considering the cross-section results,
that we can learn two things:

1. There is an evident preference for the PV form of the
    πNN vertex.

2. Class A and class B potentials for the proton distorted
    wave give similar agreement with the (p,π^+) data.

Whilst discussing calcium, we show in figure 8.6 the result
of ignoring pion distortion at 146 MeV. Here, the centre of
mass energy of the pion is only 9.5 MeV. It is interesting
to see that only S-wave pions are produced (indicated by the
flat cross-section); therefore any structure at all in the
cross-section (as well as any non-zero analysing power)
comes from the pions rescattering into P-waves which then
interfere with the S-waves (WO55).

)

We have seen that, with the two above conjectures,[1] we can get fits to the cross-section data. Before concluding that we have solved the (p,π^+) problem, we must consider the analysing power. Since we find the cross-section agreement in DWBA worsens as the momentum transfer increases, it is logical to consider the foreward angle analysing power data. Unfortunately no such data on calcium is available at present. However, good data exist on ^{12}C at 200 MeV (AU78) as well as the corresponding proton elastic data (NA81). For the (p,π^+) calculations we assume that ^{13}C consists of a ^{12}C core with a 1p1/2 neutron (ground state) or with a 2s1/2 neutron (3.09 MeV excited state).

The assumption that ^{13}C consists of a ^{12}C core and a 1p1/2 neutron may not be a good one. For the non-relativistic case it has been shown by Miller (MI74) that configuration mixing effects can alter the differential cross section by around a factor of two. This means that we should not expect to do better than a factor of two in the relativistic calculations. We are, in any event, more interested in the analysing power. As experiments have shown that the analysing power is not sensitive to the final state (AU78),(PI79b), we can expect that it might be less sensitive to configuration mixing. The vector and scalar potentials for the bound neutron are Woods Saxon wells which have radii and diffusenesses given by r=1.0 fm and a=0.4 fm. Figures 8.9 and 8.10 show the predictions of the model for

---

[1] PV coupling and class B distortion

^{12}C at 200 MeV, using class A and class B potentials and PV with PS coupling. We see from figure 8.8 that in all cases the shape of the differential cross-section is reproduced, although the two PS curves tend to be too flat. We expect the curve calculated using PV coupling and a class B proton distortion to be the most realistic; this curve comes within a factor of 3 for angles *larger* than 60° but it is otherwise a little low. For the analysing power (figure 8.10), all the curves follow the same trend, namely being negative up to around 90° and then positive up to 180°. The PS curves both start off in the wrong direction but correct themselves by 40°. The PV class A curve only dips as far as -0.3 at 50° and then goes positive, whilst the PV class B curve is in excellent agreement with the data all the way up to 90°.

This gives ample evidence for the recipe of using PV coupling and the class B potentials. Just to add to the evidence, we show in figures 8.11 and 8.12 the cross-section and analysing power predictions for the ^{16}O(p,π^+)^{17}O(g.s.) reaction at 185 MeV; the data are from (DA74). The proton and neutron potentials are taken to be the same as for calcium at this energy, but scaled down in radius. If instead of using the potential obtained by fitting the calcium data we employ those obtained from fitting the carbon data, the curves move very little.

In figure 8.13 and 8.14 we show the cross-section and analysing power predictions for the reaction ^{12}C(p,π^+)^{13}C(2s1/2, 3.09 MeV). The analysing power is in

$\frac{d\sigma}{d\Omega}$(nb/sr)

$\theta_{c.m.}$
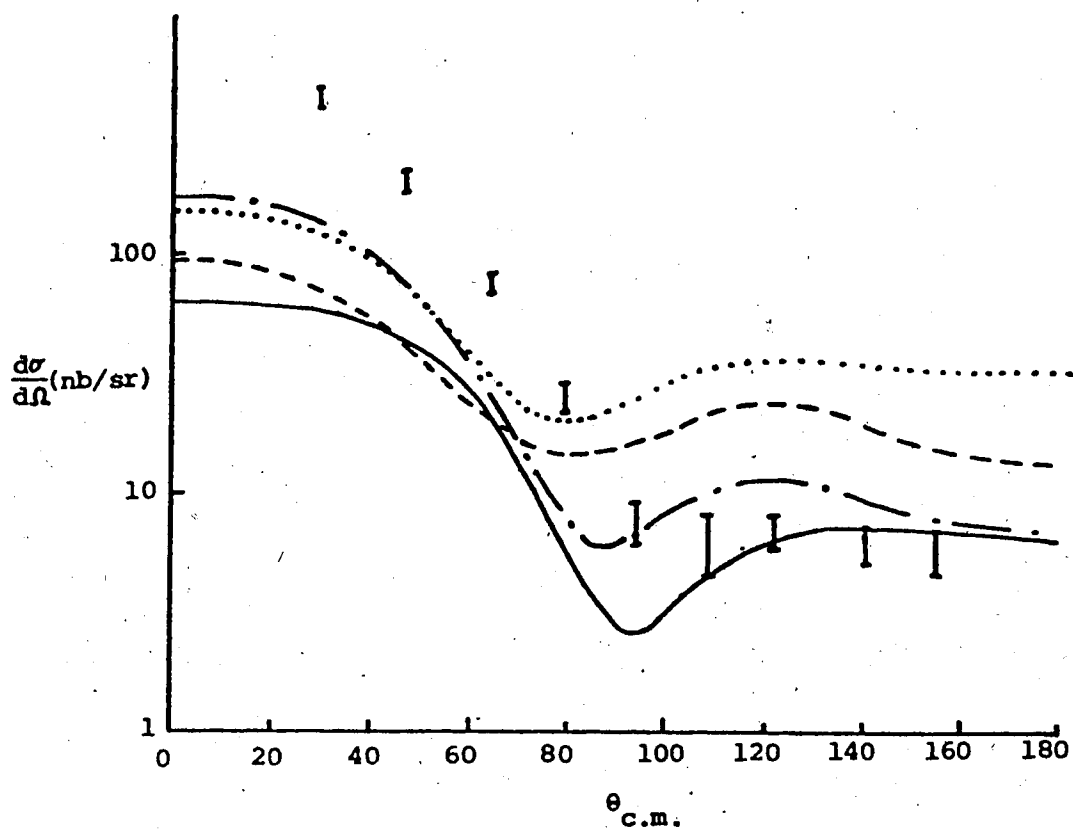
———————— PV Coupling, Class B proton distortion

— · —— · ·— PV Coupling, Class A proton distortion

— — — — — —PS Coupling, Class A proton distortion

················PS Coupling, Class B proton distortion

Figure 8.9 The cross-section prediction for ^{12}C at 200 MeV.

Figure 8.10 The analysing power prediction for ^{12}C at 200 MeV.
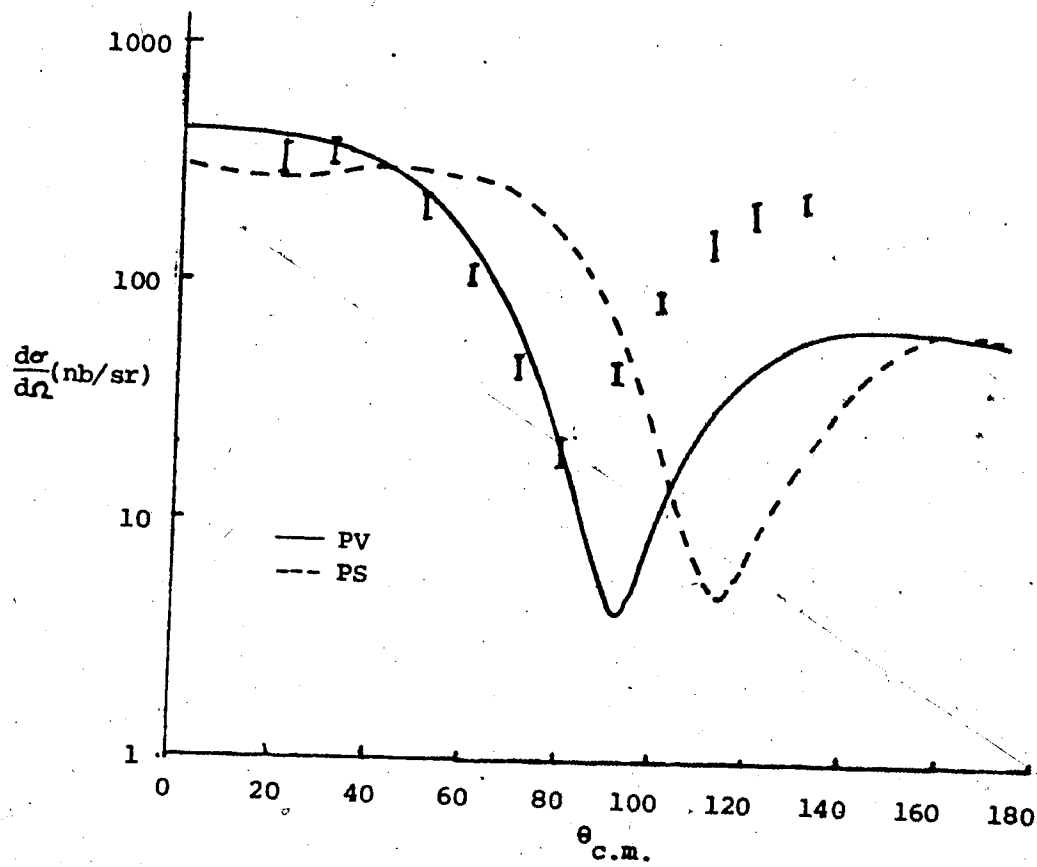
Figure 8.11 185 MeV (p,π⁺) cross Section on ¹⁶0.
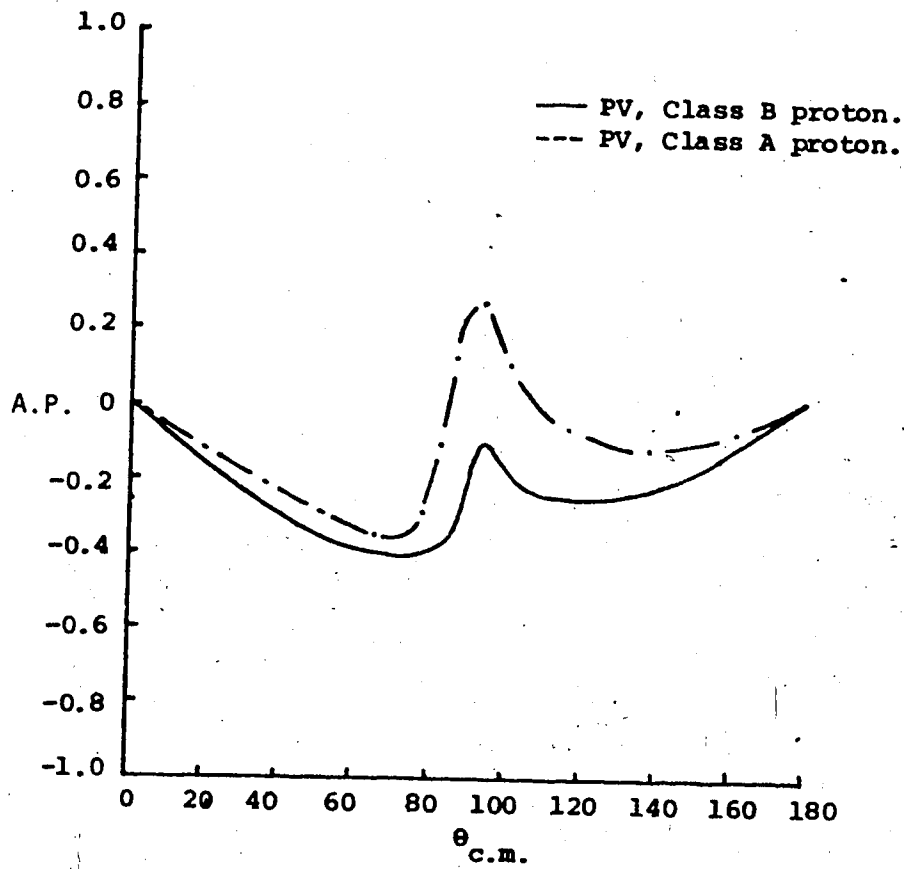
Figure 8.12 185 MeV (p,π⁺) analysing power on ¹⁶O.
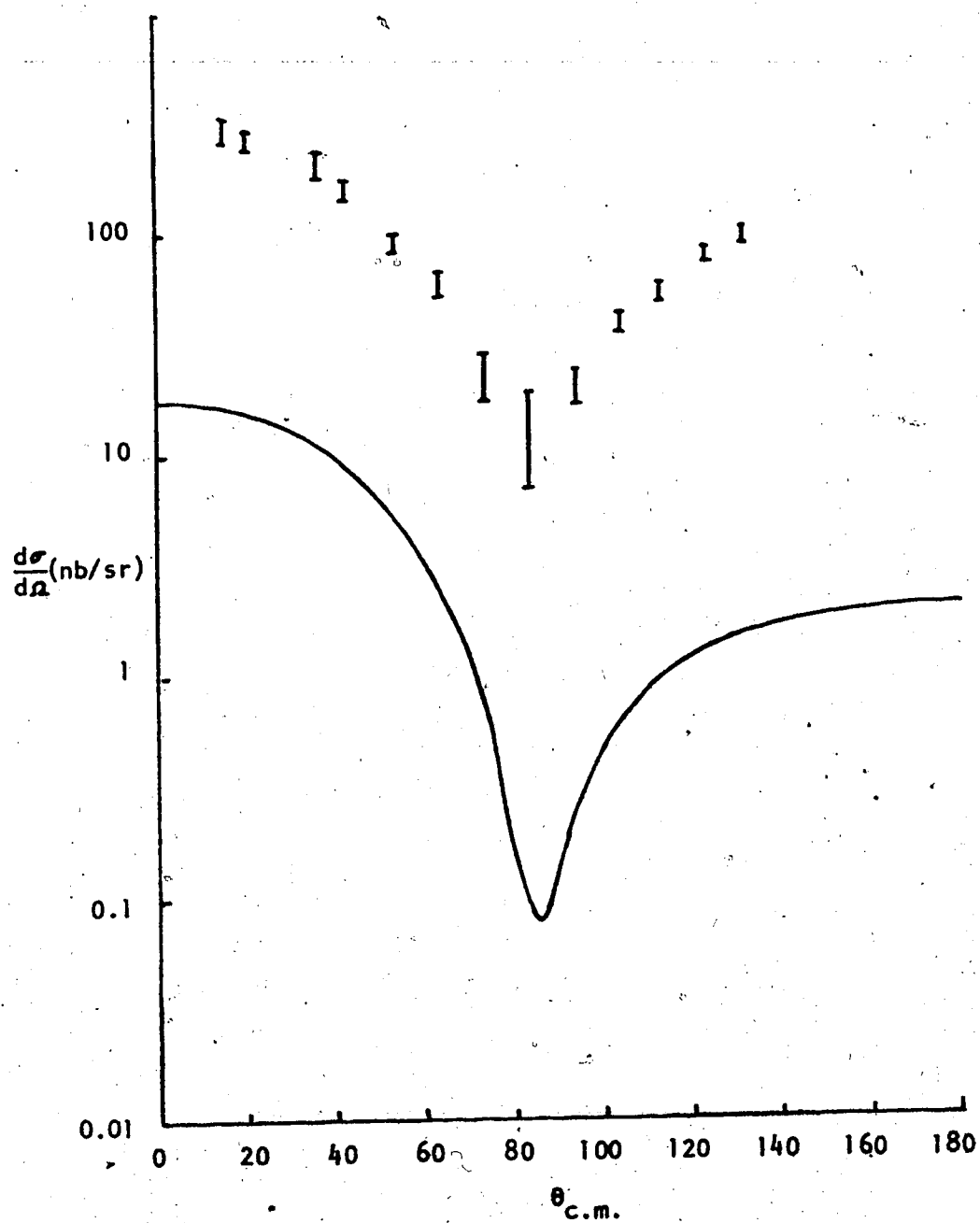
Figure 8.13 185 MeV $^{12}C(p,\pi^+)^{13}C(3.09)$ cross-section.
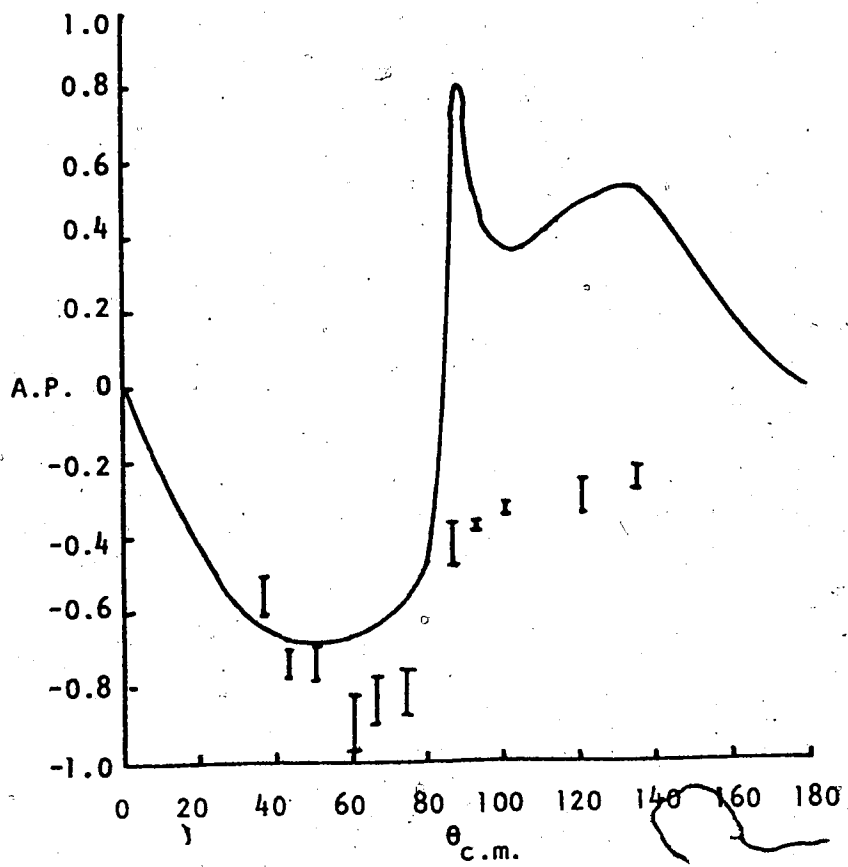
Figure 8.14 185 MeV $^{12}C(p,n^+)^{13}C(3.09)$ analysing power.

good agreement with the foreward angle data, and the shape
of the cross-section is excellent: the normalisation problem
in the cross-section remains somewhat of an anomaly,
possibly configuration mixing is *very* important for this
state.

It is pleasing to see that the 3 analysing powers shown
here all have the same general shape, namely being negative
in the foreward direction and positive in the backward
direction. Whilst we have not shown the analysing power
predictions from the calcium calculations, they too have the
same shape.

9. CONCLUSION

In this Chapter we summarize the information which we can extract from the present study. The Chapter is divided into two sections: what we can learn about the proton-nucleus interaction and what we can learn about the (p,π^+) reaction. Whilst there is much proton elastic scattering and (p,π^+) data available, we have mainly restricted ourselves to analysing the proton elastic scattering data for which (p,π^+) data exist at the same (or a neighbouring) energy.

9.1 The Proton-Nucleus Interaction

We have found that the relativistic approach to proton-nucleus elastic scattering appears to work quite well for most nuclei. The only nucleus that causes problems is ^{4}He, possibly because the nucleus is so light. Generally the fits are at least as good as those generated non-relativistically from a Schrödinger equation.

We can get good fits, even for nuclei with non-zero spin and non-zero isospin, with just using vector and scalar potentials; this indicates that the relativistic Hartree Fock arguments about other Lorentz-type potentials not contributing significantly can be applied to higher energies as well as in nuclear structure. The idea of using vector and scalar mesons to describe proton-nucleus elastic scatting is not new. Duerr (DU56) first derived the model by using arguments about the energy dependence of the effective

non-relativistic optical potential. This work, as well as the work of Arnold et al. (AR78), confirms Duerr's hypothesis. At higher energies flux absorption is very important: we appear to be able to account for it very well by merely making the vector and scalar potentials complex. The reaction cross-sections calculated after fitting the elastic data invariably come out in agreement with the measured values where available. This indicates that the bulk of the proton nucleus interaction can be described in terms of only complex vector and scalar potentials. Notice that for nuclei with non-zero spin and isospin (i.e. ^{8}Be) we can fit the data even though we expect a contribution from the pion field. This pion field is necessary to calculate observables such as the depolarisation (just as in the non-relativistic case where the spin-spin term is necessary). However we expect its effect on the cross-section and analysing power to be small since it is a '1/A' effect.

One feature that emerges naturally is that the non-relativistic equivalent real central potential has a repulsive core at energies above 100 MeV and is energy dependent. These features are now fairly well established.

Both for class A and class B fits the effective non-relativistic real central potential is predicted to be energy dependent. The fact that the 160 MeV parameters are good at predicting the 181 MeV, and 200 MeV data is an indication that the energy dependence is probably of the

right magnitude, but we do not expect it to be exact.

Since the imaginary potential arises from coupling to the open inelastic channels rather than from some fundamental interaction as in the case of the real potential, it is perhaps unreasonable to ask that its energy dependence should come out correctly. The analysis by Nadasen et al (NA81) shows that from 40 meV to 180 MeV the imaginary potential is roughly constant. This is actually the case for the small W (class B) fits as shown in figure 7.14. The large W fits (class A) predict a large energy variation (AR80). However we must be cautious not to exclude them for this reason, since at higher energies we anticipate the imaginary potential will vary more with increasing energy. This has been shown in the study on ^{4}He by Leung and Sherif (LE78).

If we must at some point choose between the two classes of potentials, then the small W class (class B) appears most realistic for the following reasons (in order of increasing importance)

1. The physics of a little flux being absorbed by both potentials is more realistic than one swallowing far too much flux and the other putting most of it back into the elastic channel.

2. The wavefunctions calculated from both classes of potential correctly predict the (p,π^+) cross-sections, but only class B distortions correctly predict the analysing power data on ^{12}C (at least for the smaller

momentum transfers).

3. The energy dependence of the effective non-relativistic imaginary potential is more in line with the ordinary non-relativistic analyses (NA81).

9.2 Pion Production

By examining the graphs in Chapter 3 for the single particle wavefunctions in momentum space, we can see that at the momentum transfers encountered in the (p, π^+) reaction the lower components are just as large as the upper components. Thus any non-relativistic theory which uses a Foldy Woulthousen reduction of the vertex (i.e. treating g as small) is doomed to failure. Indeed, to date there is no non-relativistic calculation that gives both the energy and angular dependences of the cross-sections, let alone having simultaneously the correct analysing power.

Provided we use a proton distorted wave generated from a class B optical potential which affords a good fit to the elastic data, PV coupling for the πNN vertex, the Stricker potential to distort the outgoing pion and a bound state generated using the strong oppositely signed potentials, then we can say the following:

1. The observed cross-sections in the case of $^{40}Ca(p, \pi^+)^{41}Ca$ in the energy range 146-185 MeV can be reproduced to a good approximation. The agreement at forward angles is quite good for energies above 160 MeV.

2. The cross-sections for proton induced pion production on

^{12}C leading to the ground state and the state at 3.09 MeV are qualitatively reproduced. In particular, the backward peaking of the differential cross-section of the excited state is correctly predicted by the model, in contrast to the non-relativistic result for this state (PI79b).

3. For angles less than 90° the analysing powers are well reproduced. One feature which is most promising is that the analysing powers to the ground and excited (3.09 MeV) states in ^{12}C are similar, in agreement with the experimental data (AU78). This is a feature which has not been present in any theory so far.

From comparing the pseudovector and pseudoscalar couplings we can see immediately that the PS coupling does not agree with the data to the same extent that the PV coupling does (generally the cross-section minima tend to be too far out in angle and the analysing power has the wrong sign for small angles). This is striking evidence to add to the requirements of PCAC to eliminate PS coupling as a candidate for the πNN vertex.

From figures 8.3 and 8.4 we can see that the (p,π^+) reaction is very sensitive to the pion distortion. The fact that the Stricker potential can give such good agreement with the data allows us to say that as long as we do not go *too* far off shell then the Stricker potential describes well the pion-nucleus interaction up to 50 MeV.

9.3 Future Development

In this thesis we have developed a model for the (p,π^+) reaction in the framework of a relativistic DWBA formalism. This DWBA formalism is by no means limited to (p,π^+), it can also be applied to such reactions as (p,p'), (p,γ), (p,d) and $(p,2p)$.

The second of these, (p,γ), is very attractive since it shares the proton distortion and bound state wavefunctions with (p,π^+), but does not have any of t. incertainties associated with the pion rescattering. Thus (p, γ), along with the proton elastic scattering data, can be expected to reduce ambiguities in the proton distortion and the bound state wavefunctions.

The (p,d) and $(p,2p)$ reactions can also probe the higher momentum components of the nuclear wavefunctions, thus they too can be expected to add information to that attainable from (p,γ).

One interesting application of the model is to notice that we have a good fit to the proton elastic scattering data on ^8Be. This nucleus has neither zero spin nor zero isospin, which means we can expect it to have a significantly large pion field, which will give rise to a pseudo-scalar potential. This potential can be calculated by a simple folding model and should give rise to a definite prediction for the depolarisation parameter. This parameter has been measured (RO81): thus we have a good test of the idea that the class A potentials are realistic, and are

somehow causing the calculations to behave in a manner which resembles a coupled channel calculation.

There are 2 competing mechanisms to the (p,π^+) stripping mechanism as shown in figure 9.1.
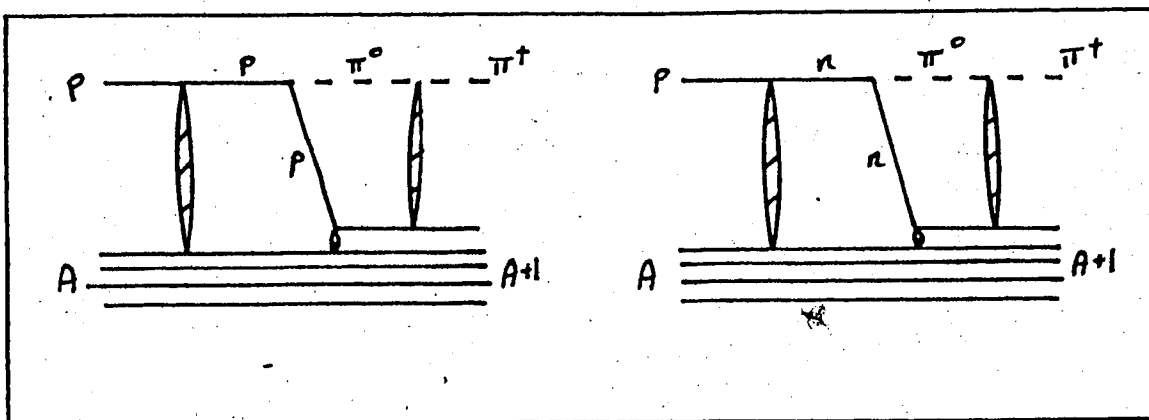
Figure 9.1 Competing mechanisms for the (p,π^+) reaction

These should be of the order of the (p,π^-) reaction, which the data show to have a cross-section about a factor of 10 lower than that of the (p,π^+) reaction. The reason for this is that the (p,π^-) reaction goes by a charge exchange and so we can expect it to be less probable. The agreement with the data on ^{40}Ca confirms that these effects are indeed small. An added attraction to calculating the contributions from the graphs shown in figure 9.1, is that we can extract the T-matrix for the (p,π^-) reaction.

Even in its present form, the (p,π⁺) reaction can be
used as a probe of the off-shell parts of the pion-nucleus
potential. It would be interesting to see the effects of
treating the pion relativistically, i.e. putting the
Stricker potential into a Klein-Gordon equation instead of a
Schrödinger equation. As Johnson and Ernst have indicated
(JO79), the wavefunctions so generated are quite different
in the nuclear interior; thus we may expect to see
significant differences in the calculated (p,π⁺)
observables.

Bibliography

AB70 M.Abramowitz and I.A. Stegen. *Handbook of Mathematical Functions*. Dover Publications N.Y. (1970).

AL78 M.A. Alberg, E.M. Henley, J.F. Walker and G.A. Miller. Nucl. Phys. <u>A306</u> (1978) 447.

AM80 R.D. Amado, F. Lenz, J.A. McNeil and D.A. Sparrow. Phys. Rev. <u>C22</u> (1980) 2094.

AR79 L.G. Arnold, B.C. Clark and R.L. Mercer. Phys. Rev. <u>C19</u> (1979) 917.

AR80 L.G.Arnold, B.C. Clark,R.L. Mercer and P. Schwandt. OSU Preprint OSU-TR-80-351

AU78 E.G. Auld, A. Haynes R. Johnson, G. Jones, T. Masterson, E.L. hie . Ottewell, P. Walden and B. Tatischeff. Phys. Rev. Lett. <u>41</u> (1978) 462.

BA69 M.V. Barnhill. Nucl. Phys. <u>A131</u> (1969) 106.

BE69 P.R. Bevington. *Data Reduction and Error Analysis for the Physical Sciences. McGraw Hill (N.Y.) 1969*.

BJ64 *J. D. Bjorken and S.D. Drell. Relativistic Quantum Mechanics*. McGraw-Hill (1964).

BL67 J. BLATT. Journal of Computer Physics <u>1</u> (1967) 382.

BO74 Y. LeBornec,B. Tatischeff,L. Bimbot, I. Brissaud, J.P. Garron, H.D. Holmgren,F.Reide and N. Willis. Phys. Lett. <u>49B</u> (1974) 434.

BO76 Y. LeBornec,B. Tatischeff,L. Bimbot, I. Brissaud,H.D. Holmgren,J. Källne, F. Reide and N. Willis. Phys. Lett. <u>61B</u> (1976) 47.

BR77 R. Brockman and M. Dillig. Phys. Rev. C15 (1977) 361.

BR78 R. Brockman. Phys. Rev. C18 (1978) 1510.

CH51 G.F. Chew, M.L. Goldberger, J.M. Steinberger and
C.N. Yang. Phys. Rev. 84#3 (1951) 581.

CH68 I. Cheon. Prog. T. Phys. Supp. Extra. (1968) 146.

CO10 P.H. Cowell and A.C.D. Cromelin. *Appendix to Greenwich
Observatory for 1909 Edinborough* (1910) 62.

DA73a S. Dahlgren,P. Grafstrom, B. Höistad and A. Asberg.
Nucl. Phys. A211 (1973) 243.

DA73b S. Dahlgren,P. Grafstrom, B. Höistad and A. Asberg.
Nucl. Phys. A204 (1973) 53.

DA74 S. Dahlgren,P.Grafstrom, B. Höistad and A. Asberg.
Nucl. Phys. A227 (1974) 245.

DU56 H.P. Duerr. Phys. Rev. 103 (1956) 469.

ED62 S.F. Edwards and A.D. Kanaris. Nucl. Phys. 33 (1962)
388.

EI73 J.M. Eisenberg, R. Guy, J.V. Noble, and H.J. Weber.
Phys. Lett. 43B (1973) 20.

EL53 L.R.B. Elton. Proc. Phys. Soc. (London) A66 (1953) 806.

ER66 M. Ericson and T.E.O. Ericson. Ann. Phys. 36 (1966)
323.

FE77 H. Fearing Phys. Rev. C16 (1977) 313.

FE80 H.W.^Fearing. TRIUMF Preprint TRI-PP-80-27. (To be
published in Progress in Particle and Nuclear Physics).

FO49 L.L. Foldy and R.E. Marshak Phys. Rev. $\underline{75}$ (1949) 1493.

FR74 J.L. Friar, Phys. Rev. $\underline{C10}$ (1974) 955.

GE54 M. Gell-Mann and K. Watson. Ann. Rev. Nucl. Sci. $\underline{4}$ (1954) 219.

GE60 M. Gell-mann and M. Levy. Nuovo Cimento $\underline{16}$ (1960) 705.

GI77 W.R. Gibbs and A.T. Hess. Phys. Lett. $\underline{68B}$ (1977) 205.

GI78 S.K. Yound and W.R. Gibbs. Phys. Rev. $\underline{C17}$ (1978) 837.

GR74 Z. Grossman, F. Lenz and M.P. Locher. Ann. Phys. $\underline{84}$ (1974) 348.

GR79 A.R. Green and E. Maqueda. Nucl. Phys. $\underline{A316}$ (1979) 215.

GR80 J.M. Greben and R.M. Woloshyn Nucl. Phys. $\underline{A333}$ (1980) 399.

HE43 Heitler and Peng. Proc. Roy. Irish. Acadamy $\underline{49A}$ (1943) 1.

HQ76 B. Höistad Invited Talk to the Topical Meeting on Intermediate Energy Physics, March 31 to April 10 1976.

HO77 B. Höistad. *Proceedings of the Seventh International Conference on High Energy Physics and Nuclear Structure.* Zürich. (1977) 215.

HO78 B. Höistad, T. Johannson and O. Jonsson . Phys. Lett. $\underline{79B}$ (1978) 385.

HO79 B Höistad, S. Dahlgren, T. Johannson and O. Jonsson. Nucl. Phys. $\underline{A319}$ (1979) 409.

HU81 D.A. Hutcheon, E.D. Cooper, P. Kitching, H.S. Sherif, J.M. Cameron, R.P. Liljestrand, C.A. Miller,

W.J. McDonald, D.M. Sheppard, W.C. Olsen, G.C. Neilson, D.K. McDaniels, J.R. Tinsley, L.W. Swenson, P. Schwandt, C.E. Stronach and L. Ray. *Elastic Scattering of Protons on ^{40}Ca and ^{208}Pb at 200-500 MeV*.Abstract submitted to Ninth International Conference on High Energy Physics and Nuclear Structure (Paris 1981).

IU79 Indiana University Cyclotron Facility Annual Report 1979.

JA80 M. Jaminon, C. Mahaux and P. Rochus. Phys. Rev. C22 (1980) 2027.

JE77 J.P. Jeukenne, A. Lejeune and C. Mahaux. Phys. Rev. C16 (1977) 80.

JO70 W.B. Jones and J.M. Eisenberg. Nucl. Phys. A154 49.

JO79 M.B. Johnson and D.J. Ernst. Phys. Rev. C20 (1979) 1064.

KE73 M.P. Keating and J.G. Willis. Phys. Rev. C7 (1973) 1336.

KE80 B.D. Keister. Nucl. Phys. A350 (1980) 365.

KU77 K. Kume and H. Ohtsubo. Prog. T. Phys. 58 (1977) 575.

LE76 T.S.H. Lee and S. Pittel. Nucl. Phys. A256 (1976) 509.

LE78 S.W.L. Leung and H.S. Sherif. Can. J. Phys 56 (1978) 1116.

LI73 T.K. Lim Phys. Lett. 44B (1973) 341.

LI78 M.J. Lighthill. *Fourier analysis and Generalised Functions* Cambridge University press (1978).

ME58 A. Messiah *Quantum Mechanics*. J. Wiley and Sons inc.

(1958).

ME72 R.L. Mercer. PhD Thesis. Univ. of Illinois (1972).

ME80 D.F. Measday and G.A. Miller. Annual Review of Nuclear
and Particle Science $\underline{29}$ (1970) 121.

ME66 M.A. Melkanoff, T. Sawada and J. Raynal. J. Comp. Phys.
$\underline{6}$ (1966) 1.

ME81 H.O. Meyer, P. Schwandt, G.L. Moake and P.P. Singh.
Phys. Rev. $\underline{C23}$ (1981) 616.

MI72 L.D. Miller and A.E.S. Green. Phys. Rev. $\underline{C5}$ (1972) 241.

MI74 G.A. Miller. Nucl. Phys. $\underline{A224}$ (1974) 269.

MI76 L.D. Miller and H.J. Weber. Phys. Lett. $\underline{64B}$ (1976) 279.

MO48 C. Morette and H.W. Pang. Proc Roy. Irish Academy $\underline{51A}$
217.

MO80 G.A. Moss, L. Greeniaus, J.M. Cameron, D.A. Hutcheon,
R.L. Liljestrand, C.A. Miller, G. Roy, B.K.S. Koene,
W.H.T. Van Oers, A.W. Stetz, A Willis and N. Willis
Phys. Rev. $\underline{C21}$ (1980) 1932.

NA81 A. Nadasen, P. Schwandt, P.P. Singh, W.W. Jacobs
A.D. Bacher, P.T. Dedevec, M.D. Kaitchuck and
J.T. Meek. Phys. Rev. $\underline{C23}$ (1981) 1023.

NO24 B.V. Noumerov. Monthly notices of the Royal
Astronomical Society. $\underline{84}$ (1924) 592.

NO75 J.V. Noble. Nucl. Phys. $\underline{A244}$ (1975) 526.

NO76 J.V. Noble. Phys. Rev. Lett. $\underline{37}$ (1976) 123.

NO76b J.V. Noble. Proceedings of the International Topical

Conference on Meson Nuclear Physics. Ed. P.D. Barnes,
R.A. Eisenberg, L.S. Kisslinger. (N.Y. AIP pp 221-236)

PI79a H.M. Pilkuhn. *Relativistic Particle Physics.*
Springer-Verlag, N.Y. Inc. (1979) 71.

PI79b P.H. Pile, R.D. Bent, R.E. Pollock, P.T. Debevec,
R.E. Marrs, M.C. Green, T.P. Sjoreen and F. Soga. Phys.
Rev. Lett $\underline{42}$ (1979) 1461.

PI79c P.H. Pile, T.P. Sjoreen, R.E. Pollock, R.D. Bent,
M.C. Green, W.W. Jacobs, H.O. Meyer and F. Soga. IUCF
report (1979) 63.

RO57 M.E. Rose *Elementary Theory of Angular Momentum.*
J. Wiley & Sons N.Y. (1957).

RO65 P.G. Roos and N.S. Wall. Phys. Rev. $\underline{140}$ (1965) B1237.

RO67 L.S. Rodberg and R.M. Thaler *Introduction to the
Quantum Theory of Scattering.* Academic Press (1967).

RO73 E. Rost and P.D. Kunz. Phys. Lett. $\underline{43B}$ (1973) 17.

RO81 G. Roy, H.S. Sherif, G.A. Moss, L.G. Greenius,
C.A. Miller, R. Liljestrand, D.P. Gurd, G.M. Stinson,
E.D. Cooper, J. Soukup, H. Wilson and R. Abegg.
Abstract submitted to Ninth International Conference on
High Energy Physics and Nuclear Structure. Paris 1981.

SC57 J. Schwinger. Ann. Phys. (N.Y.) $\underline{2}$ (1957) 407.

SE74 K.K. Seth and S.G. Iversen. Phys. Lett. $\underline{53B}$ (1974) 171.

SH81a H.S. Sherif and R.S. Sloboda. Phys Lett $\underline{99B}$ (369)
1981.

SH81b H.S. Sherif *Private communication.*

SH79 *H.S. Sherif, S.W. Leung, A.W. Thomas and G. Brookfield.*

Phys. Lett. <u>83B</u> *(1979) 293.*

SI78 E.R. Siciliano and R.M. Thaler. Phys. Rev. Lett. <u>41</u> (1978) 927.

ST78 K. Stricker. *Contributed paper to the Los Alamos Summer School on Nuclear Science* June 1978.

ST79 K. Stricker, H. McManus and J.A. Carr. Phys. Rev. <u>C19</u> (1979) 929.

ST80 K. Stricker, J.A. Carr and H. McManus. Phys. Rev. <u>C22</u> (1980) 2043.

TH81 A.T. Thomas. *Private communication.*

TS80 M.Tsangrides, J.G. Wills and R.D. Bent. IUCF Annual Report (1979) 60.

WA74 J.D. Walecka. Ann. Phys. <u>83</u> (1974) 491.

WE78 H.J. Weber and J.M. Eisenberg. Nucl. Phys. <u>A312</u> (1978) 201.

WO55 L. Wolfenstein. Phys. Rev. <u>98</u> (1955) 766.

WO80 R. Woloshyn. Nucl. Phys. <u>A336</u> (1980) 499.

YE54 D.R. Yennie, D.G. Ravenhall and R.N. Wilson. Phys. Rev. <u>95</u> (9154) 500.

APPENDIX A. NUMERICAL INTERGRATION

Here we discuss the numerical solution of equations of the
form

$$y''(r) = f(r) y(r)$$

<div align="right">A.1</div>

This equation is of the type encountered in not only the
proton and pion distorted waves, but also in the bound state
calculation. We employ a modification of the Noumerov method
(NO24) due to Raynal(ME66).

The Noumerov method itself is a modification of a
method proposed by Cowell (CO10). The essence of the Cowell
method is as follows,

Taylor's theorm gives us,

$$y(r+h) = \sum_{n=0}^{\infty} \frac{h^n y^{(n)}(r)}{n!}$$

<div align="right">A.2</div>

$$y(r-h) = \sum_{n=0}^{\infty} \frac{(-h)^n y^{(n)}(r)}{n!}$$

<div align="right">A.3</div>

therefore

$$y(r+h) + y(r-h) = 2 \sum_{n=0}^{\infty} \frac{h^{2n} y^{(2n)}(r)}{(2n)!}$$

<div align="right">A.4</div>

if we differentiate this equation, use equation A.1 and
subtract from equation A.4 after multiplying by $h^2/12$ we get

$$y(r+h)(1-T(r+h)) + y(r-h)(1-T(r-h)) = y(r)(2 + 10T(r)) + o(h^6)$$

A.5

where we have defined

$$T(r) = \frac{h^2}{12} f(r)$$

A.6

From equation A.6 we see that if we know y(0) and y(h) then we can get y(2h). This makes the method self-starting since we put y(0)=0, choose an arbitrary small number for y(h) and obtain the overall normalisation later from matching to the Coulomb wave-functions in the elastic scattering case, or by the requirement of unit total probability for the bound state.

One problem that occurs for the larger values of 'L' is that the solution grows initially like r^L and so can overflow the machine after a few steps. We can get around this by noticing that if our regular solution is growing like r^L then the irregular solution will be shrinking like r^{-L}. This means we can pick a starting point away from the origin, and the errors made in assuming y(nh)=0 go rapidly to zero.

Noumerov suggested the following substitution;

$$w(r) = y(r)(1 - T(r))$$

A.8

The Cowell formula becomes

$$w(r+h) + w(r-h) = \left(\frac{2 + 10\,T(r)}{1 - T(r)} \right) w(r)$$

A.8

This runs very quickly on a computer, roughly twice as fast as the Cowell method. It does have a drawback however, that is if we want y(r) as an array we have to divide each time by (1 - T(r)) - generally if the potentials are complex so is T(r), this penalty exactly redresses the balance, and so Noumerov and Cowell methods take the same time. If, as in the case of the search program *RUNT* where we are only interested in the phase shift the Noumerov method keeps its factor of 2 advantage in speed.

A modification to speed things up further (ME66) in the Noumerov method is to notice that in evaluating

$$\frac{2 + 10\,T(r)}{1 - T(r)}$$

A.9

we have a complex divide. Since we are discarding terms of order h^6 we may write this as

$$\frac{2 + 10\,T}{1 - T} = (2 + 10T)(1 + T + T^2 + \ldots) = 2 + 12T(1+T) + o(h^6)$$

A.10

The modified Noumerov algorithm becomes

$$w(r+h) + w(r-h) = \left(2 + 12\, T(r)\big(1+T(r)\big)\right) w(r)$$

It turns out this formula is actually more accurate than the Noumerov method, the sign of the terms $o(h^6)$ being discarded are usually opposite to those discarded earlier. The interested reader is referred to (ME66).

One furthur note for the practioner. Clearly we are going to use the modified Noumerov method in *RUNT* where we do not want to keep the wave-function. Like most Physics computer programs *RUNT* is written in FORTRAN. The standard FORTRAN compiler will handle an expression such as 12*T by making a complex number 12 + 0i and performing the four multiplies and two adds required of a complex multiply. Clearly an expression such as T/12 where 12 is first complexified is horribly inefficient!! To get around these difficulties it is best to handle real and imaginary parts separately and thereby avoid complex arithmatic altogether.

At Rmax we extract the phase-shift by comparing to a linear combination of Coulomb Wavefunctions. In the pion case we match the functions at two points, for the proton case we use the function and its derivative. We can get the derivative from the Noumerov method by using the following formula

$$y'(r) = \frac{w(r+h)[1 - 2T(r+h)]}{2h(1 - T(r+h))} - \frac{w(r-h)(1 - 2T(r-h))}{2h(1 - T(r-h))} \qquad A.12$$

APPENDIX B. THE RELATIVISTIC COULOMB WAVEFUNCTIONS

The derivation and evaluation of these functions is a long
and tedious buisness. We divide this section into 2 parts,
the derivation of the functional form and then the
evaluation of the functions. To avoid unnecessary
mathematical derivations we make numerous references to the
Handbook of Mathematical Functions (AB70).

B.1 Deriving the analytic forms

We start from the equations 4.20 and 4.21. We set
$V_v(r) = Ze^2/r$ and $V_s(r) = 0$. This gives us the two coupled
differential equations

$$\left(\frac{Ze^2}{\hbar c\, r} - \frac{E-mc^2}{\hbar c}\right) f_c(r) - \left(g_c'(r) - \frac{K\, g_c(r)}{r}\right) = 0 \qquad \text{B.1}$$

$$\left(\frac{Ze^2}{\hbar c\, r} - \frac{E+mc^2}{\hbar c}\right) g_c(r) + \left(f_c'(r) + \frac{K\, f_c(r)}{r}\right) = 0 \qquad \text{B.2}$$

where we have used the definitions,

$$f_{c,s}(r) = \frac{f_c(r)}{r}, \qquad g_{c,s}(r) = \frac{i\, g_c(r)}{r} \qquad \text{B.3}$$

After many substitutions to simplify the notation and
algebra we get

$$\left(\frac{\eta_{(+)}}{x} - 1\right)U(x) - V'(x) + \frac{K}{x}V(x) = 0 \qquad \text{B.4}$$

$$\left(\frac{\eta_{(-)}}{x} - 1\right)V(x) + U'(x) + \frac{K}{x}U(x) = 0 \qquad \text{B.5}$$

where the new quantities are given by

$$\eta_{(\pm)} = \frac{\alpha}{k}\varepsilon_{(\pm)} , \qquad \varepsilon_{\pm} = \frac{E \pm mc^2}{\hbar c} \qquad \text{B.6}$$

$$U(x) = \frac{f_c(r)}{\sqrt{\varepsilon_{(+)}}} , \qquad V(x) = \frac{g_c(r)}{\sqrt{\varepsilon_{(-)}}} \qquad \text{B.7}$$

$$x = kr , \qquad \alpha = \frac{Ze^2}{\hbar c} \qquad \text{B.8}$$

The potential is real and so two independent real solutions to the equations can be found. Let us introduce a complex function and its complex conjugate by

$$F(x) = U(x) + iV(x) \qquad \text{B.9}$$

$$F^*(x) = U(x) - iV(x) \qquad \text{B.10}$$

We can therefore eliminate $U(x)$ and $V(x)$ in favour of F and its complex conjugate. This gives two simultaneous equations for F and its complex conjugate. We can eliminate F^* in favour of F by differentiating one equation and substituting into the other. After much tedious but straightforward algebra we can get

$$F''(x) + \frac{1}{x} F'(x) - \left\{ \frac{\eta_{(+)} + \eta_{(-)}}{x} - 1 - \frac{\eta_{(+)}\eta_{(-)} - K^2}{x^2} - \frac{i}{x} \right\} F(x) = 0$$

B.11

If we compare this equation to equation 13.1.35 in (AB70) we see that F can be written in terms of the Confluent Hypergeometic Function 'M'. We compare B.11 to the equation 13.1.35 and equate co-efficients. We can immediately identify

$$h(x) = 2ix$$

B.12

and from equating co-efficients in the second term

$$f'(x) = i + \frac{1 - b - 2A}{2x}$$

B.13

and also if we equate powers of x^0, x^{-1} and x^{-2} in the third term we have

$$ib - 2i\alpha = i - (\eta_{(+)} + \eta_{(-)})$$

B.14

and

$$(b-1)^2 = 4\left(K^2 - \eta_{(+)}\eta_{(-)} \right)$$

B.15

equation B.15 gives us

$$b = 1 \pm 2s$$

B.16

where we have introduced

$$S = \sqrt{K^2 - \alpha^2} \quad = \sqrt{\left(J + \tfrac{1}{2}\right)^2 - \alpha^2}$$

B.17

Now, using this in B.14 gives us

$$\alpha = s - \qquad = s - i\gamma$$

B.18

where γ is the [illegible] parameter

$$\gamma = \frac{zE}{\hbar c} = \frac{ze^2}{\hbar v}$$

B.19

Now, equation B.15 had two possible solutions depending on which sign of the square root we take. Expressing $f(x)$ in terms of the variable s gives us

$$F(x) = e^{-ix} x^s M(s - i\gamma, 2s+1, 2ix)$$

B.20

so going back to f and g we get

$$\begin{pmatrix} f_c(r) \\ g_c(r) \end{pmatrix} = \begin{pmatrix} \sqrt{\epsilon_{(+)}} \; Re \\ \sqrt{\epsilon_{(-)}} \; Im \end{pmatrix} (kr)^s e^{-ikr} M(s - i\gamma, 2s+1, 2ikr)$$

B.21

We obtain two independent solutions by putting

$$S = \pm\sqrt{K^2 - \alpha^2}$$

B.22

If we examine B.21 closely, we see the positive s solution is regular at the origin, all other solutions, in particular the one we have here with s negative, are irregular at the origin. We may write the most general

solution

$$\begin{pmatrix} f_c(r) \\ g_c(r) \end{pmatrix} = \begin{pmatrix} \sqrt{\varepsilon_{(+)}} & Re \\ \sqrt{\varepsilon_{(-)}} & Im \end{pmatrix} \left\{ \begin{array}{l} \lambda_R (kr)^s e^{-ikr} M(s-i\gamma, 2s+1, 2ikr) \\ + \lambda_I (kr)^{-s} e^{-ikr} M(-s-i\gamma, 1-2s, 2ikr) \end{array} \right\}$$

B.23

A moments thought will tell us we haven't quite finished. Consider the regular solution

$$f_c(r) = \sqrt{\varepsilon_{(+)}} \; Re\left\{ \lambda_R (kr)^s e^{-ikr} M(s-i\gamma, 2s+1, 2ikr)\right\}$$

B.24

We have a constant λ_R which arose from the solution of the complex differential equation. In general therefore λ_R will itself be a complex number. It appears that we have 4 real arbitrary constants arising in the general solution (2 regular, 2 irregular) to the two real coupled first order differential equations. What has happened is that in going from two first order equations to one second order equation we have differentiated. This step has introduced the possibility of new solutions, and so we must put back B.24, and its irregular counterpart into the origonal first order equations to check that it is indeed a solution to the origonal problem.

If we assume λ_R is complex and write it as

$$\lambda_R = N_R e^{i\phi}$$

B.25

we can substitute back in and get a constraint on ϕ

$$e^{-2i\phi_R} = \frac{-\left(K + \frac{i\alpha mc}{\rho}\right)}{s + i\gamma}$$

B.26

The derivation of this result is quite tedious, involving the use of the Kummer Transformation as well as recurrence relations for the Confluent Hypergeometric functions.

Now in equation B.26 it appears that in general ϕ must have an imaginary part. To see that this is not so we show the magitude of the r.h.s. to be unity

$$\frac{K + \frac{i\alpha mc}{\rho}}{s + i\gamma} = \frac{\rho^2 K^2 + \alpha^2 m^2 c^2}{\rho^2 K^2 - \rho^2 \alpha^2 + \rho^2 \gamma^2}$$

$$= \frac{\rho^2 K^2 + \alpha^2 mc^2}{\rho^2 K^2 + \alpha^2\left(\frac{E^2 - \rho^2 c^2}{c^2}\right)} = 1$$

B.27

Now the irregular solution is obtained from the regular one by the recipe $s \rightarrow -s$ and so for the irregular solution we have immediately

$$e^{-2i\phi_I} = -\left(\frac{K + \frac{i\alpha mc}{\rho}}{-s + i\gamma}\right)$$

B.28

We now have to decide on the value of N in equation B.25. This of course depends on the normalisation convention we are using. In the absence of the Coulomb interaction we

choose a normalisation by requiring

$$\psi^{m_s}(\underline{r},t) \longrightarrow \frac{e^{i\underline{k}\cdot\underline{x}}}{(2\pi)^{\frac{3}{2}}} \sqrt{\frac{E+mc^2}{2mc^2}} \begin{pmatrix} 1 \\ \dfrac{\underline{\sigma}\cdot\underline{P}c}{E+mc^2} \end{pmatrix} \chi(m_s)$$

B.29

We have seen that we get an extra logarithmic phase in the arguement of the exponential for the Coulomb case, but this does not affect the normalisation we seek.

We can expand the exponential in B29 in partial waves and if we use the Dirac equation to get the lower component we have

$$\psi^{m_s}(\underline{r},t) = \frac{e^{-iEt}}{2\pi} \sum_{\substack{LJM \\ m_L}} i^L Y_L^{*m_L}(\hat{k}_i)(L\,\tfrac{1}{2}\,m_L\,m_s|JM)$$

$$\left\{ \begin{array}{c} \sqrt{\dfrac{E+mc^2}{\pi mc^2}} \quad j_L(kr)\, \mathcal{Y}_{L\,\frac{1}{2}\,J}^M(\Omega) \\[3mm] sgn(K)\sqrt{\dfrac{E-mc^2}{\pi mc^2}} \quad j_{L'}(kr)\, \mathcal{Y}_{L'\,\frac{1}{2}\,J}^M(\Omega) \end{array} \right\}$$

B.30

with the usual conventions (see Chapter 4)

$$L' = 2J - L, \quad K = (L-J)(2J+1), \quad sgn(K) = \begin{cases} +1 & K > 0 \\ -1 & K < 0 \end{cases}$$

B.31

Thus for the radial functions we have the normalisation

$$f_L(r) \longrightarrow \frac{1}{K}\sqrt{\frac{E+mc^2}{\pi mc^2}} \sin\left(kr - \frac{L\pi}{2}\right)$$

B.32

If we use the asymptotic form of the Confluent Hypergeometric Function (AB70 equation 13.5.1) we can get, after some algebra,

$$f_c(r) \longrightarrow \frac{N_R \sqrt{E_+} \; \Gamma(2s+1) e^{\frac{\pi \eta}{2}}}{2^s \left| \Gamma(1+s+i\eta) \right|} \cos\left(\phi_R - kr - \arg\Gamma(1+s+i\eta) + \eta \ln 2kr + \frac{\pi s}{2} \right) \qquad \text{B.33}$$

This gives us the normalisation for the regular solution

$$N_R = \frac{1}{k} \frac{\hbar c}{\pi m c^2} \frac{2^s e^{-\frac{\pi \eta}{2}} \left| \Gamma(1+s+i\eta) \right|}{\Gamma(1+2s)} \qquad \text{B.34}$$

and

$$N_I = \frac{1}{k} \frac{\hbar c}{\pi m c^2} \frac{2^{-s} e^{-\frac{\pi \eta}{2}} \left| \Gamma(1-s+i\eta) \right|}{\Gamma(1-2s)} \qquad \text{B.35}$$

Equation B.33 can be compared directly to 4.56. We see that we can obtain the Coulomb Phase-Shift by

$$\Sigma_k = \arg\Gamma(1+s+i\eta) + \frac{\pi}{2}(1-s+1)^s - \phi_R \qquad \text{B.36}$$

After all this algebra it is sad to report that one problem remains. The solution to this problem is straightforward in analytic terms, but it causes rather unpleasant problems in the numerical evalution of the phase-shifts later on.

Consider the asymptotic forms for the two solutions we have found

$$f_c^{(R)}(r) \longrightarrow \frac{1}{k} \sqrt{\frac{E+mc^2}{\pi m c^2}} \cos\left(kr - \eta \ln 2kr + \arg\Gamma(1+s+i\eta) - \frac{\pi s}{2} - \phi_R \right) \qquad \text{B.37}$$

$$g_c^{(I)}(r) \longrightarrow \frac{1}{k}\sqrt{\frac{E+mc^2}{\pi mc^2}}\cos\left(kr - \frac{\gamma}{\ln 2kr} + \arg\Gamma(1-s+i\gamma) + \frac{\pi s}{2} - \phi_I\right) \qquad \text{B.38}$$

we can write

$$f_c^{(I)}(r) \longrightarrow -\frac{\gamma}{k}\frac{E+mc^2}{\pi mc^2}\sin\left(kr - \frac{\pi s}{2} - \frac{\gamma}{\ln 2kr} + \arg\Gamma(1+s+i\gamma) - \phi_R + \xi\right) \qquad \text{B.39}$$

If $\xi = 0$ the solutions are 90° out of phase and we extract the phase-shift as outlined in Chapter 4. If ξ is a half odd integer multiple of π, then the two solutions we have are linearly dependent and we will have to look elsewhere for an irregular solution.

It turns out that

$$\xi = \pi(s + 1/2) + \tan^{-1}\left(\cot\pi s \tanh\pi\gamma\right)$$

$$\text{B.40}$$

If we think of the Coulomb interaction as being weak, then γ is small and we have

$$\xi = \pi(s + 1/2) + \gamma/s \qquad \text{B.41}$$

as we have feared, ξ is close to a half odd integer multiple of π.

In order to extract the phase-shift we need a linear combination of regular and irregular functions to get an (irregular) function which is asymptotically 90° in advance of the regular solution in phase. Such a solution turns out

to be

$$f_c^{(I)}(r) = cc \cdot r \left\{ f_c^{(s)}(r) - cosec\,\theta \right\} f_c^{(-s)}(r)$$

<div align="right">B.42</div>

where

$$\theta = -\pi s - \tan^{-1}\left(\tan \pi s \tanh \pi \nu\right) + \frac{(-1)^K \pi}{2} r$$

<div align="right">B.43</div>

the $(-1)^K$ arises to ensure the solution is 90° in advance of rather then 90° behind the regular solution.

Equation B.42 finally gives us the irregular solution. The difficulty we will encounter is that since ν is small and therefore the two solutions are almost linearly dependent, the subtraction in B.42 can lose us up to 6 significant figures.

This method is the same as that used by (ME72) and (EL53). It would be and interesting and useful project for someone to come up with a nice way of calculating the irregular solution which did not involve this subtraction.

B.2 Numerical Evaluation of the Coulomb Wavefunctions

Here we evaluate the functions with

$$S = \pm\sqrt{K^2 - \alpha^2}$$

<div align="right">B.44</div>

and chose a linear combination of them to obtain the irregular solution with the correct asymptotic phase. Since this subtraction involves a large loss of precision it is important to evaluate the functions very accurately in the first place.

The numerical integration method of Elton and the power series method of Mercer, it seems to this author may not be sufficient for this purpose and so a more direct analytic method is developed and employed. We have from equation B.42

$$\begin{pmatrix} f_c(r) \\ g_c(r) \end{pmatrix} = \begin{pmatrix} \frac{E+mc^2}{\hbar c} & N_s \, Re \\ \frac{E-mc^2}{\hbar c} & N_s \, Im \end{pmatrix} (kr)^s e^{i\phi_R} e^{-ikr} M(s-i\gamma, 2s+1, 2ikr)$$

B.45

and the irregular solution from $s \to -s$. Let us concentrate for now on just the regular solution.

To evaluate Ns we need to evaluate a complex Gamma function. Since this function is not standard FORTRAN we evaluate it by one of two means

1. If $\gamma < 1$ we use the recurrence relation

$$\Gamma(s+1) = s \, \Gamma(s)$$

B.46

to reduce the problem to one with $0 < s < 1$. We then use the Mclauren series for the reciprocal

$$\frac{1}{\Gamma(z)} = \sum_{n=1}^{\infty} a_n z^n \quad ; \quad a_1 = 1, \quad a_2 = .5772, \dots$$

B.47

(see (AB70) 6.1.34)

If $\gamma > 1$ or $S > 20$ we are better off using the recurrence relation to get us to where $|s + i\gamma| > 20$ and using the asymptotic series for the logarithm of

the gamma function

$$\ln \Gamma(z) \sim (z - 1/2) \ln z - z + 1/2 \ln 2\pi$$

$$+ \sum_{m=1}^{N} \frac{B_{2m}}{2m(2m-1) z^{2m-1}}$$

B.48

(AB70,6.1.41)

where Bn are the Bernoulli numbers.

The evaluation of all the other parts is now straightforward except the 'M' function. This function is defined by a series which is uniformly convergent on $[0, \infty)$,

$$M(a,b,z) = 1 + \frac{a z}{b} + \frac{a(a+1)}{b(b+1)} \frac{z^2}{2!} + \frac{a(a+1)(a+2)}{b(b+1)(b+2)} \frac{z^3}{3!} + \dots$$

B.49

$$\equiv \sum_{n=0}^{\infty} \frac{a_{(n)}}{b_{(n)}} \frac{z^n}{n!}$$

B.50

Since we have the limit

$$\lim_{n \to \infty} \left| \frac{a_{(n)}}{b_{(n)}} \right| = \text{constant}$$

B.51

and since also Z is a pure imaginary number the series has identical properties to the series for exp(ix). It is well known that this series is useless for calculations if x is larger than, say 20, since we lose 8 figures from subtractions. Since we are interested in values of |Z| ~ 60 this series is completely useless.

The large |Z| can however be turned to advantage if we try for an asymptotic series. From the definition of the 'M'

function in equation B.49 we can employ the techniques of (LI78) to get the result

$$M(\alpha, b, z) = \frac{e^{i\pi\alpha}}{\Gamma(b-\alpha)} z^{-\alpha} \sum_{n=0}^{R-1} \frac{\alpha_{(n)} (1 + \alpha - b)_{(n)} (-z)^{-n}}{n!}$$

$$+ \frac{e^{z}}{\Gamma(\alpha)} z^{\alpha-b} \sum_{n=0}^{S-1} \frac{(b-\alpha)_{(n)} (1 - \alpha_{(n)}) z^{-n}}{n!} \qquad \text{B.52}$$

(see also (AB70) eqn. 13.5.1)

For our large values of $|Z|$ these series converge very quickly as long as s is small. If s is of order unity the series looks like

$$\sum_{n=0}^{N} \frac{n!}{z^{n}} \qquad \text{B.53}$$

The terms rapidly get smaller, but the series ultimately diverges. This is because the series is asymptotic. The saving grace of such a series is that the error involved in stopping the series after a finite number of terms is $\leq$ the size of the next term. For small $|Z|$ the accuracy obtainable from the series is seriously limited, but for $|Z| > 10$ we can always get 17 figures of accuracy, which is as much as the computer we are using can handle anyway.

We are interested in not only s ~ 1 but also s ~ $|Z|$. In this latter case the terms of the series look like (take $|Z|$=50)

$$\sum_{n=1}^{R} \frac{(50)_n (50)_n}{(50)_n \, n!}$$

B.54

so that the ratio of terms is

$$\frac{T_{n+1}}{T_n} = \frac{(50+n)^2}{50\,n}$$

B.55

the terms never get smaller!! The series only is useful then if we have s << |Z|. The only way round this dilemma of calculating the higher partial waves is to use a recurrence relation to get us from small s to large s. Unfortunately such a relation does not give us *all* the results we seek as in the non-relativistic case since the values of 's' we seek are not separated by integers. Suppose we are interested in evaluating the function for s=58.7, then we must first evaluate the series with s=.7 and s=1.7 and then recur up. The next value of s might be 59.69 and so we would have to start over with s=.69 and s=1.69. Using some graph-theoretic techniques and starting from the recurrence relations given in (AB70) we can derive the required relation

$$M(s-i\gamma, 2s+1, z)\left[\frac{(s-1-i\gamma)(s+i\gamma)}{(2s-2)(2s-1)^2 \, 2s}\right] z^2$$

$$+ M(s-1-i\gamma, 2s-1, z)\left(1 - \frac{z(1+2i\gamma)}{(2s-1)(2s-3)}\right) = M(s-2-i\gamma, 2s-3, z)$$

B.56

This relation is stable if s < kr but as in the spherical Bessel functions when we want to calculate an s > kr we must

use a backward recurrence method for the regular solution.

APPENDIX C. REDUCED MASS TRANSFORMATION

Here we give the formalism for calculating the reduced mass for the case of two relativistic projectiles. There are 3 common *recipies* for the reduced mass which one plugs into a Dirac or Klein-Gordon equation, namely

$$\mu = \frac{m_1 m_2}{m_1 + m_2} \qquad \text{C.1}$$

$$\mu = \frac{m_1 m_2}{E_1 + E_2} \qquad \text{C.2}$$

$$\mu = \frac{E_1 E_2}{E_1 + E_2} \qquad \text{C.3}$$

The first and third are the extreme non-relativistic and extreme relativistic results. The second is a hybrid result given by (PI79a) where it is shown to give the correct result in first order as compared with a field-theoretic calculation. If we write down a two particle Dirac Hamiltionian or a two particle Klein-Gordon Hamiltonian, then we cannot find a linear transformation (as in the Schrödinger case) which separates out the centre of mass motion, hence the need for a *recipe*.

The method presented here for calculating μ starts from the premise that the reduced mass needed comes as a result of *recoil* and so should not depend on whether we have Fermions or Bosons present, just on their masses and energies. We write the mass-energy relation as

$$E^2 = p^2 c^2 + m^2 c^4 \qquad \text{C.4}$$

$$\Rightarrow \quad T = \frac{p^2}{2m\left(1 + \frac{T}{mc^2}\right)} \qquad \text{C.5}$$

where T is the kinetic energy. The two particle Hamiltonian then is

$$H_{12} = \frac{P_1^2}{2m_1\left(1 + \frac{T_1}{2m_1 c^2}\right)} + \frac{P_2^2}{2m_2\left(1 + \frac{T_2}{2m_2 c^2}\right)} + V_{12}(r_1 - r_2) \qquad \text{C.6}$$

We make the approximation of replacing the kinetic energy operators by their *free* eigenvalues. This is a reasonable approximation providing that the energy exchange in the centre of mass is small (identically zero for elastic scattering) and

$$V_{12}(r_1 - r_2) \ll m_1 c^2, m_2 c^2 \qquad \text{C.7}$$

We definine effective masses by

$$m_1^* = m_1\left(1 + \frac{T_1}{2m_1 c^2}\right) \quad , \quad m_2^* = m_2\left(1 + \frac{T_2}{2m_2 c^2}\right) \qquad \text{C.8}$$

The Hamiltonian now looks just like a two particle Schrödinger Hamiltonian and so we write

$$r = r_1 - r_2 \qquad \text{C.9}$$

$$R = \frac{m_1^* r_1 + m_2^* r_2}{m_1^* + m_2^*} \qquad \text{C.10}$$

then

$$H = m_1 + m_2 + \frac{P_r^2}{2\mu^*} + \frac{P_R^2}{2M^*} + V_{12}(r)$$

C.11

where

$$\mu^* = \frac{m_1^* m_2^*}{m_1^* + m_2^*}$$

C.12

$$M^* = m_1^* + m_2^*$$

C.13

This then has the centre of mass and relative motion separated. We want the relative piece to look like;

$$H_r = \sqrt{P_r^2 + \mu^2} + V_{12}(r) = \frac{P_r^2}{2\mu^*} + V_{12}(r) + \mu$$

C.14

so as before;

$$\mu^* = \mu\left(1 + \frac{T_{cm}}{2\mu c^2}\right)$$

C.15

where

$$T_{cm} = T_1 + T_2$$

C.16

Thus we can get μ from m_1, m_2, T_1 and T_2. As input to the calculation we have P_r and μ. We can calculated the reduced centre of mass energy from the mass-energy relation

$$E_r^2 = P_r^2 c^2 + \mu^2 c^4$$

C.17

APPENDIX D. THE PROGRAM *RUNT*

In this Appendix we outline the structure of the search program *RUNT*. *RUNT* is based on the formalism of Chapter 4. In essence *RUNT* reads in two sets of elastic scattering data (cross-section and analysing power) for a given nucleus and energy; then varies the potential parameters so as to obtain a fit to the data by a χ^2 minimisation technique.

RUNT is written in double precision. Its speed is such that a typical search starting from guessed parameters takes around 2-5 minutes on the University of Alberta's Amdahl-V8 computer.

We describe the program one subroutine at a time.

D.1 Main Line

This reads in the initial parameters, calls subroutine USEFUL and then subroutine SEEK.

The input cards are ordered as follows:

1. RMAX,NSTEP (F10.4,I3)

   The matching radius (fm) and the number of integration steps.

2. ANGMIN,ANGMAX,NANG (2f10.4,I3)

   ANGMIN/MAX are the smallest and largest angles at which a curve is required from a given set of potential parameters; NANG is the number of evenly spaced angles at which the elastic observables are calculated.

3. TPROT (F10.4)

The laboratory kinetic energy of the incident proton (MeV).

4. LMAX (I3)

The number of partial waves to be used.

5. VV,RV1,AV1 (3F13.7)

The strength (MeV), radius (fm) and diffuseness (fm) of the real vector potential (see Chapter 7). The radius is multiplied by $A^{1/3}$ where A is the number of nucleons in the target nucleus.

6. WV,RV2,AV2 (3F13.7)

Same as card 5 but for the imaginary vector potential.

7. VS,RS1,AS1 (3F13.7)

Same as card 5 but for the real scalar potential.

8. WS,RS2,AS2 (3F13.7)

Same as card 5 but for the imaginary scalar potential.

9. ZP,ZT,RCOUL (3F12.6)

The charge on the incident and target nuclei in units of the electron charge (which is taken as negative), and the radius of the uniform charge distribution (units of fm).

10. WP,WT (2F12.6) The atomic weights of the projectile and target nuclei in units of a.m.u.

D.2 Subroutine USEFUL

This subroutine does the odd calculations needed by the other subroutines.

It scales up the potential radii according to the

formula

The subroutine then calculates all the kinematic quantities, relativistically. Finally the subroutine calculates quantities to do with the Coulomb interaction and performs a few tests on the input data to ensure the program is going to give sensible results.

D.3 Subroutine SEEK

As its name suggests, this is the subroutine responsible for carrying out the search.

After the experimental data are fed in, the main loop starts.

1. The program reads (from unit 5) a sequence of 13 letters, either T's or F's. Each T or F refers to the variables to be searched on in the order

   VV RV1 AV1 WV RV2 AV2 VS RS1 AS1 WS RS2 AS2 RCOUL

   A T signifies the variable in question is to be searched on, whilst an F signifies that it is to retain its present value throughout the search.

2.

   The next card has on it one of 3 words:

   a. AUTO Subroutine CURFIT is called which varies the

parameters requested until the χ^2 is reduced. The variables are updated with their new values which are then printed along with the χ^2.

b. BOOB The program backs up a step and a new set of T's and F's can be read in.

c. HAND The program now requests input from unit 5. The values of the parameters which are to be searched on are given in one line and the program calculates the χ^2 and prints it out.

D.4 Subroutine CURFIT

This subroutine automatically varies the potential parameters to lower the χ^2 between the experimental data and the fitted curve. The search is based on an algorithm due to Marquadt. (BE69).

Curfit calls subroutine DERIV which calculates the partial derivatives of the χ^2 with respect to the potential parameters. Both CURFIT and DERIV need to call subroutine FUNCTN which calculates the cross-section and analysing powers from a given set of potential parameters.

D.5 Subroutine FUNCTN

This subroutine takes a given set of potential parameters and returns values for the differential cross-section and analysing power at the same angles as the experimental data so that subroutine CHISQ can calculated the χ^2.

FUNCTN first calls subroutine DW which returns the phase-shifts for each partial wave, and then uses the method of Yennie et al (YE54) to calculate the two scattering amplitudes from which the observables are calculated. If desired the reaction cross-section is also calculated.

D.6 Subroutine DW

This subroutine takes its name from the distorted wave which, in the DWBA program, it calculates. Since we are interested only in the phase-shift, the modified Noumerov method (Appendix A) is used. Since approximately 45% of the CPU time is used in doing the numerical integration, this piece of the code is written as optimally as possible.

The first call to DW sets up the potentials and the functions $\ker(r)$ and $d'(r)/d(r)$ which are introduced in Chapter 4. Subsequent calls skip this calculation.

The values of the integrated wavefunction and its derivative are calculated at RMAX, and then passed to subroutine MATCH which returns the phase-shift.

For the special case of $L=1$, the integration is started by a power series method since the term in the Cowell method $y(r)T(r)$ is non-vanishing at the origin.

D.7 Subroutine MATCH

On first entry this subroutine calls subroutine RELKOU which returns the regular and irregular Dirac Coulomb wavefunctions and their derivatives at RMAX. If the Coulomb interaction is turned off then the subroutine calls subroutine BESSEL to do the calculation.

Using these regular and irregular wavefunctions, the phase-shift is calculated.

D.8 Subroutine RELKOU

This subroutine calculates the Dirac Coulomb wavefunctions according to the algorithm described in Appendix B. The subroutine is self contained except for calls to subroutine CGAMMA which calculates the values of the complex gamma function (also by the methods outlines in Appendix B).

D.9 Subroutine BESSEL

This subroutine simply calles SBESS and SNEUM which calculate the spherical Bessel functions and spherical Neumann functions by recurrence relations.

D.10 Subroutine CURVES

This subroutine is called from SEEK if no variables are to be searched on, i.e. if thirteen 'F's in a row are given.

The subroutine calls FUNCTN and returns NANG values for

the elastic observables on a regular grid between ANGMIN and ANGMAX.

D.11 Subroutine MATINV

As the name suggests, this subroutine inverts a square matrix. This subroutine is called from CURFIT and is described in (BE69).

APPENDIX E. THE PROGRAM *SAPPHIRE*

In this Appendix we outline the structure of the DWBA program *Sapphire*.

This program calculates the T-Matrix elements using the formalism of Chapter 6, which itself calls on the results of Chapters 3, 4 and 5.

Sapphire has many options, which means it is a large program; not just in the number of computer cards needed to store it but also *Sapphire* occupies 248 pages of virtual memory.

Sapphire is written in double precision; a typical run takes 6-10 seconds of CPU time. *Sapphire* can handle up to 75 partial waves, however in practice it is limited by its ability to handle only 800 integration steps. This means that without extending the array sizes, *Sapphire* can perform the DWBA calculations only up to incident proton energies of around 300 MeV.

Below we describe the program one subroutine at a time.

E.1 Main Line

This subroutine is responsible for reading in (and writing out) the main controls and input data. The main line then calls the necessary subroutines which perform the various tasks as required. The input cards are ordered as follows:

1. NPLOT,DWBA,ELAST,PLOT,LFASE,ELPI,KARENS,FT,VTYPE

(I3,8L1)

Where,

   a.   IF NPLOT=1, then the differential cross-section and analysing power are written on unit 7 in a format suitable for reading by any standard plotting program.

   b.   If DWBA=T, the DWBA calculation is done.

   c.   If ELAST=T, then the proton elastic scattering observables are calculated.

   d.   If PLOT=T then many intermediate curves are plotted out on a graphics terminal. This is especially useful for debugging.

   e.   If FASE=T then the proton and pion phase-shifts are printed out.

   f.   If ELPI=T, then the pion elastic scattering differential cross-section is calculated.

   g.   If KARENS=T then the Stricker potential is used for the pion distortion. If KARENS=F, then the potential desired is controlled by the parameters on card 17.

   h.   If FT=T then the Fourier transform of the bound state wavefunctions is calculated.

   i.   If VTYPE=T, then the pseudovector vertex is used in the DWBA calculation: if VTYPE=F then the pseudoscalar vertex is used.

2.   RMAX,NSTEP (F10.4,I3)

The cut off for the radial integrals and the number of

integration steps.

3. ANGMIN,ANGMAX,NANG (2F10.4,I3)

    ANGMIN/MAX are the smallest and largest angles at which
    a curve is required. NANG is the number of evenly
    spaced angles at which the observables are calculated.

4. TPROT (F10.4)

    The laboratory kinetic energy of the incident proton
    (MeV).

5. LMAX (I3)

    The number of pion partial waves used in the
    calculation of the pion differential cross-section and
    also the DWBA calculation. LMAX+LBOUND partial waves
    are used in the calculation of the proton elastic
    scattering observables.

6. IBOUND,NODES,PARB (2I3,F11.4)

    a. IBOUND determines the type of potential used in
        calculating the bound state wavefunctions. In all
        cases the requirement that the state should have
        the correct binding energy is used.

        1) IBOUND=1, VVEC/VSCA=PARB is used as a
        constraint.

        2) IBOUND=2 VVEC and VSCA are varied independently
        to fit the binding energy and spin-orbit splitting
        of the state.

        3) IBOUND=3 VSCA is set to zero.

        4) IBOUND=4 VVEC is set to zero.

    b. NODES determines the number of nodes needed in the

upper component of the bound state, the nodes at zero and infinity are <u>not</u> counted.

c.   PARB is the ratio of VVEC to VSCA used if IBOUND=1 is given. A typical value would be -0.81.

7.   VVEC,RVEC,AVEC (3F17.8)

The strength (MeV), radius (fm) (to be multiplied by $A^{1/3}$, where A is the nucleon number of the target nucleus) and diffuseness (fm) for the vector potential used in calculating the bound state.

8.   VSCA,RSCA,ASCA (3F17.8)

Same as 7, but for the scalar potential.

9.   EBIND,ESPLIT (2F16.10)

The binding energy and spin-orbit splitting (if known) of the bound state in MeV.

10.   FJBOND,LBOUND (F10.4,I3)

The 'J' and 'L' quantum numbers for the bound state.

11.   RMATCH,ERB (2F16.10)

RMATCH is the radius at which the outward integrated wavefunction meets the inward integrated wavefunction, and the derivative mis-match calculated. (Typical value 4 fm).

ERB is the maximum allowed derivative mis-match at RMATCH. A typical value would be 10^{-5}.

12.   QMAX,NQ (F10.4,I3)

Should the bound state in momentum space be required, then it is calculated in NQ evenly spaced steps from zero to QMAX fm^{-1}.

13. VV,RV1,AV1 (3F13.8)

The strength (MeV), radius (fm) (which will later be multiplied by $A^{1/3}$ and diffuseness (fm) for the real vector potential used in calculating the proton distorted wave.

14. WV,RV1,AV1 (3F13.8)

Same as above but for the imaginary vector potential.

15. VS,RS1,AS1 (3F13.8)

Same as above but for the real scalar potential.

16. WS,RS2,AS2 (3F13.8)

Same as above but for the imaginary scalar potential.

17. ZI,ZF,RCOUL (3F17.8)

   a. ZI/ZF are the initial and final channel charges (i.e. the product of incident and target charges and the product of the charges on the pion and final nucleus).

   b. RCOUL is the radius(fm) of the uniform charge distribution used in calculating the proton distorted wave (which will be multiplied by $A^{1/3}$).

18. WP,WT,WF (3F17.8)

The atomic masses (a.m.u.) of the projectile, target and final nuclei. (Must be as accurate as possible).

19. A1,A2,A3,A4 (8F15.6)

   a. If KARENS=T then the A3 and A4 are not used, and A1 and A2 become the 4 variable imaginary pieces in the Stricker potential as given in table III of (ST79).

b. If KARENS=F then the pion distortion potential is of the form

$$E_\pi V_\pi (r\phi) = A_1 \rho(r) + A_2 \nabla \rho(r) \underline{\nabla}$$

E.1

Where $\rho(r)$ is the density normalised to the number of nucleons,

20. GEON1,GEON2,GEOC,NPROT,NNEUT,IPOT (3F15.6,3I4)

    a. IPOT determines the potential geometry used.

      1) If IPOT=1 then Woods Saxon geometry is used

$$\rho(r) = \frac{1}{\ldots \frac{r - GEON1}{GEON2}}$$

E.2

$$\rho_c(r) = \begin{cases} 1 & r < GEOC \\ 0 & r > GEOC \end{cases}$$

E.3

      2) If IPOT=2 then modified Gaussian geometry is used

$$\rho(r) = \left(1 + GEON1\left\{\frac{r}{GEON2}\right\}^2\right)e^{-\left(\frac{r}{GEON2}\right)^2}$$

E.4

$$\rho_c(r) = \rho(r)$$

E.5

    b. NPROT and NNEUT are the number of protons and neutrons in the final nucleus.

21. PHITT (F12.4)

This is actually read in from subroutine PIDW. It is

best set to zero since it represents an experimental phase-shift equivalent potential transformation. Specifically, for the $l=1$ partial wave,

$$y_1(r) \rightarrow y_1(r)e^{i\,PHITT\sqrt{\frac{P(r)}{P(0)}}}$$

E.6

E.2 Subroutine USEFUL

This performs little calculations which are needed by the other subroutines. These include potential radius scaling, kinematics, Coulomb parameters and a few tests on the input data.

E.3 Subroutine IAIB

This subroutine calculates the radial integrals given in equations 6.21 and 6.22. This subroutine first calls one of four possible bound state subroutines, depending on the value of IBOUND.

IAIB next calls DW which returns a proton distorted wave, then PIDW, which returns a pion distorted wave. Having all the ingrediants, the quadrature is done using the trapizoidal rule.

E.4 Subroutine TOUTER

This subroutine calculates the T matrix. Touter starts the sums over the quantum numbers $L\,J\,\ell_\pi$, and then calls

subroutine TINNER to do the sum over the remaining quantum numbers.

E.5 Subroutine TINNER

This subroutine is called by TOUTER, it calculates the T matrix for a given set of quantum numbers

To do this TINNER evaluates the spherical harmonics with $\theta=\pi/2$ and $\phi=0$, then calls subroutines to calculate the Wigner 3J and 6J symbols and uses the I_A and I_B calculated in subroutine IAIB.

E.6 Subroutine BONDV/BONDS

These subroutines call subroutine INTGER which returns a value of the derivative mis-match at RMATCH. They adjust VVEC/VSCA (Whilst setting the other to zero) so as to make the derivative mis-match less than ERB. Newton's method is used.

E.7 Subroutine BOND1

This subroutine calls subroutine INTGER which returns a value of the derivative mis-match at RMATCH. It adjusts VVEC and VSCA subject to the constraint VVEC/VSCA=PARB.

E.8 Subroutine BOND2

This subroutine varies VVEC and VSCA independently to fit both the binding energy and spin-orbit splitting of the bound state. It does this by calling subroutine INTGER for not only the bound state required but also for the spin-orbit split state, thereby obtaining derivative mis-matches for both states. VVEC and VSCA are then varied so as to make *both* of these mis-matches less than ERB, using the two dimensional Newton's method.

BOND2 contains the entry point BONDRS which is called from BONDV, BONDS and BOND1. BONDRS calculates the $f(r)$ and $g(r)$ from the $y(r)$ and $y'(r)$ obtained from the numerical integration.

E.9 Subroutine INTGER

This subroutine integrates the bound state differential equation up to RMATCH from both sides, calculates the derivative mis-match and returns it to the calling program.

E.10 Subroutine DW

On first call to this subroutine, the subroutine sets up the arrays $ker(r)$ and $d'(r)/(rd(r))$ as described in Chapter 4. The subroutine then uses a modification of the Cowell method to calculate the wavefunction $[y(r)]$. Subroutine MATCH is called which gives the phase-shift and normalisation. The $f(r)$ and $g(r)$ are then calculated from

the y(r) and y'(r) obtained from the numerical integration.

E.11 Subroutine MATCH

This subroutine takes the values for y(RMAX) and y'(RMAX) from DW, calls either RELKOU or BESSEL (depending on whether the Coulomb interaction is present or not) and then calculates the phase-shift and normalisation for the proton distorted wave.

E.12 Subroutines CLEBO,F3J,F6J,S6J

These calculate the Clebsch gordon co-efficient with all 3 projection quantum numbers set to zero, the Wigner 3J symbol and the Wigner 6J symbol respectively.

E.13 Subroutine DWBAOB

This subroutine takes the T matrix and calculates from it the differential cross-section and analysing power for the (p,n^+) reaction. Also the phase shifts are written out after the entry point PHPNT.

E.14 Subroutine START

For the special case of l=1, the Cowell method is not self starting since the y(r)T(r) term does not vanish at the origin.

It turns out that the most accurate way around this problem is to start with a power series. Is just so happens that this power series is that corresponding to the non relativistic Coulomb wavefunctions.

E.15 Subroutine ERRORS

This subroutine is called whenever there is an error or warning message to be given by the program.

E.16 Subroutine ELSCAT

This subroutine takes the phase-shifts as calculated by subroutine DW, and then uses Yennie's method to calculate the elastic scattering amplitudes and observables. The reaction cross-section is also calculated.

E.17 Subroutine LEGTAB

This tabulates the values of the Legendre polynomials and first associated Legendre polynomials for all values of L from 0 to 150.

E.18 Subroutine SIGTAB

This tabulates the Dirac Coulomb phase-shifts.

E.19 Subroutine PIDW

On first call this subroutine sets up the array Bulk(r) as described in Chapter 5. PIDW then uses the Cowell method (modified) to calculate y(r) and y'(r). After calling MATPI which returns the phase-shift and normalisation, PIDW calculates the pion distorted wave.

E.20 Subroutine MATPI

This calls subroutine COU which calculates the non-relativistic Coulomb wavefunctions, then extracts the phase shift and normalisation for y(r).

E.21 Subroutine PIEL

This subroutine takes the pion phase shifts and calculates the pion elastic scattering amplitude and cross section using the technique of subtracting off the point charge Coulomb amplitude.

E.22 Subroutine FORIER

This takes the bound state wavefunctions and calculates the (three dimensional) Fourier transform of them.

E.23 Subroutine VERFIX

This subroutine "fixes" the pseudoscalar vertex so that it will give the answer corresponding to the pseudovector vertex. It does this by multiplying the bound state wavefunctions by an expression containing the binding and proton distorting potentials (see Chapter 6).